An interactive task-ambient cooling control featuring personal thermal comfort and non-intrusive sensing techniques

PhD Dissertation submitted in partial fulfillment
of the requirements for the degree of

Doctor of Philosophy
in
Building Performance and Diagnostics

By

Siliang Lu
August 2019

School of Architecture
College of Fine Arts
Carnegie Mellon University
Pittsburgh PA, 15213

Doctoral Committee

Erica Cochran Hameen (Chair), Ph.D., Assistant Professor

School of Architecture, Carnegie Mellon University

Ömer Tugrul Karaguzel, Ph.D., Assistant Professor

School of Architecture, Carnegie Mellon University

Berangere Lartigue, Ph.D., Associate Professor

LMDC, Paul Sabatier University, Toulouse, France

Acknowledgment

To my committee members

I would like to express my appreciation to all the thesis committee members for having accepted to be in my committee board. First of all, my special thanks go to Prof. Omer T. Karaguzel, for having honored me by being one of my committee members, and also for his supervision and encouragement, when I participated in the collaborative VIFI project with LBNL and LSU. I sincerely thank Prof. Berangere Lartigue for having accepted to read and review the manuscript of my work, with her proficiency and expertise. I would also like to thank her for her great advice on my work, especially building energy simulations and help me improve my oral defense by taking time to make several dry runs with me.

I want to deeply thank Prof. Erica Cochran Hameen, my thesis advisor, for giving me this precious opportunity to work under her supervision. During all the four years of my PhD study, her patience, her indispensable advice, her constant guidance, her scientific rigor and her confidence in me, all these have enabled me to overcome the challenges in my research. I really appreciate her effort to helping me get CSC financial support when I prepared materials in New York City before my PhD study, which has encouraged me to accomplish the goal of the research and to finish my thesis. I also really appreciate her time to help me improve my oral defense during spring and summer.

To my colleagues in the project

The work in this thesis has been inspired by previous work done by Prof. Bing Dong, Prof. Jooho Choi and Dr. Jie Zhao. Many thanks to them for their great work. I am grateful to Prof. Jie Shi and Prof. Yue Zou and their colleagues, for their generous help to provide experimental test beds for me in Tongji Univeristy and Donghua Univeristy last spring and summer. Meanwhile, I would like to thank Weilong Wang, Chaochao Lin and Shihan Wang for their intelligence in working with me on my research last spring. I also thank those participants for joining in my experiments and providing their useful feedbacks so that I can setup the database for my research. My gratitude also extends to Prof. Wei Wang for his useful advice on the writing part.

To Intelligent Workplace and School of Architecture people

I would like to express my sincere thanks to Prof. Volker Hartkopf and Prof. Vivian Loftness, for their wonderful leadership of this dynamic and innovative research team. My warmest thanks

also go to Darlene Covington-Davis, for her understanding of my difficulties and her essential assistance throughout my PhD study. I also appreciate Prof. Nina Baird, Zhiang Zhang, Chenlu Zhang, Yujie Xu, Wanni Zhang, Linhao Li, Youngjoo Son, Xianla Li, Shihao Zhang, Hetal Parekh, Flore Marion, James Katungyi, Jing Yang, Jiarong Xie ans Suzy Li for their nice presentations on their works that have broadened my vision on building science and architectural technology. It is a great pleasure for me to work with them in the same office. I am also grateful to all my BPD friends during master and doctoral studies, especially Yuzhe Liu, Yuqi Pan, Xiaowen Gu, Han Li, Nilesh Bansal, Akash Mehta and those friends in AECM and CD. I am very grateful to all the team members who have created a friendly atmosphere and organized some excellent and unforgettable activities such as Potluck and cookie event in the working time and after working.

To my family and my friends

I wish to thank my parents and all my family members, for their love, their understanding, and their encouragement. This thesis cannot be finished without their support. My thanks also go to one of my best friends Sida Wang, for her great company and encouragement all the time. Finally, I would like to thank all my friends in CMU, in Pittsburgh, in the US or elsewhere, whom I have not seen for years and who have always shown their useful support and help when I need.

Abstract

The Heating, Ventilation and Air-Conditioning (HVAC) system plays a key role in shaping building performances. Effective and efficient HVAC operations not only achieve energy savings but also create a more comfortable indoor environment for occupants. Moreover, compared to the private office environment, the open-plan office environment has become a trend in most office buildings since it not only creates opportunities for employees to communicate with one another and improves productivity but also reduces construction cost. However, the open-plan office building layout is also faced with problems such as interruptions from other people and unsatisfactory shared indoor temperature and humidity levels. Therefore, it is of great importance to develop a new paradigm for the HVAC system framework so that everyone can work under their preferred thermal environment while also achieving improved energy performance. But how can we achieve personal thermal comfort and energy efficiency without being intrusive?

This dissertation proposes a new integrative task-ambient cooling control featuring personal comfort models with non-intrusive sensing techniques for open-plan office spaces. The research mainly consists of four parts:

- Development of a personalized cooling control to create a comfortable local thermal environment automatically with non-intrusive sensing techniques and machine learning algorithms. The sensing system consists of an indoor air temperature sensor, relative humidity sensor DHT22, and an infrared temperature sensor AMG8833.
- Quantification of the energy savings of the proposed task-ambient cooling system by cooling set-point optimization of the ambient conditioning system and the automatic operations of the task conditioning systems with personal thermal comfort models.
- Development of a data-driven approach with CFD simulator to analyze the benefits of energy savings in a typical office space while maintaining acceptable thermal comfort with the proposed task-ambient cooling system.
- Development of an energy co-simulation with the proposed task-ambient cooling system to analyze the benefits of energy savings in a typical shared office space while maintaining acceptable thermal comfort with comfort database I & II.

As a result, in terms of energy savings, five 3-hour sessions in the field study have shown that the proposed system can achieve 9.6% in HVAC energy savings on average compared with

baseline system. Moreover, the energy co-simulation study has shown the energy performances with the proposed task-ambient cooling system could be optimized to save HVAC electric demand power by 5.3% on average compared with baseline system.

Additionally, in terms of thermal comfort, the performances in the field study have shown the recall scores of the thermal sensation model and the thermal satisfaction model with data from all female subjects are 84.7% and 76.5%, respectively. Meanwhile, the recall scores of the thermal sensation and the thermal satisfaction model with data from all male subjects are 87% and 82.5%, respectively. Furthermore, an automated feedback collection mechanism was implemented to update personal comfort models by collecting override actions by occupants (collecting the information of thermal environment conditions when occupants manually change on/off overriding the programmed automation system). As a result, participants were more satisfied with updated personal comfort models.

Overall, the proposed task-ambient cooling system featuring personal thermal comfort and non-intrusive sensing techniques not only optimizes energy performance, but also provides a more comfortable thermal environment in open plan office spaces.

Keywords: Adaptive and personal thermal comfort; Non-intrusive infrared sensing; Task-ambient cooling system.

Table of contents

Chapter 1 Background of the interactive task-ambient conditioning system

1.1 Overview of occupant thermal comfort

Most people spend 90% of their time indoors (Bratman et al., 2012) since buildings can provide satisfactory environments for human beings. Indoor environment quality (IEQ) is always used to evaluate the quality of the built environments created with different building systems such as acoustic quality, air quality, spatial quality, visual quality and thermal quality. As one of the key building systems, Heating, ventilation and air-conditioning (HVAC) system affects all of these qualities, particularly indoor air quality (IAQ) and indoor thermal quality. The effective and efficient HVAC operations not only achieve energy savings but also create a more comfortable environment for occupant indoors. Nowadays, open-plan offices have become a trend since it increases the communications but also reduces construction cost. However, open-plan office building is also faced with problems like unsatisfactory shared indoor temperature and humidity due to different thermal preferences. Therefore, a great solution to satisfy individual thermal comfort is to develop personal comfort models so as to predict occupant thermal comfort level and take it into consideration for the operations of occupant-responsive HVAC system in real open-plan offices.

As defined by ANSI/ASHRAE 55 (ASHRAE, 2013) and ISO7730 (Roelofsen, 2011), thermal comfort is the condition of mind that expresses satisfaction with the thermal environment and is assessed by subjective evaluation. Therefore, thermal comfort is the combined result of physical environment and psychological activities. In the course of thermal comfort theory, static thermal comfort and adaptive thermal comfort have become two main categories. In terms of static thermal comfort, predicted mean vote (PMV) and predicted percentage of dissatisfied (PPD) developed by Fanger (Fanger, 1970) are the most widely accepted thermal model, as shown in Figure 1-1. PMV and PPD have six variables applied to be the indicators of thermal comfort, which are indoor air temperature, indoor relative humidity, indoor air velocity, mean radiant temperature, clothing insulation and metabolic rate. Moreover, since PMV predicts the average vote of a large group of people based on 7-point thermal sensation scale, it describes the overall thermal sensation of multiple occupants in a shared thermal environment. However, since PMV was derived from strictly controlled climate chamber, which was different from real office buildings, the performances of thermal comfort prediction needs improving.

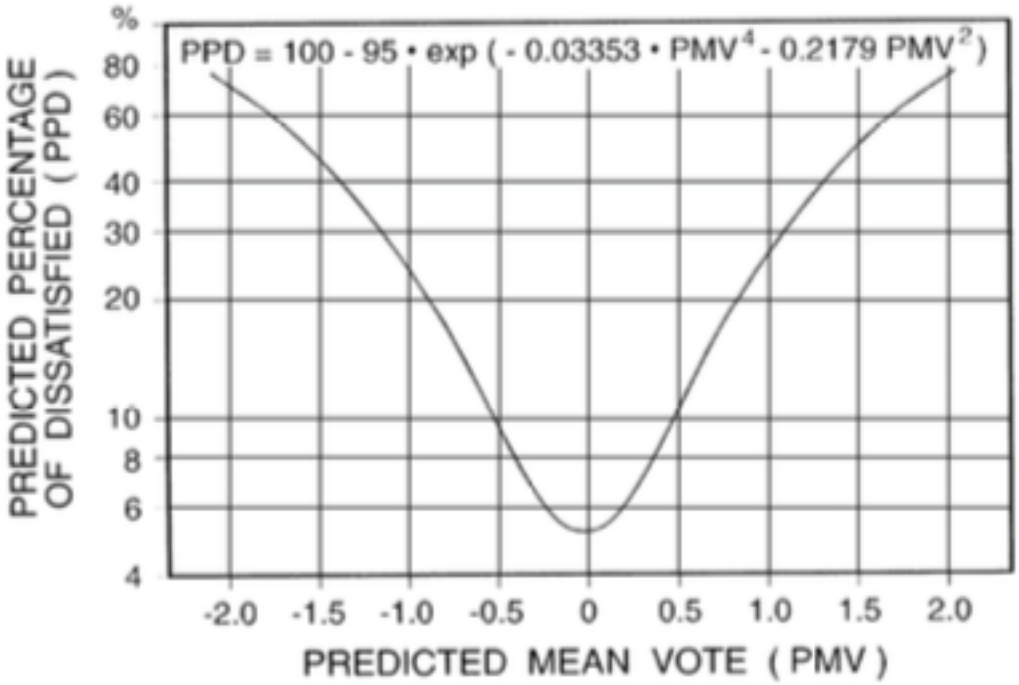

Figure 1-1 Relationship between PMV and PPD (ASHRAE 55, 2010)

In order to overcome the disadvantages of static thermal comfort, adaptive thermal comfort aims to provide insights in highlighting interactions between occupants and buildings, which increases opportunities for personal and responsive control, thermal comfort enhancement, energy consumption reduction and climatically responsive and environmentally responsible building design (De Dear et al., 1998). The adaptive model is premised that the occupant is no longer a passive recipient of the given thermal environment. Instead, the occupant is able to interact with all levels of the person-environment system via feedback loops in the real thermal environment. Meanwhile, in adaptive thermal comfort, researchers believe thermal comfort is not only affected by physical environment but also affected by factors such as gender, age and nationality. One of the milestone projects of adaptive thermal comfort is the ASHRAE RP-884 database (Comfort database I) consisting of 22,000 samples, which aims to test the adaptive thermal comfort hypothesis and develop an adaptive thermal comfort model. Moreover, a newly released dataset called ASHRAE global thermal comfort database II (Comfort database II) consisting of 81,846 samples intends to support diverse inquiries about adaptive thermal comfort in field settings (Földváry et al., 2018). These two databases have been widely used to investigate various adaptive thermal models, which have the potential to be integrated into personalized HVAC controls. With comfort database I, Lee et al. (2017) proposed a method for learning thermal preference profiles

by formulating a combined classification and inference problem with 5-cluster model. Moreover, the thermal preference of a new user is inferred by mixture of sub-models for each cluster where clusters are used to group occupants with similar thermal preferences characteristics. In addition, instead of predicting 7-point thermal sensation described in ASHRAE 55, the paper predicts thermal preferences with 3 classes, namely "want cooler", "want warmer" and "no change". Besides, Auffenberg et al. (2015) proposed a personalized thermal model using Bayesian network to learn and adapt to a user's individual preferences by predicting thermal sensation of occupants within a specific area, such as San Francisco with ASHRAE RP-884 dataset. However, the results were not promising that the highest accuracy of the model was only 30%. In addition, Wang et al. (2019) has proposed to use k-nearest neighbor (KNN) and multivariate Gaussian distributions to detect outliers with different thermal acceptability and thermal preferences from majority votes with the comfort database I & II. Besides, Gao et al. (2019) adopted a deep neural network based approach for predicting the occupants' thermal comfort with comfort database I, and then adopted Deep Deterministic Policy Gradient (DPPG) for learning the temperature and humidity control policy. The results have shown better prediction performances for thermal comfort and achieved higher thermal comfort and energy efficiency than baseline. Moreover, Lu et al. (2019) has developed personalized thermal comfort models with KNN, support vector machine (SVM) and random forest (RF) to predict thermal sensations based on comfort database I and conducted a Q-learning based temperature set-point controller with the personalized thermal models. However, since the majority vote in the database regarding thermal sensation is neutral, the thermal sensation prediction was hard to detect other states.

However, even if comfort databases I&II have provided good opportunity to study adaptive thermal comfort, since each occupant has few samples in the databases and they aim to develop a generic adaptive thermal comfort model based on large populations, it may not be suitable for personal thermal comfort predictions and for fine-grained individual thermal comfort management by differentiating individual thermal comfort differences. Therefore, researchers have proposed a new category of thermal comfort model named personal comfort model, which predicts an individual's thermal comfort responses (Kim et al., 2018). Meanwhile, for both adaptive thermal comfort and personal thermal comfort, three response types were common to use, as shown in Figure 1-2.

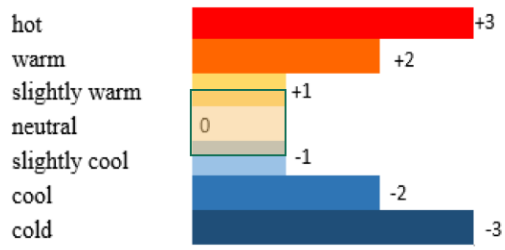

(a) 7-point thermal sensation

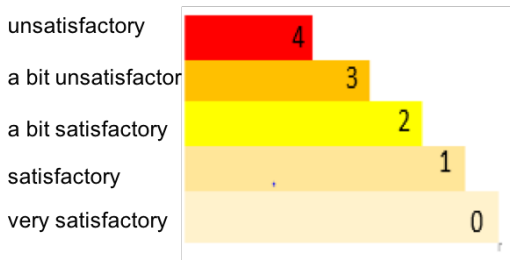

(b) 5-point thermal satisfaction

(c) 3-point thermal preference

Figure 1-2 Three types of thermal comfort metrics

Besides making the most of existing comfort databases, researchers on thermal comfort also proposes skin temperature to indicate thermal comfort inspired by thermoregulation theory. Thermoregulation is a dynamic equilibrium with the environment where body regulates its internal core temperature in terms of heat generation and heat exchange with the environment (Jazizadeh et al., 2018). In detail, if the ambient temperature is below skin temperature, heat is dissipated from the body by radiation and convection. On the other hand, if the skin temperature is lower than ambient temperature, heat will be absorbed by the body so that the skin temperature increases. Even if heat exchange also occurs due to the metabolic process of the human body, since occupants usually sit or walk without too much metabolic heat production in office buildings, whether the individual is thermally comfortable or not is more related to skin temperature.

Motivated by this, many researchers have proposed thermal comfort models with mean skin temperature or the most representative local skin temperature. Liu et al. (2015) used mean skin temperature of 10 measurement locations, including forehead, chest, upper arm, back, abdomen, elbow, hand, thigh, calf and foot to evaluate thermal comfort for a person in a sleeping posture under steady thermal environment. The results turned out that the mean skin temperature at the three different thermal comfort levels was statistical significant. In terms of local skin temperature, Choi (2010) tested skin temperatures of 10 body locations to select the best location for thermal comfort inference, including forehead, upper arm, belly, wrist, hand, thigh, calf and foot. The

results turned out that wrist was the most responsive area to infer thermal comfort with the lowest p-value. Moreover, Sim et al. (2016) established multiple linear regression models to estimate thermal sensations with variables based on skin temperature. As a result, the models using temperatures of the fingertips and wrist showed the highest accuracy. Wei Li et al. (2018) also proposed multiple linear regression models to estimate thermal sensation under various active states using wrist skin temperature-related variables. The study indicated skin temperature, its time differential and heart rate could be used for estimating individual thermal sensation. Even if these empirical thermal sensation models achieved high accuracy, the studies were only conducted in a steady-state thermal environment.

In addition, most of the existing thermal comfort models have been based on regression at present. However, thermal comfort predictions can also be seen as classification problem where various classification algorithms can be implemented. A recent research on thermal comfort inference utilized the wearable device of a pair of eyeglass with infrared (IR) arrays, and demonstrated that 82.8% of prediction accuracy for detecting uncomfortable conditions was obtained with hidden markov model (HMM) (Ghahramani et al., 2018). Moreover, Huang et al. (2015) used wearable devices like wearable fitness trackers to measure physical movements, sweat level and skin temperature so as to infer individual thermal comfort with machine learning algorithms including random forest (RF) and support vector machine (SVM). In addition, Dai et al. (2017) implemented SVM to predict thermal demands using skin temperature collected from various locations with wearable sensors. As a result, SVM classifiers with linear kernel were preferred to Gaussian kernel, which achieved over 90% accuracy. Based on the literature review, classification models have performed so well as regression models.

Besides different methods of thermal comfort models, the development of sensing technique has also promoted the development of adaptive and personal thermal comfort. The current sensing technique used for thermal comfort inference can be mainly divided into two categories. One is wearable sensing devices and the other is contactless sensing devices. For wearable devices, wrist band has been the most popular one (Choi, 2010; Sim et al., 2016; Li et al., 2018; Ghahramani et al., 2018; Huang et al., 2015; Dai et al., 2017). For instance, Ghahramani et al. (2016) proposed a wearable infrared eyeglass frame to measure skin temperature at different points of the skin, including nose, front face, back of ear and cheekbone so as to infer thermal preferences.

Even if wearable devices can directly measure variables like skin temperature to indicate thermal comfort, the major disadvantage is intrusiveness. Therefore, contactless measurement methods have drawn much more attention nowadays, especially infrared (IR) thermography. IR thermography utilizes the emitted infrared radiation to measure surface temperature of an object. In order to measure surface temperature with IR thermography correctly, emissivity of the object has to be known since most of actual objects are grey bodies. Nowadays, IR thermography has been widespread and applied into various functions, such as building diagnostics in HVAC industry, fault detection as well as thermal comfort analysis. An empirical study utilized an infrared (IR) sensor called Lepton to estimate occupant thermal comfort level by measuring skin temperature measured from different face regions. The results have shown that ears, nose and cheeks are most indicative to thermal comfort (Li et al., 2018). In addition, Ranjan and Scott (2016) have used IR camera to dynamically detect and predict thermal comfort. They classified thermal preferences based on skin temperature of forehead, cheeks, jaws, upper neck, lower neck, palm core, palm and back of hand, and found that the face outperformed other body regions. Moreover, Han et al. (2017) utilized infrared imaging to measure skin temperature and control the indoor environment with self-learning algorithms. As a result, 98% of the occupants' feedback demonstrated the control system was able to achieve satisfactory thermal environments.

In addition to infrared camera, other types of camera can also be implemented to measure skin temperature-related variables like RGB camera and depth camera. A recent study has proposed a red-green-blue-depth-temperature (RGB-DT) framework consisting of a thermographic camera, a depth-sensor and a color camera to measure body temperatures at different body parts, including hand, elbow, shoulder, chest as well as left and right heads (Cosma et al., 2018). A feedback form was used to collect thermal comfort information from different subjects. Moreover, Jazizadeh and Jung (2018) have used RGB camera with Photo plethysmography (PPG) technique to amplify subtle variations of blood perfusion of human face in different temperature ranges. However, the proposed system was not evaluated in a regular temperature range between 20℃ and 30℃ in a real office building.

To summarize, contactless sensing technique can solve the issue of intrusiveness while maintain high performance of thermal comfort inference. Moreover, the adaptive and personal thermal comfort are more realistic to the actual indoor environment than static thermal comfort and the performances can be enhanced with machine learning algorithms. Therefore, developing

adaptive and personal thermal comfort models with contactless sensing techniques has become an interesting research area recently. However, most of the current contactless sensors such as vision-based sensors are much more expensive than conventional sensors such as temperature/humidity sensors. Hence, it is unlikely to spread the sensing system in a large-scale office environment.

1.2 Overview of occupant-responsive HVAC system

With profound studies on relations between building energy performances and human dimensions that occupant behaviors actually play a significant role in energy consumption in the buildings (D'Oca et al., 2018), the occupant-responsive HVAC system has been seen as future trend for developing the intelligent building systems due to the outstanding performances of energy savings and occupant comfort improvement in both field studies and building simulations.

Among various occupant-responsive HVAC control system, task-ambient conditioning (TAC) system has drawn much more attention than before. Task ambient conditioning (TAC) system is defined as any space conditioning system that allows thermal conditions in small, localized zones to be individually controlled by building occupants, while still automatically maintaining acceptable environmental conditions in the ambient space of the building (Bauman et al., 1996). Since TAC system not only takes individual thermal preferences into account but also maintains the overall acceptable thermal environment, it has become one of the most promising air-conditioning systems in open-plan office buildings. Moreover, due to rapid development of building automation system (BAS), many researchers have investigated advanced control strategies so as to operate advanced HVAC system effectively in the open-plan office buildings. Zhang et al. (2010) developed a task-ambient system that heated only the feet and hands, and cooled only the hands and face, to provide comfort in a wide range of ambient environment. The simulated annual heating and cooling energy savings with such TAC system was as much as 40%. In addition, as one of the most popular personalized cooling devices, personalized fan such as desktop fan and ceiling fan has several advantages. Firstly, fans offer a straight-forward, economic, and independently operable technique to increase movement of air so as to ultimately improve thermal comfort in a room (Sekhar, 1995). Moreover, when operated with Air-conditioning (AC) system, the downwash propelled by foil (rotating) drives the supply air to blend with the existing air, mitigating the uncomfortable thermal stratification. Lastly, since the energy consumption of the distributed personalized fans are lower than centralized air-conditioning system (Anderson et

al., 2015), fans contribute to improve energy efficiency of task-ambient conditioning system (TAC) by elevating temperature set-point dead band of the ambient conditioning system.

Shetty et al. (2019) have developed desk fan usage preference models, including fan state and fan speed with tree-based methods among six users. The results have shown 97.73% accuracy have been achieved in predicting fan state with the test set and importance of different features vary among different individuals. In addition, Makhoul et al. (2013) conducted a computational fluid dynamic (CFD) simulation to study the enhancement of ceiling mounted personalized ventilation (PV) when assisted by desktop fans to reduce thermal plume. Thermal comfort models were developed based on skin temperature, core temperature, as well as sensible and latent heat flux calculated with multi-segmented bioheat model. The bioheat model were co-simulated with CFD model by exchanging data related to thermal environment, including mean radiant temperature, air temperature and air velocity. The simulation results have shown the desk-mounted fans were able to reduce the convection plumes around the occupant and achieved energy saving by up to 13% when compared with conventional mixing ventilation systems. In addition, PV aims to deliver conditioned air directly to the indoor spaces with various ambient conditioning systems such as underfloor air distribution (UFAD) (Sekhar & Zheng, 2018) so as to reduce energy consumption and improve individual thermal comfort. Sekhar & Zheng proposed an integrated personalized ventilation and local fan-induced active chilled beam (PV-ACB) air conditioning system and was analyzed based on thermal stratification with CFD. However, even if CFD simulations have revealed improvements in thermal comfort, both of them have used static thermal models such as PMV, which may not be appropriate to evaluate thermal comfort in real office environment.

Moreover, personal comfort system (PCS) is an innovation to integrate low-energy PCS to create micro-zones into centralized HVAC operations in open plan office environments (Anderson et al., 2015). The project has invented the low-energy heated and cooled chairs with wireless internet connectivity and tested the performances in different real office environments in California. The PCS adjusts the local thermal environment based on occupant behavioral models of changing heating/cooling set-points of the chair. Meanwhile, the whole framework gets further optimized with communication between chairs and the centralized HVAC system. However, due to variation of how this building is operated, the field measurement of the whole HVAC energy consumption did not conclusively show whether PCS saved energy or not.

For most of existing TAC systems, the control of the task component is partially or entirely decentralized and completely under the control of the occupants. As a result, TAC system cannot be fully optimized since the task system states are not responsive to dynamic thermal environment and occupant thermal comfort until the occupant takes action on his/her own. On the contrary, the performances of TAC system have great potential to be optimized by connecting the distributed task components with the ambient component such as PCS.

In the well-connected TAC system where the individual thermal preferences based on interactions with the task conditioning system are transmitted to the ambient conditioning system wirelessly, the ambient conditioning system plays a role in coordinating individual task conditioning system and optimizing the overall thermal environment. So far, there are mainly two strategies to optimize ambient conditioning system. One is to create a group thermal comfort model based on individual thermal models and the other is to implement advanced control strategies such as multi-agent control.

Zhao et al. (2014) proposed a group thermal model by taking the convex hull of the individual complaint regions of the group people as the group complaint regions and using the compliment set of the complaint regions as the comfort zone of the group. Moreover, Xu et al. (2014) also proposed a group thermal model by combining multiple thermal models, which are probability distributions for different thermal comfort levels, into a single probability distribution. Even if the group thermal model simplifies the dynamic ambient conditioning control, it may cause larger prediction biases on the group thermal model if the individual thermal model has biases.

In artificial intelligence, agents are physical or virtual entities that intelligently interact in an environment by both perceiving and affecting it. In multi-agent system (MAS), agents can additionally communicate and coordinate with each other as well as with their environment (Dounis & Caraisco, 2009). Hence, in multi-agent framework, the most important components are agents and the coordinator. Among various control logics applied in the framework of multi-agent control system, fuzzy control, model predictive control (MPC) and reinforcement learning (RL) control have been widely investigated. Moreover, for building control system, many researchers have applied multi-agent framework in the occupant-centric HVAC system. Klein et al. (2012) proposed a multi-agent comfort and energy system (MACES) to simulate the energy savings and occupant thermal comfort improvements in an office building. MACES was tested with multiple actual schedules and constructed agents representing building devices, occupants and meetings.

The simulation has shown 12% energy reduction and 5% comfort improvements. In addition, Ghahramani et al. (2014) introduced a knowledge-based approach for improving HVAC system operations through coupling personalized thermal comfort preferences and energy consumption patterns. In their approach, zone temperature set points were selected through solving a constrained optimization problem for energy, with comfort, indoor air quality, and system performance constraints. The agents were represented with multiple occupant discomfort profiles and coordinated by solving the optimization with iterative relaxing algorithm. Moreover, Zhao (2015) conducted building simulations to optimize both energy performances and occupant thermal comfort with MPC where the occupant behavior models were developed to predict energy consumption and PMV data was collected from real subjective feedbacks. With the occupant behavior models and subjective feedbacks, occupant behaviors can be represented as agents. In addition, Dalamagkidis et al. (2007) developed a RL controller taking into account user preferences as agents in order to achieve energy savings, high comfort and indoor air quality. Lastly, besides centralized HVAC system, as mentioned before, multi-agent control system can also be applied into TAC system. Jain et al. (2018) investigated the impact of occupancy prediction errors on thermal comfort and energy consumption with MPC control system. The results have shown that with the task conditioning system, the controller was more robust to prediction errors.

To summarize, multi-agent control system is one of the most suitable systems for building energy and thermal comfort management. Moreover, with the development of better thermal models and more robust inter-connected network, the benefits in terms of thermal comfort from multi-agent control in TAC system will be increased.

1.3 Motivations

Based on literature review on thermal comfort research and occupant-responsive HVAC control system, it can be concluded that the recent studies related to thermal comfort have been focused on development of different sensing techniques to develop adaptive personal thermal comfort models, as well as integration of such models into occupant-responsive HVAC system. Kim et al. (Kim et al., 2018) presented a unified framework for personal comfort models and discussed challenges for applications of personal comfort models in the real world. It was found that most recent adaptive and personal thermal comfort research is focused on developing statistical thermal comfort models by collecting data and implement various machine learning algorithms to achieve higher prediction accuracy. However, few studies on adaptive and personal

thermal comfort further apply the models into advanced HVAC controls such as reinforcement learning control. Moreover, compared to sensing approaches like wearable devices, contactless sensing devices such as IR camera are much less intrusive and have drawn much more attention than before. However, it is expensive to use IR camera in a large-scale office buildings. Therefore, this dissertation proposes and evaluates a new task-ambient cooling system featuring personal comfort models with non-intrusive sensing techniques for open-plan office buildings with field studies, CFD and energy simulations. Table 1-1 shows the skin temperature measurement method benchmark for thermal comfort inference and performance benchmark based on three metrics, including intrusiveness, privacy and cost-effectiveness. Moreover, with field studies in real open-plan offices, the proposed system was evaluated based on actual feedback from users. In addition, with CFD and energy simulations, the proposed system was evaluated with more detailed analysis on thermal comfort in terms of airflow patterns, temperature distribution and energy consumption. Finally, it will bring about more insightful suggestions on the task-ambient cooling system before real deployment in large-scale.

Table 1-1 Skin temperature measurement method and performance benchmark

	Cheekbone	Frontal face	Nose	Ear	Wrist	Lower neck	Palm	Non-intrusiveness	Privacy	Cost-effectiveness
Li et al., 2017	✓		✓	✓					✓	
Dai et al., 2017					✓				✓	✓
Choi, 2010					✓				✓	✓
Ghahramani et al., 2016		✓							✓	✓
Metzmache et al., 2018		✓						✓	✓	
Han et al., 2017		✓						✓	✓	
Li et al., 2018					✓				✓	✓
Abdallah et al., 2016					✓				✓	✓
Sim et al., 2016					✓				✓	✓
Hasan et al., 2016					✓				✓	✓
Ghahramani et al., 2018						✓			✓	
Ranjan & Scott, 2016						✓	✓	✓	✓	
Jung et al., 2018		✓						✓		
Huang et al., 2015					✓				✓	✓
Cosma et al., 2018		✓					✓	✓	✓	
Lu et al., 2019	✓							✓	✓	✓

1.4 Research hypotheses

Moreover, this dissertation aims to validate the following main hypothesis with three sub-hypotheses:

- Main Hypothesis: An interactive task-ambient cooling system will provide higher energy savings than a conventional air-conditioning (ambient only) system, while maintaining thermal comfort in open-plan office buildings.

- Sub-hypothesis 1: Task conditioning system can be operated automatically based on the personal thermal comfort models.
- Sub-hypothesis 2: Personal thermal comfort model can be continuously improved by collecting occupant override actions.
- Sub-hypothesis 3: An interactive task-ambient cooling system can be optimized by minimizing sensible cooling loads with the constraints of individual thermal comfort.

1.5 Chapter overview

The whole dissertation can be mainly divided into three parts. In addition to introduction, the whole dissertation consists of the development of the non-intrusive task conditioning system and the evaluation of the task-ambient cooling controls, which are discussed with the following chapters in detail. All of these chapters have made contributions to the development of the interactive task-ambient cooling system, as shown in Figure 1-3. In all, the whole methodology includes a controlled experiment, a field study to develop personal thermal comfort model and evaluate the task-ambient cooling control using machine learning as well as two simulation studies using CFD and energyplus, respectively.

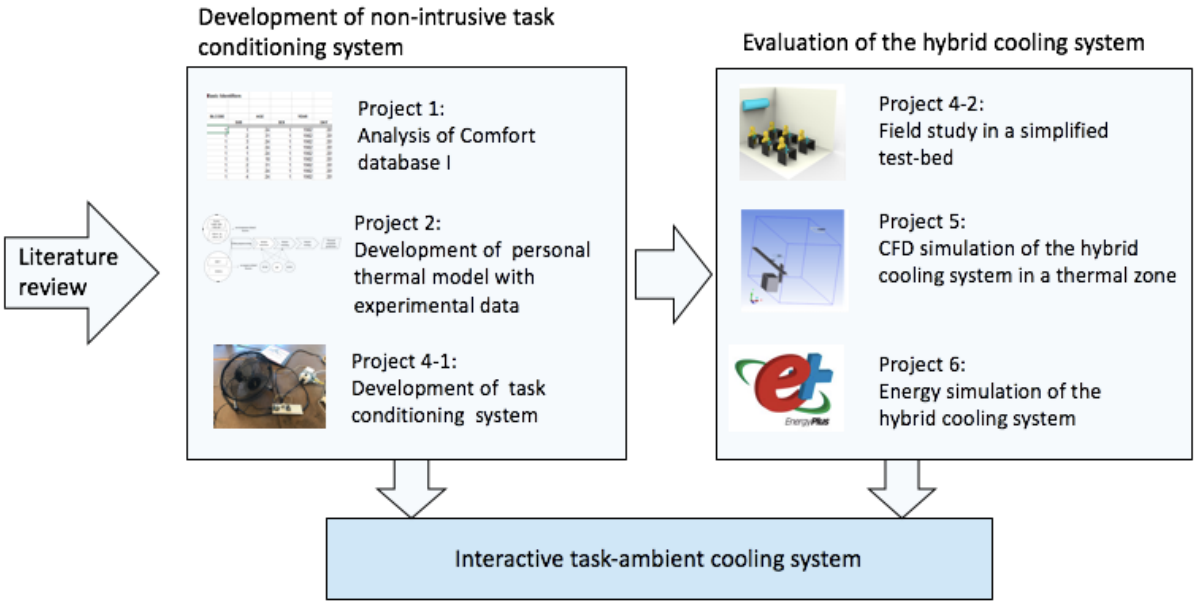

Figure 1-3 Overview of the whole dissertation

In addition to overview of each chapter, Table 1-2 shows the deliverables of each chapters and the correspondent algorithms, baseline models as well as software used.

Table 1-2 Project deliverables for each research chapter

RESEARCH PROJECTS	PROJECT DELIVERABLE	DATASET	MACHINE LEARNING ALGORITHM	BASELINE MODEL	PROGRAMMING /SIMULATION ENGINE
PROJECT 1	**1. Adaptive thermal comfort model**	Comfort database I	SVM	PMV	Python
			RF		
			KNN		
PROJECT 2	**2. Personal comfort model**	Data from experimental study	SVM	PMV	Python
			RF		
PROJECT 4-1	**3. Personalized task conditioning system**	-	-	-	Arduino IDE
PROJECT 4-2	**4. Personal comfort model**	Data from field study	SVM	Classification model with indoor air temperature only	Python
	5. Hybrid cooling framework		-	-	Ouimeaux
PROJECT 5	**6. Personal preference distribution in CFD simulator**	Data from experimental study	SVM		Ansys
			RF		
		Comfort database I & II	SVM		
			RF		
PROJECT 6	**7. Synthetic personal preference distribution**	Comfort database II	GMM	-	Energyplus
			KDE		
	8. Energy simulation for the hybrid cooling system	-	-		

Chapter 2: *Data-driven simulation of a thermal comfort-based temperature set-point control with comfort database I.* This chapter aims to develop the data-driven thermal comfort model with comfort database I and the second part is to develop a Q-learning based temperature set-point controller based on combination of thermal comfort predictions from the thermal comfort model and some domain knowledge from ASHRAE 55.

Chapter 3: *Comfort-based and non-intrusive personalized model in office buildings.* This chapter aims to develop personal comfort models with three different feature sets trained with two machine learning algorithms. In order to collect occupant data, an experimental study was conducted in an open-plan office in Shanghai with the non-intrusive sensing system consisting of indoor air temperature and relative humidity sensor DHT22 and an IR camera.

Chapter 4: *A case study of the interactive task-ambient conditioning cooling control in Shanghai.* This chapter aims to develop personal comfort models with machine learning algorithms by collecting data from a sensing system consisting of indoor air temperature and relative humidity sensor called DHT22, an infrared temperature sensor called AMG8833 (GridEye) and a micro-controller called ESP8266 with WIFI module. Moreover, the performances of the proposed personalized cooling system controlled with personal thermal models were also enhanced in an open-plan office in Shanghai during the cooling season by optimization of the whole TAC system.

Chapter 5: *Data-driven personal comfort models combined with CFD simulation for the local fan-induced air-conditioning system*. This chapter aims to conduct CFD simulations with the best adaptive thermal models developed with based on the data from both comfort database II as well as an empirical study in an open-plan office at the end of August in Tongji University, Shanghai.

Chapter 6: *Energy co-simulation study of the task-ambient cooling control based on synthetic thermal preference distributions.* This chapter aims to conduct energy co-simulations to evaluate energy savings based on the optimization of the ambient conditioning system with constraints of thermal preference predictions with synthetic thermal preference distributions based on comfort database II in an open plan office room.

1.6 Related thesis publications

Academic journals

[J1] Lu, S., Wang, W., Lin, C., & Cochran Hameen, E. (2019). Data-driven simulation of a thermal comfort-based temperature set-point control with ASHRAE RP884. *Building and Environment*, *156*, 137-146.

[J2] Lu, S., Wang, W., Wang, S., & Cochran Hameen, E. (2019). Thermal Comfort-Based Personalized Models with Non-Intrusive Sensing Technique in Office Buildings. *Applied Sciences*, *9*(9), 1768.

International conferences

[C1] Lu, S., Wang, S., Cochran Hameen, E., Shi, J., & Zou, Y. Comfort-based integrative HVAC system with non-intrusive sensing in office buildings. Computer-aided Architectural design research in Asia, CAADRIA 2019, Wellington, New Zealand, April 2019.

[C2] Lu, S., Cochran Hameen, E., Zou, Y. An interactive building control for the integrative HVAC system featuring personalized cooling in office buildings. ASHRAE annual conference, Kansas City, Missouri, June 2019.

[C3] Lu, S., Cochran Hameen, E. Simulation Study of Individual Thermal Comfort with the Integrated Personalized Fan and VAV System. Building simulation, Rome, Italy, September 2019.

Chapter 2: Data-driven simulation of a thermal comfort-based temperature set-point control with ASHRAE RP884 database (comfort database I)

Table 2-1 Nomenclature

Abbreviation	Description
ASHRAE RP884	ASHRAE RP-884 Adaptive model project
ASHRAE 55	ASHRAE Thermal environmental conditions for human occupancy
ASH	ASHRAE thermal sensation scale
PMV	predicted mean vote
comfort database	Global thermal comfort database II
TAC	task ambient conditioning
SVM	support vecor machine
RF	random forest
KNN	k-nearest neighbor
GMM	gaussian mixture model
BIC	Bayesian information criteria
MDP	markov decision process
RL	reinforcement learning
DP	dynamic programming
MC	monte carlo
TD learning	temporal difference learning
Q-learning	off-policy TD learning
SARSA	on-policy TD learning

This chapter aims to propose a reinforcement-learning based temperature set-point controller based on statistical personalized thermal comfort models developed with the subset of RP884 database where data were selected from office buildings in three major climates. Moreover, it has provided the comprehensive understanding of adaptive thermal comfort in the real environment. This chapter has mainly two contributions. The first contribution is to implement various machine learning algorithms beyond common methods such as regressions, including k-nearest neighbor (KNN) (Altman, 1992), support vector machine (SVM) (Smola et al., 2004), random forest (RF) (Liaw & Wiener, 2002) to develop thermal comfort models over multiple climate zones and compare with PMV regarding the performances of predicting thermal comfort with 7-point ASHRAE sensation scale (ASH) (ASHRAE 55, 2013). The second contribution is to implement

and evaluate the model-free reinforcement learning-based temperature set-point controller with the statistical thermal comfort model in a simplified data-driven simulator.

With the sub-hypothesis 2 that adaptive thermal comfort model can improve the performances of occupant-responsive HVAC control in terms of thermal comfort, the methodology can be divided into two parts. The first part is to develop the data-driven thermal comfort model with ASHRAE RP884 database and the second part is to develop a tabular Q-learning based temperature set-point controller based on combination of thermal sensation predictions from the adaptive thermal comfort model and some domain knowledge from ASHRAE 55 (2013). Both parts were implemented in Python.

2.1 Development of the thermal comfort model with ASHRAE RP884 database

Figure 2-1 describes the development of thermal comfort models. The classification follows the standard machine learning pipeline, including data preprocessing, classification model selection, classification model training, and model testing. Besides classification, an unsupervised clustering was also implemented to identify the thermal sensation distribution under different indoor thermal conditions.

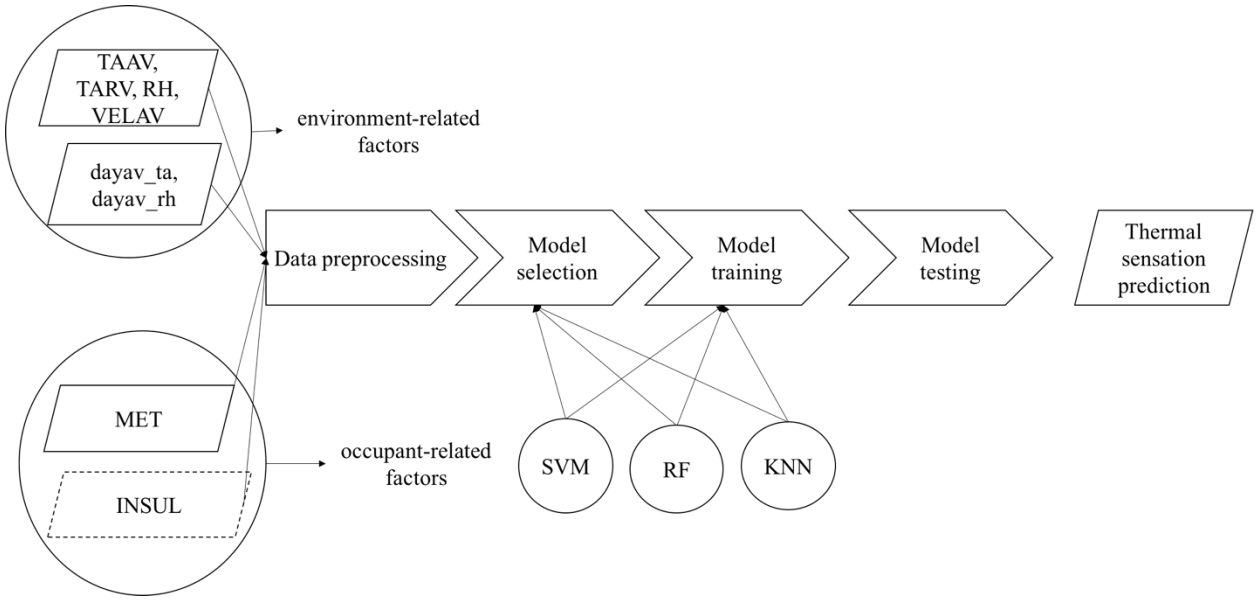

Figure 2-1 Thermal comfort model pipeline

2.1.1 Data description and preprocessing

The dataset used in the project is the subset of ASHRAE RP884 database, which was collected from various studies on thermal comfort and reformatted into the same structure across the world. The original dataset includes 22000 instances. However, the subset used in the paper was truncated

and well cleaned based on the major climates and air-conditioned office buildings during summer and winter, including Mediterranean, humid subtropical and west coast marine climates. Therefore, the total number of instances of the subset is 5530. Moreover, the original RP884 database collects over 80 attributes under different office environments. However, most of features have large amount of missing data and lack of consistency, including physical factors such as gender and age. Therefore, as shown in Table 2-2, features from sensor measurements plus clothing insulation are extracted from the original codebook and Figure 2-2 shows ASH scale used as prediction labels in the study. Moreover, the extracted features were ranked with feature selection algorithm based on tree-based feature selection to analyze the most important factor to thermal comfort.

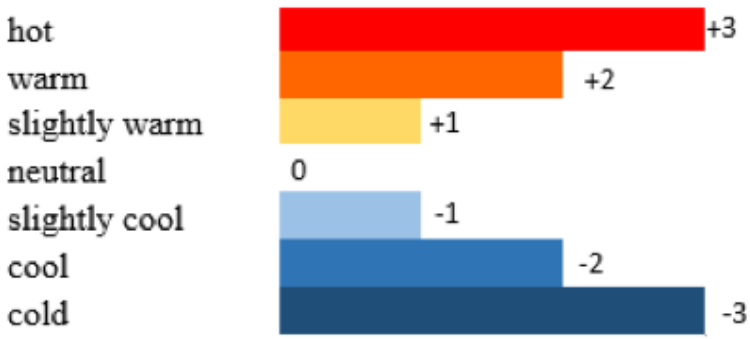

Figure 2-2 ASHRAE thermal sensation scale

Table 2-2 The extracted features from the original feature space

Feature name	Description
TAAV	Average of three heights' air temperature [^{o}C]
RH	Relative humidity [%]
Dayav_ta	Outdoor average of min/max air temp on day of survey [^{o}C]
Dayav_rh	outdoor average min/max relative humidity on day of survey [%]
MET	Average metabolic rate of subject [met]
INSUL	Clothing plus upholstery insulation [clo]
TRAV	Average of three heights' mean radiant temperature [^{o}C]

VELAV Average of three heights' air speed [m/s]

2.1.2 Clustering:

Before developing a temperature set-point controller such that the system could automatically adapt the comfortable environment for occupants, it is important to have an overview over the indoor thermal environment conditions (i.e. indoor air temperature, relative humidity) among different open-plan office buildings and how occupants' thermal sensations distribute across the world. In order to see how distinctive thermal conditions are in the dataset, similar thermal environments were grouped into a cluster. Unsupervised clustering is a learning method where the parameters are learned with unlabeled data. Among unsupervised clustering, the most two common yet efficient algorithms are K-means (Faber, 2004) and Gaussian mixture model (GMM) (Reynolds, 2015). K-means clusters the dataset with hard assignments that each cluster has a unique centroid point and each data point belongs to only one cluster. However, GMM clusters the dataset with soft assignments that each data point is assigned to a mixture of clusters where the mean and variance matrix of each cluster, the probability that a data point belongs to a cluster $p(\boldsymbol{x}|cluster = i)$ and the mixture proportion of a cluster $p(cluster = i)$ are generated. The clustering process follows the conditional probability as below:

$$\mathrm{p}(\boldsymbol{x}|\mathrm{cluster} = \mathrm{i}) \sim \mathrm{N}(\mu, \sigma) \quad (2\text{-}1)$$

$$\mathrm{p}(\boldsymbol{x}) = \sum_{\mathrm{i}} \mathrm{p}(\mathrm{x}|\mathrm{cluster} = \mathrm{i})\mathrm{p}(\mathrm{cluster} = \mathrm{i}) \quad (2\text{-}2)$$

where $\boldsymbol{x}(x_1, x_{2\ldots,} x_n)$ is an instance in the feature space consisting of all environment-related features and the dataset can be estimated with *k* clusters. As shown above, since each cluster follows normal distribution, the probability density of the whole dataset $p(\boldsymbol{x})$ can be estimated with the sum of weighted clusters.

Moreover, during testing, the new data point is assigned to a cluster with the highest probability that the data point belongs to. Since GMM is a better clustering method to approximate a general distribution and clusters may overlap with each other, instead of K-means clustering, GMM was implemented that each cluster is assigned with a mean and a co-variance matrix in this study.

In addition, since GMM algorithm clusters the data as appropriately as possible by conducting maximum likelihood estimation to get parameters of each cluster, the optimal number of cluster has to be determined further. Bayesian information criterion (BIC) (Schwarz, 1978) is also a model

selection method to find out suitable parameters. In this study, the best number of cluster was selected with Bayesian information criterion (BIC) where the optimal k could get the lowest BIC score, which aims to find the true model with high probability and it is assumed one of the models is the true model. In this study, when selecting the number of cluster, the one with the lowest BIC is preferred. Suppose we formulate a collection of candidate models, $M_1, M_2 \dots M_n$. The mathematical formula of BIC for each candidate model is shown as below:

$$\text{BIC} = -2lnL\left(\hat{\theta}|x_1, x_2 \dots x_n\right) + kln(n) \quad (2\text{-}3)$$

where L is likelihood function, $\hat{\theta}$ is the number of cluster, x is the data, k is the dimension of the feature space and n is the number of data.

2.1.3 Classification algorithms:

After clustering, several classification algorithms have been implemented to train and evaluate the prediction performances of thermal comfort models with the best parameters by model selection. Cross-validation is one of the common methods of model selection, which aims to find the model that gives the best prediction. It can be used for both parametric models and non-parametric models. In general, the data are split into a training set and a test set. The models fit on the training set and are used to predict the test set. Usually, many such splits are used and the result are averaged over splits. In other words, n-fold cross-validation means that the original dataset is split into n folds where one-fold is used as test set and the rest is used as training set. Then, the n models are developed with different training sets and the final classification result is the average of results of all n models on the test sets. Based on the specific dataset, 5-fold cross-validation was implemented in this study for tuning parameters of each classifier to select the best model.

Besides, since the feature space is high-dimensional, K-nearest neighbor (KNN), support vector machine (SVM) and random forest (RF) were implemented to train the classifiers as supervised learning methods. In addition, 90% of normalized dataset was separated into training set and the rest of the data was for development set and test set. Moreover, even if neutral sensation doesn't necessary mean thermal comfort, it is a precondition of comfort (Auliciems & Szokolay, 1997). Therefore, in this study, we conformed to the conclusion occupant feels thermally comfortable when they feel the thermal environment is neutral. In other words, occupant is considered to be comfortable if the voted sensation is 0.

2.1.3.1 K-nearest neighbor

KNN is one of the simplest machine learning algorithms. It follows voting scheme and is a non-parametric method for classification and regression where k is a tuning parameter, indicating the number of training data used for predicting the label. With smaller k, the bias will be lower while the variance will be higher. On the contrary, with larger k, the bias will be higher while the variance will be lower. The pseudocode of KNN is shown below:

Inputs: X_{train}: training data with all features; Y_{train}: thermal sensation labels of X_{train}; X_{test}: testing data with all features

for $x_i \in X_{train}$ do

Compute the distance $d(X_{test}, X_{train})$

End for

Construct set I containing indices of Y_{train} where the corresponding X_{train} has k smallest distances $d(X_{test}, X_{train})$ among all training data.

Return the majority label of Y_i $where\ i \in I$

2.1.3.2 Support vector machine

Besides KNN, SVM can be used to develop supervised classification models with high-dimensional and non-linear data. Similar to GMM, since the data is unlikely to be separated linearly, with SVM classification, soft margin usually performs better than hard margin. Moreover, compared to quadratic programming to solve the optimization problem, kernelized SVM can be computed much more efficiently. The optimization function with soft margin is shown in the following equation, which can be further kernelized (Guo & Niedermeier, 2007).

Inputs: S=$\{(x_1, y_1), (x_2, y_2)\ldots,(x_n, y_n)\}$, where $x_i \in X_{train}$ and $y_i \in Y_{train}$

$$\text{Obj. } \operatorname{argmin}_{w,\xi_1,\xi_2\ldots\xi_n} ||w||^2 + C\sum_i \xi_i \quad (2\text{-}4)$$

$$\text{s.t. } y_i w * x_i \geq 1 - \xi_i \quad (2\text{-}5)$$

$$\xi_i \geq 0 \quad (2\text{-}6)$$

where $\boldsymbol{w}$ is a weight vector, C is a penalty parameter controlling how much you want to avoid misclassifying each training example and ξ_i is a slack variable indicating if the sample is misclassified. With larger C, the optimization will select smaller margin of the hyper plane while with smaller C, the optimization will select larger margin of the hyperplane.

Moreover, the above constrained optimization problem can be converted into minimization of the unconstrained optimization problem with hinge-based loss function, as shown below:

$$\operatorname{argmin}_w ||\boldsymbol{w}||^2 + C\sum_i \max(0, 1 - yf(x_i)) \quad (2\text{-}7)$$

where $max\ (0, 1 - yf(x_i))$ is the loss function.

Even if the above optimization problem with many features can be solved with quadratic programming, the computational cost is higher. Therefore, the optimization problem can be further kernelized by replacing the term $(1 - yf(x_i))$ in the loss function with various kernel functions with the form of $K(q, q_i)$ where q and q_i are the combination of y and x. In this study, linear kernel, polynomial kernel and Gaussian kernel were implemented to select the best model.

2.1.3.3 Random forest

Unlike KNN and SVM, random forest is an ensemble learning method that averaging the accuracy of a number of decision trees constructed with bootstrapping sampling at training time. However, random forest adds additional randomness to the model that it looks for the most important feature among a random subset of features and random subset of the whole dataset instead of all features and the whole dataset while splitting the node. Compared to building deep decision trees with high-dimensional feature space, owing to randomness, RF builds several smaller trees, thus suffering less from overfitting. As a result, it generally can develop better model than decision trees.

Moreover, since RF has the ability to measure the relative importance of each feature according to information gain, it can also be used for feature selection. Equation 2-8 shows the information gain formula. Since the larger the information gain is, the more important the feature will be, the feature with highest conditional entropy has the highest importance. Therefore, as mentioned before, RF was not only implemented for developing statistical thermal comfort models but also was used for feature importance ranking in preprocessing. During model selection, the hyper-parameters of the number of trees and the tree depth are selected with cross-validation.

$$\mathrm{I}(\mathrm{Y}, X_i) = H(Y) - H(Y|X_i) \quad (2\text{-}8)$$

where

$\mathrm{I}(\mathrm{Y}, X_i)$ is information gain of Y given the feature X_i;

H(Y) is entropy of a random variable Y;

$H(Y|X_i)$ is entropy of a random variable given the feature X_i.

2.1.3.4 Model evaluation metrics

Confusion matrix is used to describe the performance of a classification model. The confusion matrix of binary classification is shown in Table 2-3:

Table 2-3 Confusion matrix

	Predicted: Negative	**Predicted: Positive**
Actual: Negative	True negative	False positive
Actual: Positive	False negative	True positive

Each cell in the table is the number of the testing samples with the correspondent prediction and the actual results. Besides confusion matrix, recall is used to give a comprehensive evaluation over the statistical thermal comfort models. Based on the table, the calculation formula is shown in Equation (8). Recall measures the ability of a model to find all correctly classified instances within a dataset.

$$\text{Recall} = \frac{\text{True positive}}{\text{True positive} + \text{False negative}} \quad (2\text{-}9)$$

2.2 Thermal comfort-based temperature set-point controller

The goal is to develop a controller which learns to take the right action so that the thermal sensation state can reach the optimal state. Therefore, a tabular Q-learning based algorithm were implemented to get the optimal policy by maximizing the accumulative sum of state values. Figure 2-3 shows the whole framework of the intelligent control system with the statistical thermal comfort model. As shown in the figure, the temperature set-point is determined by Q-learning controller with the input of thermal comfort prediction and sensor data in the simulated environment. Moreover, in the real application, the new sensor data could be further stored to update the thermal comfort model after a certain period of time.

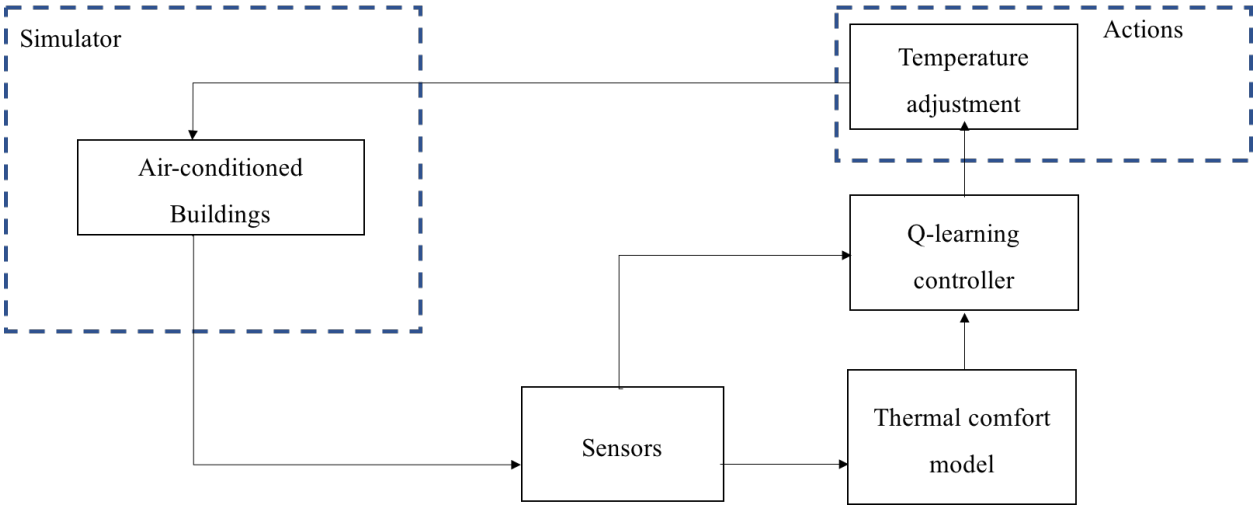

Figure 2-3 The framework of the reinforcement learning-based temperature set-point controller

2.2.1 Q-learning algorithm:

Reinforcement learning (RL) is a markov decision process (MDP) consisting of states, actions, reward function, state transition probability matrix and a discount factor and RL control aims to find the optimal policy consisting of an action sequence to gain the maximum value, which is the expected value of the cumulative future rewards from a start state to the terminal state (Sutton & Barto, 2018). The general diagram of reinforcement learning is shown below. As shown in Figure 2-4, the state and the reward will change at every step after selecting an action. In this study, the agent is trained with episodic environment, which means the agent is trained with multiple episodes with random start state so that it can explore completely.

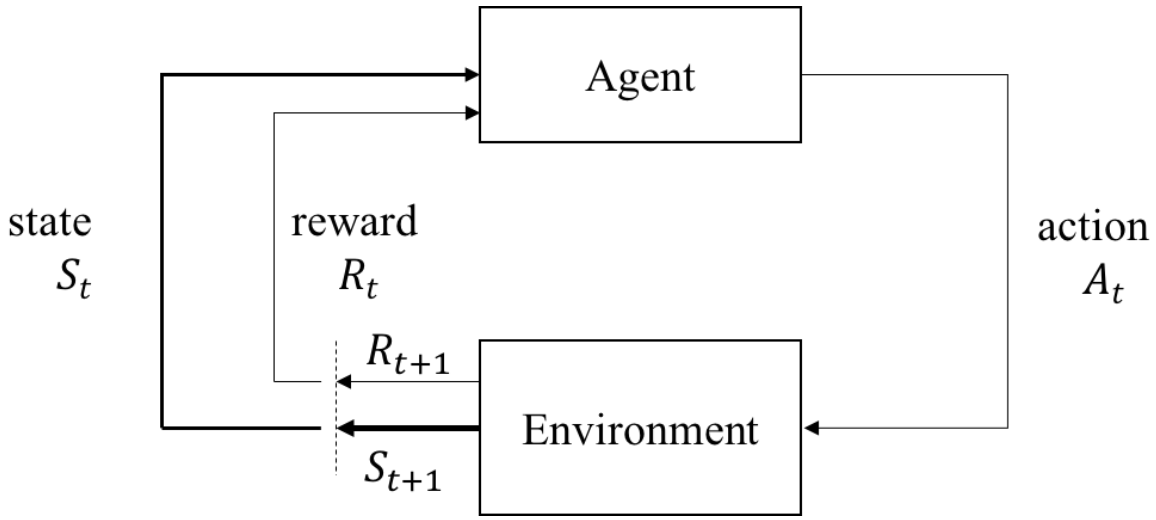

Figure 2-4 The general diagram of reinforcement learning

In order to ensure the value will converge and maximized ultimately, the value function under policy π is defined as:

$$v_\pi(s) = E_\pi[G_t|S_t = s] = E_\pi[\sum_{k=0}^{\infty} \gamma^k R_{t+k+1}|S_t = s] \quad (2\text{-}10)$$

where γ is discount factor, G is actual return, R is reward and S is state.

Alternatively, maximizing state-action value Q, which is the value of taking action a in state s under policy π can also find out the optimal policy. Therefore, the mathematical formula of state-action value function is defined as:

$$q_\pi(s,a) = E_\pi[G_t|S_t = s, A_t = a\,] = E_\pi[\sum_{k=0}^{\infty} \gamma^k R_{t+k+1}|S_t = s,\ A_t = a\,] \quad (2\text{-}11)$$

where γ is discount factor, G is actual return, R is reward, S is state and A is action.

Moreover, there are three major categories of reinforcement learning, which are dynamic programming (DP), Monte-Carlo (MC) and temporal-difference (TD) learning (Sutton & Barton, 2018). Among these three categories, TD learning is the combination of DP and MC to update the value or state-action at time t. The simplest TD method is defined as:

$$\mathrm{V}(S_t) \coloneqq \mathrm{V}(S_t) + \alpha[R_{t+1} + \gamma V(S_{t+1}) - V(S_t)] \quad (2\text{-}12)$$

where α is the learning rate, $R_{t+1} + \gamma V(S_{t+1})$ is called TD target and $R_{t+1} + \gamma V(S_{t+1}) - V(S_t)$ is called TD error.

Meanwhile, TD learning can be further categorized into on-policy TD learning called SARSA and off-policy called Q-learning. On-policy means the value update is dependent on the current policy followed in the training. On the other hand, off-policy is the term meaning that the value update is independent with the policy being followed. It can guarantee to learn the optimal policy regardless of the current situations. Compared to SARSA, Q-learning can get optimal policy while SARSA can only get near-optimal policy, particularly in the simulated environment with low cost and fast iterations. Therefore, in order to develop the comfort-based controller based on thermal comfort model, Q-learning is selected to be the controller algorithm. The pseudocode of Q-learning controller is shown below:

Initialize $Q(s,a)$ arbitrarily and *Q (terminate-state, *)* = 0 in the Q-table

Repeat (for each episode):

Initialize start state *S*

Repeat (for each step of episode):

Choose action *A* from *S* using policy derived from *Q* (i.e. e-greedy)

Take action *A*, observe *R, S′*

$Q\ (S,A) := Q(S,A) + \alpha[R + \gamma max_a Q(S',a) - Q(S,A)]$

$S := S'$

Until S is terminal

During evaluation process, the optimal policy consisting of a series of actions is determined with the trained Q-table by selecting the action with highest Q-value under a specific state.

2.2.2 Data-driven simulation setup:

In order to evaluate the reinforcement learning-based controller before deployment, the data-driven simulator is developed based on the statistical thermal comfort model built with RP884 dataset in the paper. Since the radiant temperature data is similar to the indoor air temperature data according to the dataset, the radiant temperature is approximated with indoor air temperature. Therefore, the state space is designed to be a tabular state space and each state consists of clothing insulation, indoor air temperature and relative humidity, which are top features to predict thermal sensations with the trained classifier. Meanwhile, the indoor air temperature is assumed to be within the range between 15 ^{o}C and 31 ^{o}C. Moreover, since the controller is only focused on temperature set-point, the action space consists of increasing 1 ^{o}C, no change and decreasing 1 ^{o}C.

Among different components in reinforcement learning, reward function is the most important one since it determines what policy the agent can get the most incentives or the hardest penalties. In this study, since the statistical thermal comfort model may predict incorrectly when the actual thermal sensations are not neutral, the reward function is designed with the combination of the predicted thermal sensation as well as some rules. The rules are designed with domain knowledge based on thermal comfort zone graph defined in ASHRAE 55 (2013) where for clothing insulation being 0.5 clo, the comfortable air temperature range is between 24 ^{o}C and 26 ^{o}C while for that being 1 clo, the comfortable air temperature range is between 23 ^{o}C and 25 ^{o}C. The reward function is shown below:

- With clothing insulation being 0.5 clo:

$$\mathrm{r(s,a)} = \begin{cases} -|pred| - 1000 & if\ temp < 16 \\ -|pred| - 1 * (24 - temp) & if\ temp \in [16,23] \\ -|pred| + 10 & if\ temp \in [24,26] \\ -|pred| - 1 * (temp - 26) & if\ temp \in [27,31] \\ -|pred| - 1000 & if\ temp > 31 \end{cases} \quad (2\text{-}13)$$

- With clothing insulation being 1 clo:

$$r(s,a) = \begin{cases} -|pred| - 1000 & if\ temp < 16 \\ -|pred| - 1 * (23 - temp) & if\ temp \in [16,22] \\ -|pred| + 10 & if\ temp \in [23,25] \\ -|pred| - 1 * (temp - 25) & if\ temp \in [26,31] \\ -|pred| - 1000 & if\ temp > 31 \end{cases} \quad (2\text{-}14)$$

where

r(s, a) is the state-action reward.

pred is the prediction result of thermal comfort models.

temp is the indoor air temperature

Since the controller is only for temperature set-point, relative humidity is assumed to be always in a comfort range (i.e. 40-60%), thus not being included in the reward function. Moreover, since the indoor air temperature changes behind the temperature set-point due to thermal mass, it is assumed that the temperature set-point will not change until the indoor air temperature reaches the set-point for each step.

2.3 Result analysis of RP884 database

2.3.1 Clustering:

Table 3 shows the ranking score of all features with feature selection. As shown in the table, the top four features are indoor radiant temperature, indoor air temperature, relative humidity and clothing insulation.

Table 3 Ranking score of all features

INSUL	**TRAV**	**TAAV**	**RH**	**VELAV**	**Dayav_ta**	**MET**	**Dayav_rh**
17%	15.30%	14.70%	13.80%	13.60%	9.40%	9.20%	7.10%

Moreover, Figure 2-5 (a)-(c) show the thermal sensation vote distribution classified into less than zero, zero and larger than zero with those top features of indoor air temperature, indoor relative humidity and clothing insulation collected in the subset. The results have shown among 1496 human subjects, the non-neutral sensation votes cannot be ignored since the number of neutral sensation vote is 2782 while that of non-neutral sensation vote is 2848.

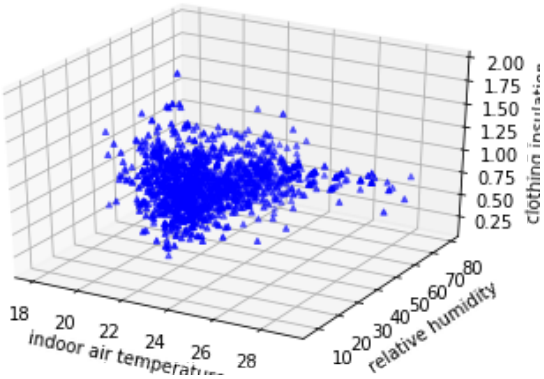

(a) sensation < 0

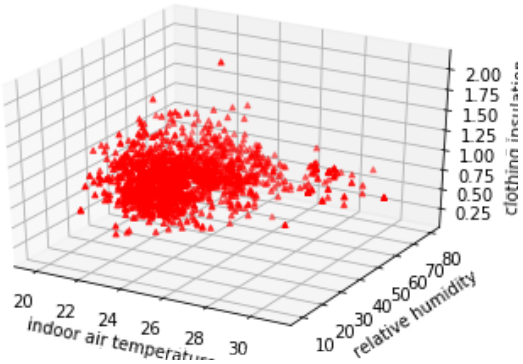

(b) sensation > 0

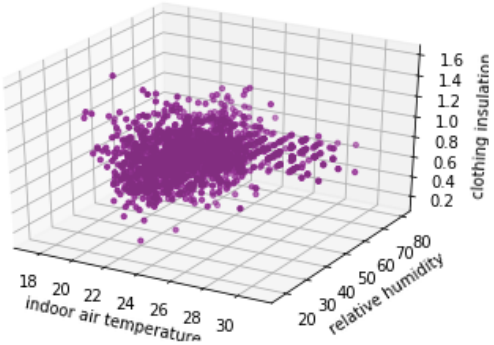

(c) Sensation = 0

Figure 2-5 Thermal sensation distribution in subset of RP884 database

Meanwhile, seven clusters were selected based on BIC score with GMM clustering, as shown in Figure 2-6. In addition, Figure 2-7 showing the thermal sensation distribution within each cluster illustrate each cluster has similar thermal sensation distribution where most of participants have thermal sensation votes as neutral. To summarize, the subset of ASHRAE RP884 database collected much fewer instances of uncomfortable conditions than those of comfortable states in regular office environments.

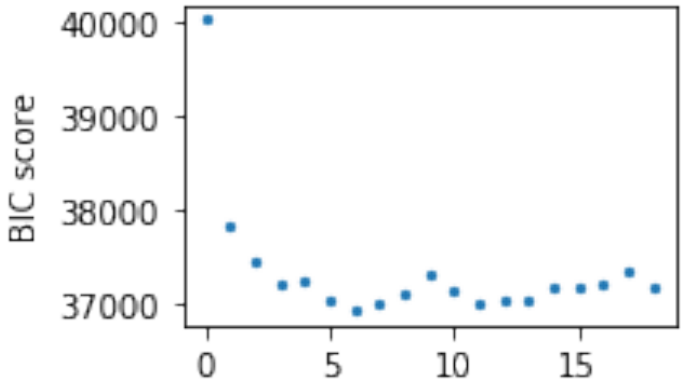

Figure 2-6 BIC score over different number of clusters

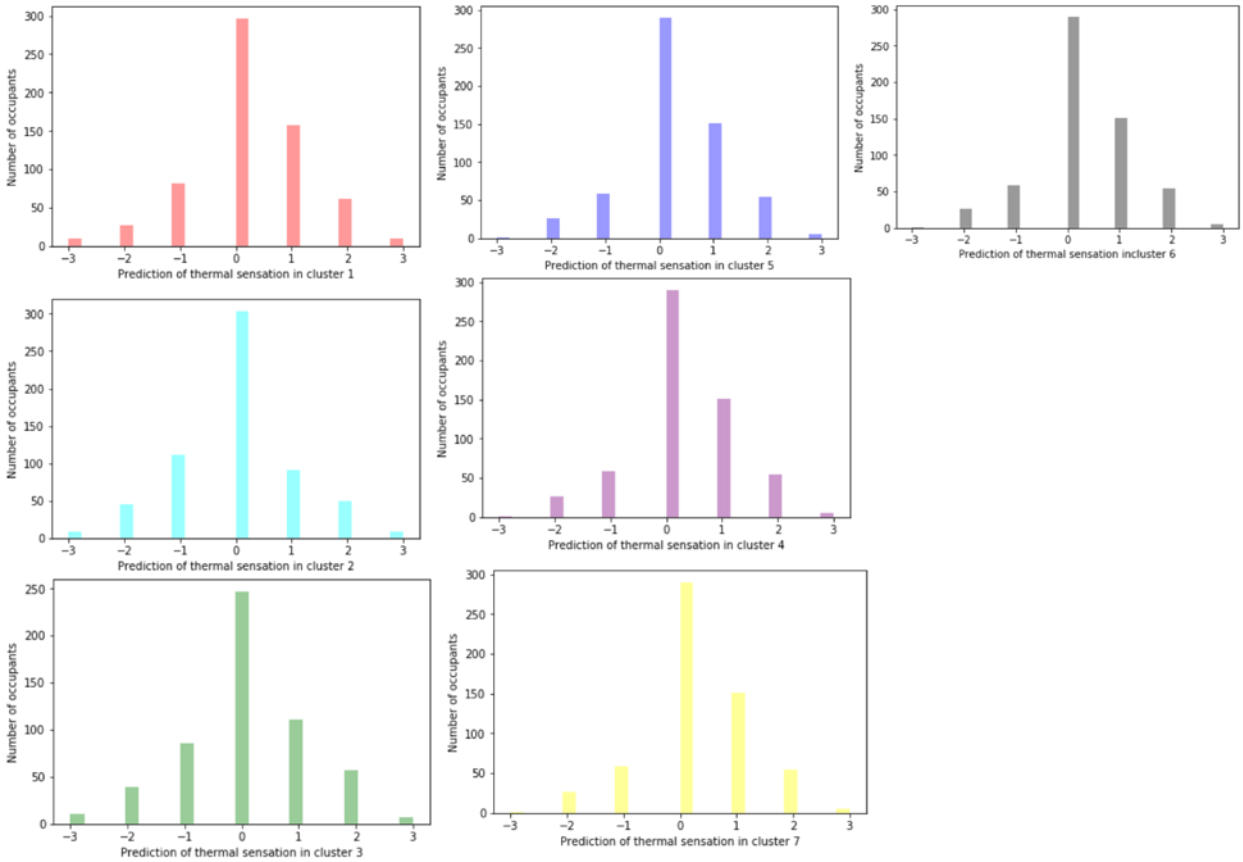

Figure 2-7 Thermal sensation distribution of the seven clusters

2.3.2 Classification:

With model selection, the k was selected as 100 in KNN, C was selected as 1 in SVM with Gaussian kernel and a total of 50 trees were ensemble in RF with tree depth of 3.

Table 2-4 shows the evaluation results with the proposed classifiers and performance benchmark with PMV. As shown in the table, there is little distinction among all classifiers, which indicates the selected classifiers have almost same performances with the imbalanced RP884 dataset. Moreover, the proposed classifiers outperform PMV in terms of recall score. This indicates that the model has predicted around 50% of testing data with correct labels. However, it is also necessary to see how the prediction results distribute among all labels.

Table 2-4 Evaluation performances of the proposed classifiers and PMV

Classifier	Recall
KNN	**49.30%**

SVM	48.70%
Random forest	48.70%
PMV	43%

Figure 2-8 (a)-(b) show the confusion matrices of all three classifiers and PMV. As mentioned before, due to the imbalance of the data that the number of instances with label of neutral sensation is much higher than those with other labels, the classifiers tend to predict all different sensations to neutral sensation. As a result, confusion matrices of the three classifiers are almost same as each other. However, unlike the proposed classifiers, even if PMV has much lower accuracy in predicting neutral sensation, the prediction accuracies of other sensations increase. This makes sense since all classifiers are built with data-dependent machine learning algorithms, the predictions are also affected by how the training data looks like. Therefore, all of the proposed classifiers aiming to minimize the number of misclassified instances will be biased to the neutral sensation with testing data. As a result, the statistical thermal comfort models need to be coupled with domain knowledge in the temperature set-point controller.

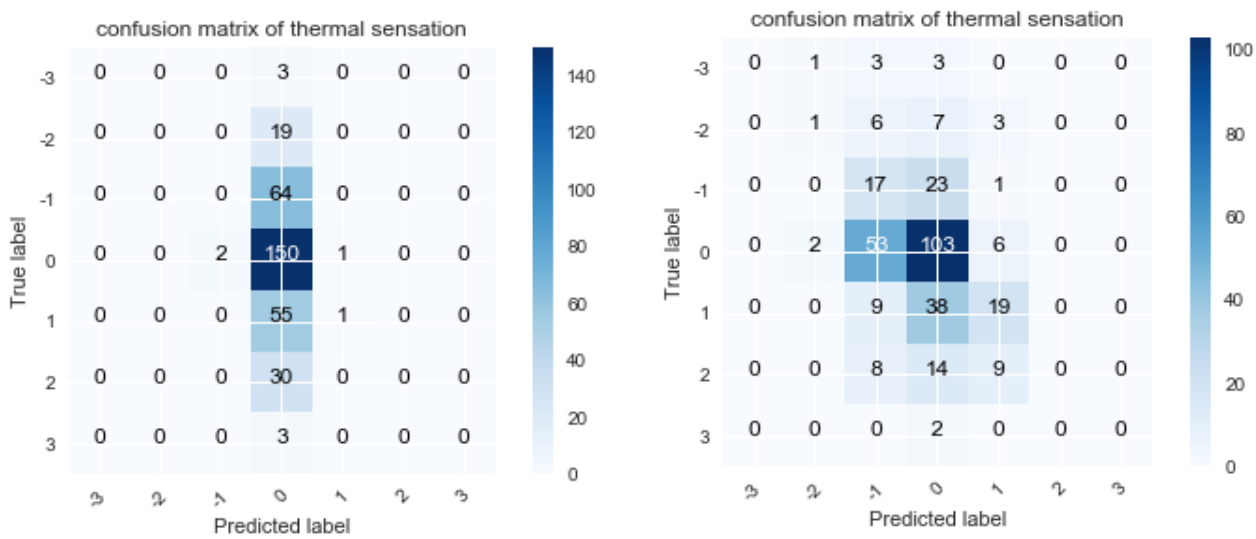

(a) (b)

Figure 2-8 Confusion matrix of sensation prediction with (a) proposed classifier (b) PMV

2.3.3 Reinforcement learning based temperature set-point control:

As mentioned in the methodology, the state consists of indoor air temperature, indoor relative humidity, clothing insulation. During training, the agent learns to reach the comfortable temperature set-point by choosing the action with e-greedy algorithm. During testing, the agent chooses the optimal action based on the trained Q-table. Figure 2-9(a)-(b) show the optimal

temperature set-point policy during evaluation with the start states of (15 °C, 60%, 0.5 clo) and (31 °C, 60%, 1 clo) after training 1000 episodes, respectively. As shown in Figure 9(a), the temperature set-point increase 1 °C at every step according to the Q-table until it reaches 24 °C where the temperature set-point no longer needs changing. Moreover, Figure 9(b) shows the temperature set-point decreases 1 °C at every step until it reaches 25 °C since it reaches the optimal state. Instead of using a set of knowledge-based rules to control the set-point, the agent is able to learn the optimal policy after training with the appropriate reward function.

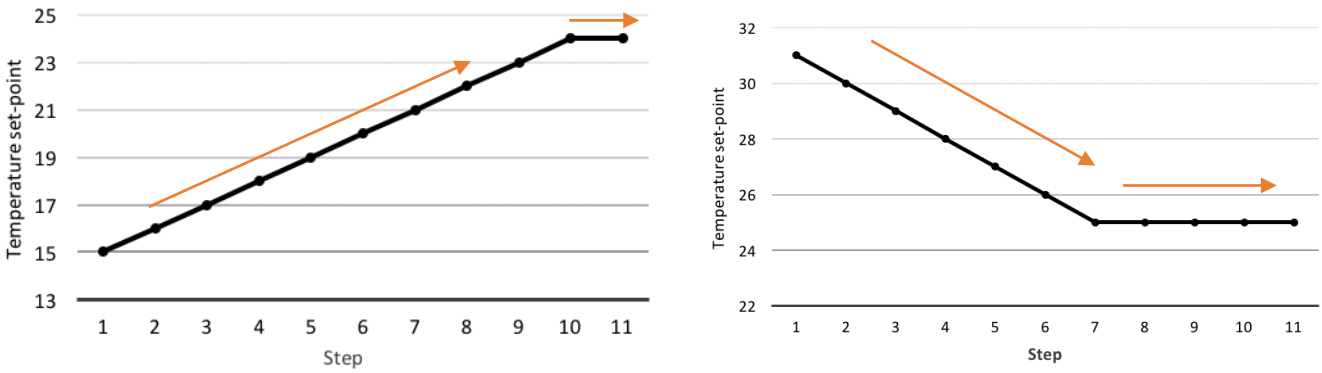

Figure 2-9 Optimal policy starting at (a) 15 °C (b) 31°C

Last but not least, the performances of 6 different starting states were evaluated. Table 2-5 shows the starting state conditions and the temperature set-point of the end-state by Q-learning based controllers trained with 10, 50, 100 episodes, respectively. As shown in the table, if the controller is trained with 10 or 50 episodes, for start state with indoor air temperature of 15 °C and 30 °C, the generated Q-table is not guaranteed to provide the optimal policy reaching the comfortable state. This is because if the agent is not trained with enough episodes, some of the states cannot be explored, thus Q-table is not fully developed.

Table 2-5 Terminal states with trained Q-table based on different number of episodes

indoor air temperature of start state[C]	indoor relative humidity [%]	clothing insulation [clo]	indoor air temperature of end state[°C]		
			10 episodes	100 episodes	1000 episodes
18	60	0.5	18	15	24
18	60	1	18	15	23
30	60	0.5	30	31	26
30	60	1	30	31	25
24	60	0.5	24	24	24

24	60	1	24	24	24

2.4 Discussions of adaptive thermal comfort models with RP884 database

This paper has implemented a reinforcement learning-based controller with statistical thermal comfort models with the subset of RP884 dataset. As reinforcement learning has drawn much more attention than before, particularly in robotic control, it has potential to be used for thermal comfort-based HVAC control as well. With the implementation of reinforcement learning controller, the results have shown that the thermal comfort-based controller can control the set-point to the optimal state with any start state after a certain number of episodes for training. Even if the current learnt policy in Q-learning is as simple as rule-based control policy, it has advantages of rule-based control when the state space is more complex than the current tabular state space such as continuous or infinite state space. Moreover, compared to rule-based control, reinforcement learning-based control is able to learn more complex logics.

In addition, a general thermal comfort model with the subset of RP884 database was developed for reward function design of the controller. As a result, due to imbalanced dataset where the majority vote is neutral sensation, the highest recall of 49.3% was achieved by training KNN classifier. Compared to the state-of-art thermal comfort model such as PMV, the statistical thermal comfort models outperform by 6% on average. However, the prediction performance is still limited. Resampling methods like over-sampling and under-sampling were both implemented. However, the results have shown that over-sampling and under-sampling decreased the recalls. Since for most of time in the real environment, occupants feel comfortable while only a few times occupants may have some complaints, it is better to have relatively higher recall and update the thermal comfort models by collecting interactions (i.e. occupants overriding the system) between the system and the users to update the thermal comfort model offline in real deployment. In addition, 6-point thermal comfort scale was also used for developing thermal comfort models. However, due to missing data, the recall scores with the proposed algorithms were much lower than those with 7-point thermal sensation scale. Even if thermal sensation is just the pre-condition of thermal comfort, since it is better predicted by measurable and objective variables, thermal sensation prediction is more suitable for the proposed controller with RP884 dataset, especially considering the real deployment. Moreover, as mentioned before, since the number of instances for occupants with very different thermal preferences from the majority is too few to build the thermal comfort

models, the performances could benefit from a newly released dataset called ASHRAE global thermal comfort database II (Comfort Database) [30]. It includes approximately 81846 complete sets of objective indoor climatic observations in the field setting collected since 2004. Based on some preliminary analysis of thermal satisfaction, occupants are more sensitive towards the indoor thermal conditions than those in the 1990s, which brings about more variant data. Therefore, it is expected that thermal comfort models using the new dataset will outperform those using RP884.

The proposed thermal comfort-based controller could be further deployed into the real building. In order to implement the system into the real office building, it is important to design a feedback strategy which will not be too interruptive to the occupants. Moreover, during deployment, the statistical thermal comfort model needs to be calibrated with new users' feedback so that the controller is able to take the optimal action after training in a more accurate simulator. In addition, besides implementing multiple personalized controller within the context of conventional centralized HVAC system, task-ambient conditioning system (TAC) [31] could also make the use of such personalized controllers. Last but not least, current controller only takes occupant thermal comfort into consideration. However, optimizing energy performance while maintaining thermal comfort could be realized by using different reward functions in reinforcement learning-based controller.

2.5 Conclusions:

In this study, a data-driven simulation of comfort-based temperature set-point control system with tabular Q-learning has been conducted. The proposed controller uses the subset of ASHRAE RP884 database to develop a thermal comfort model and some domain knowledge to design a reward function. In addition, the thermal comfort model is a classification model with machine learning methods of KNN, SVM and RF to predict thermal sensation and indicate thermal comfort. Compared to baseline of PMV, the recall of the thermal comfort model with the three algorithms has increased 6.3%, 5.4% and 5.4%, respectively. Moreover, most of correct predictions are those instances labelled as neutral due to imbalanced dataset.

Besides the statistical thermal comfort models, the reinforcement learning-based controller with tabular Q-learning control can reach the optimal comfort state after training with 100 episodes and generate the optimal policy from whatever start state in terms of indoor thermal environment. However, there are some limitations and simplifications in the controller design and more work could be done to improve the performances of thermal comfort models. In addition, more work

could also be done to implement reinforcement learning control with the integrated reward function of the statistical thermal comfort model and energy savings as well as the joint control of temperature and humidity set-points.

This study contributes to adaptive thermal comfort field by developing statistical thermal comfort models with various machine learning algorithms as well as implementing and evaluating a model-free reinforcement learning-based temperature set-point controller with the statistical thermal comfort model in a simplified data-driven simulator. However, since the database has a limitation that few instances were collected from each individual subject, the performances of thermal sensation prediction were limited for personal thermal comfort. Therefore, with more data from empirical studies shall be collected and the proposed personal comfort control system could be deployed into the real building systems.

Chapter 3: Comfort-based non-intrusive personalized models in office buildings

Table 3-1 Nomenclature

Abbreviation	Description
ASHRAE RP884	ASHRAE RP-884 Adaptive model project
ASHRAE 55	ASHRAE Thermal environmental conditions for human occupancy
ASH	ASHRAE thermal sensation scale
PMV	predicted mean vote
TAC	task ambient conditioning
SVM	support vecor machine
RF	random forest
DHT22	temperature/humidity sensor
AMG8833	infrared temperautre sensor
IR	infrared thermography
ESP8266	micro-controller with 2.4GHz WIFI module

With a comprehensive understanding of adaptive thermal comfort with ASHRAE RP884 database (comfort database I), it can be concluded that in real office environment, most occupants feel comfortable while only a few feels uncomfortable. Moreover, RP884 database only collected few instances for each subject. Therefore, it is of importance to study a more fine-grained personal thermal comfort management in the real office environment. In order to do so, occupant-related sensing techniques have to be developed so that thermal models can be developed in the real environment and occupants will not feel interruptive and intrusive during the work. Compared to sensing approaches like wearable devices, contactless vision-based occupancy sensors such as IR camera are much less intrusive and have drawn much more attention than before. However, most of recent studies using IR camera for thermal comfort use regression analysis with only skin temperature, which may not have high accuracy when predicting occupant thermal comfort. Therefore, this chapter aims to develop adaptive thermal models with three different feature sets trained with RF and SVM. In order to collect occupant data, an experimental study was conducted in an open-plan office in Shanghai with the non-intrusive sensing system consisting of indoor air

temperature and relative humidity sensor DHT22 and an IR camera. The study contributes to the field of the personalized thermal comfort by proposing new feature sets and prediction algorithms to develop adaptive thermal models, which could further be integrated into personalized system control as well as TAC system in open-plan offices. The model development part was implemented in Python while the data collection part was implemented in C++ with ESP8266 microcontroller.

3.1 Experimental Setup

Since part of this dissertation research aims to develop individual thermal models which capture the fine-grained differences between different people, instead of developing a generic thermal model, it makes more sense to develop individual thermal models. Moreover, for machine learning algorithms, the performance will increase with more amount of data. However, even if the common dataset like RP884 collected data from large group of participants, only less than 10 instances were collected for each individual. Therefore, unlike RP884, in this study, thermal models were developed based on a six-day experimental study to collect certain amount of data with two healthy subjects in their mid-twenties (one male and one female) between 3/11/2018 and 3/16/2018 in an office building in Tongji University, Shanghai.

Based on the design of non-intrusive sensing system and the literature review of principle factors to thermal comfort, the measured variables are shown in the following Table 3-1. The interval of data collection is 5 minutes, which corresponds with the survey responses. The experiment used the IR camera to measure the side face temperature and clothing surface temperature by manually selecting the face area and clothing area in the high-resolution thermal images, and then calculating the average surface temperature of those areas, respectively. Figure 3-1(a)-(b) show the participants' status in the experimental study and the correspondent thermographic photos, respectively. Before each session, the participants' clothes were reported and heart rates were measured by a free mobile app called Instant Heart Rate so as to ensure the participants have similar thermal status in the beginning. Lastly, clothing insulation was manually estimated based on ASHRAE 55 and was used for calculating PMV values. In order to get the accurate skin temperature, the emissivity was set to be 0.98.

(a) The RGB image of the two subjects

(b) The IR image of the two subjects

Figure 3-1 The experimental status of the two subjects

Table 3-1 Measured variables and sensor tools

Variable	Sensor tool	Resolution	Operating Range
Skin temperature [℃]	FLIR B8400	320x240 pixels	-20℃~120℃
Clothing surface temperature [℃]	FLIR B8400	320x240 pixels	-20℃~120℃
Indoor air temperature [℃]	DHT22	0.1℃	-40℃-80℃
Indoor relative humidity [%]	DHT22	0.1℃	-40℃-80℃
Clothing insulation [clo]	Manually identify the insulation with ASHRAE 55		

As mentioned before, even if neutral sensation doesn't necessarily mean thermal comfort, it is a precondition of comfort. Therefore, the statement that occupant feels thermally comfortable when they feel the thermal environment is neutral was in this study, and 7-point thermal sensation scale as classification labels was used, as shown in Table 3-2.

Table 3-2 ASHRAE Thermal-sensation scale

Thermal sensation vote (TSV)	Meaning
-3	very cold
-2	cold
-1	cool
0	neutral

1	warm
2	hot
3	very hot

In order to create different thermal environment conditions, an overhead air conditioner and four convective heaters were controlled in transient conditions where the air temperature increases no more than 0.2℃/min on average, as shown Figure 3-2. Moreover, Figure 3-3 shows the floorplan of the testbed where two subjects were seated in two separate desks and the camera has two locations to take photos of each subject, respectively. In addition, there were a total of 14 different sessions and each session last for at least 2 hours. Table 3-3 shows the temperature changes during each session. Since the participants attended the study for all sessions, all levels of thermal sensations were reported at least once by participants even if the majority votes belonged to neutral sensation.

(a) (b) (c)

Figure 3-2 Experimental Setup. (a) Heaters (b) FLIR B400 IR camera (c) Air-conditioning terminal

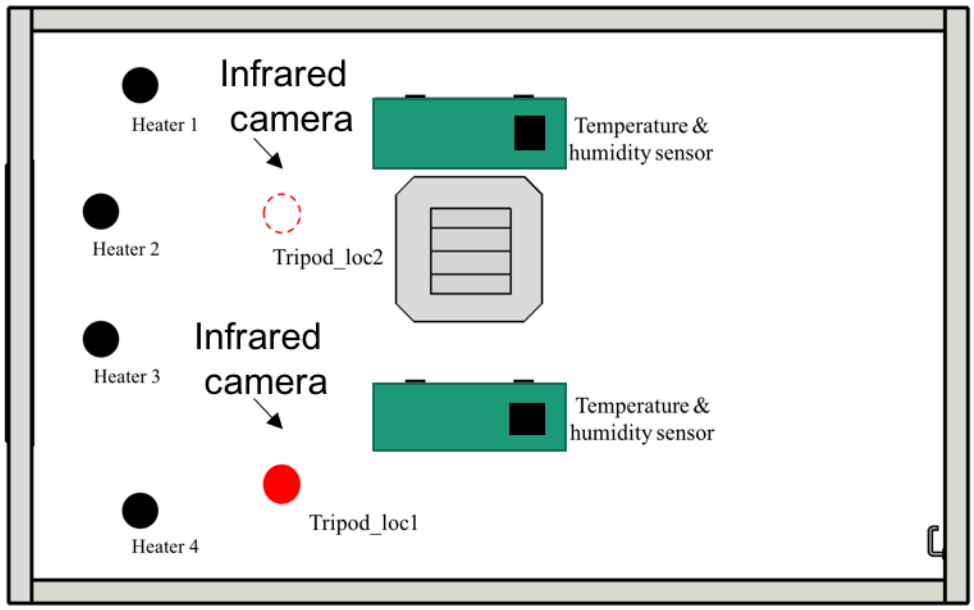

Figure 3 Floorplan of the test bed

Table 3-3 Temperature changes during each session

Date	Start time	Transition time	End time	Start temperature (℃)	Transitional Temperature (℃)	End temperature (℃)
3/11	9:50	11:00	11:50	17.4	29.3	22.3
	13:45	15:20	16:45	22.6	29	24.3
	19:30	21:45	22:30	19.3	28.5	20.9
3/12	10:10	11:10	11:30	17.7	29.5	25.3
	13:40	14:55	15:30	21.2	28.4	24.4
3/13	9:35	11:20	12:00	19	28.9	24.1
	13:40		17:30	29.9		18.5
	19:40	21:05	22:35	21.2	28.5	24.3
3/14	9:30	10:50	11:35	20.8	29	26.5
	13:35	16:50	17:35	17.3	29.3	23.8
	20:00	20:45	22:30	20.9	28	18.7
3/15	9:35	11:05	11:40	19.5	29.5	24
	13:30	14:50	16:30	21.5	30	18.1
3/16	8:50	9:00	10:20	16.1	14.4	26.2

3.2 Development of personal comfort models

The development of thermal models follows the typical machine learning pipeline, as shown in Figure 3-4. In this study, three different feature sets were used for developing the thermal models, as shown in Table 3-4.

Table 3-4 Feature sets benchmark

Base feature set	Feature set A	Feature set B
air temperature	air temperature	air temperature
relative humidity	relative humidity	relative humidity
side face skin temperature	side face skin temperature	side face skin temperature
	clothing surface temperature	side face skin temperature difference

As to baseline, PMV was used to compare with the two classification models. However, several assumptions were set when calculating PMV. Firstly, since the mean radiant temperature (MRT) and indoor air velocity were not measured and the experimental environment avoided direct radiation, MRT was approximated with indoor air temperature when calculating PMV and the indoor air velocity was calculated as 0.1 m/s since there was no draft risk. In addition, since the subjects were seated during the whole study, the metabolic rate was calculated as 1 met and there was no external work.

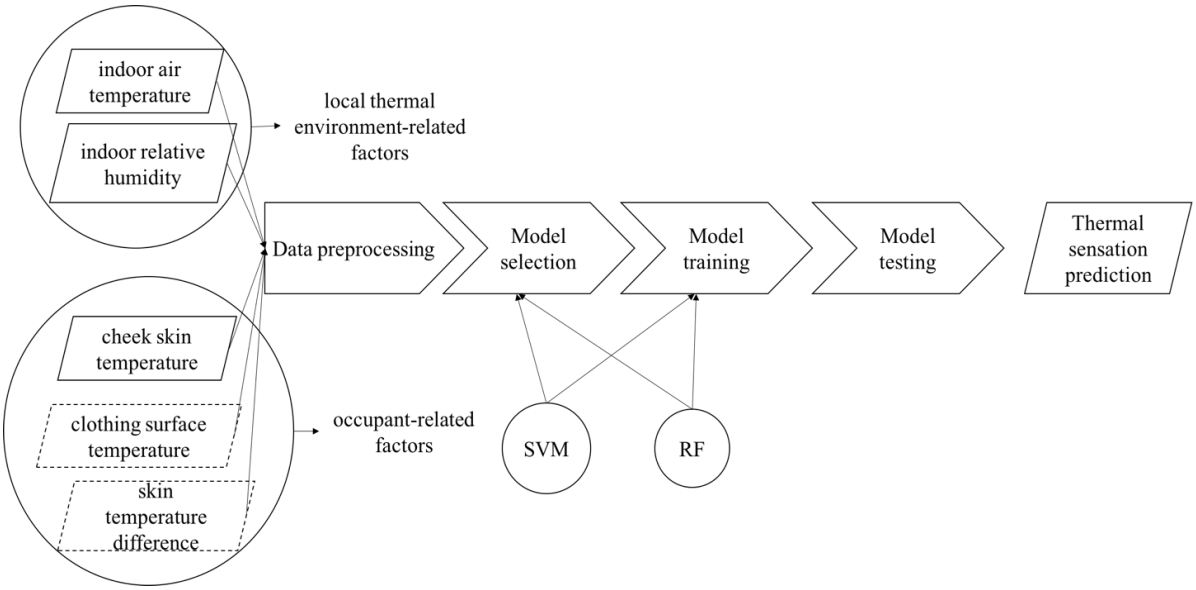

Figure 3-4 The development of thermal model pipeline

The whole dataset was split into two parts where 80% of data is the training set and 20% is the testing data. In addition, before training the best model, the hyper-parameters used in the best models were selected with 5-fold cross-validation, as shown in Table 3-5. In addition, in terms of classification algorithms, SVM and RF were implemented for classification since they can perform well with such relatively small-scale dataset. Same as chapter 1, before training the best model,

the hyper-parameters including the kernel function of SVM, tree depth and the number of trees of RF were tuned with 5-fold cross-validation.

Moreover, the prediction results of SVM and RF were compared with PMV model. Besides recall score mentioned in Chapter 1, all thermal models were also evaluated with precision and F1 scores (Kohavi, 1995), which were calculated with the confusion matrix (Table 3-6). Precision score describes how precise the model is out of the predicted results, which is the ratio between true positives and all predicted positives. Lastly, F1 score is used for seeking balance between recall and precision, which is harmonic mean of recall and precision. Precision and F1 scores can be computed with the following equations.

Table 3-5 The parameters of SVM and RF to be tuned with cross-validation

Algorithms	**Parameters**	
SVM	Penalty parameter C	1,10
	Kernel type	Gaussian, linear
RF	Tree depth	3,4
	Number of trees	50,100

Table 3-6 Confusion matrix

	Predicted Negative	Predicted Positive
Actual Negative	True negative	False positive
Actual Positive	False negative	True positive

$$\text{Precision} = \frac{\text{True positive}}{\text{True positive}+\text{False positive}} \quad (3\text{-}1)$$

$$\text{F1} = 2 * \frac{\text{Precision}*\text{Recall}}{\text{Precision}+\text{Recall}} \quad (3\text{-}2)$$

3.3 Result analysis

The raw data has a total of 775 instances, among which the male subject had 413 instances and the female subject had 362 instances. Moreover, Table 3-7 shows the number of instances collected from each thermal sensation. As shown in the table, the distribution is imbalanced where the neutral sensation is the majority vote.

Table 3-7 Data distribution over different sensations

	Very cold (-3)	Cold (-2)	Cool (-1)	Neutral (0)	Warm (1)	Hot (2)	Very hot (3)
female	3	16	29	168	73	58	15
male	7	13	24	188	100	58	23

3.3.1 Relationships between occupant-related variables and TSVs

In this study, two occupant-related variables were selected as features. One is side face skin temperature and the other is clothing surface temperature. Before developing the thermal models, the relationship between skin temperature and TSVs as well as the relationship between clothing surface temperature and thermal sensation were investigated. Figure 3-5(a)-(d) show the relationships based on the data collected with the two subjects. As a result, for female subject, the correlation coefficient between skin temperature and TSVs is 0.747 while that between clothing surface temperature and TSVs is 0.768. In addition, for male subject, the correlation coefficient between skin temperature and TSVs is 0.688 while that between clothing surface temperature and TSVs is 0.763. Therefore, clothing surface temperature has higher correlation with TSVs for both subjects.

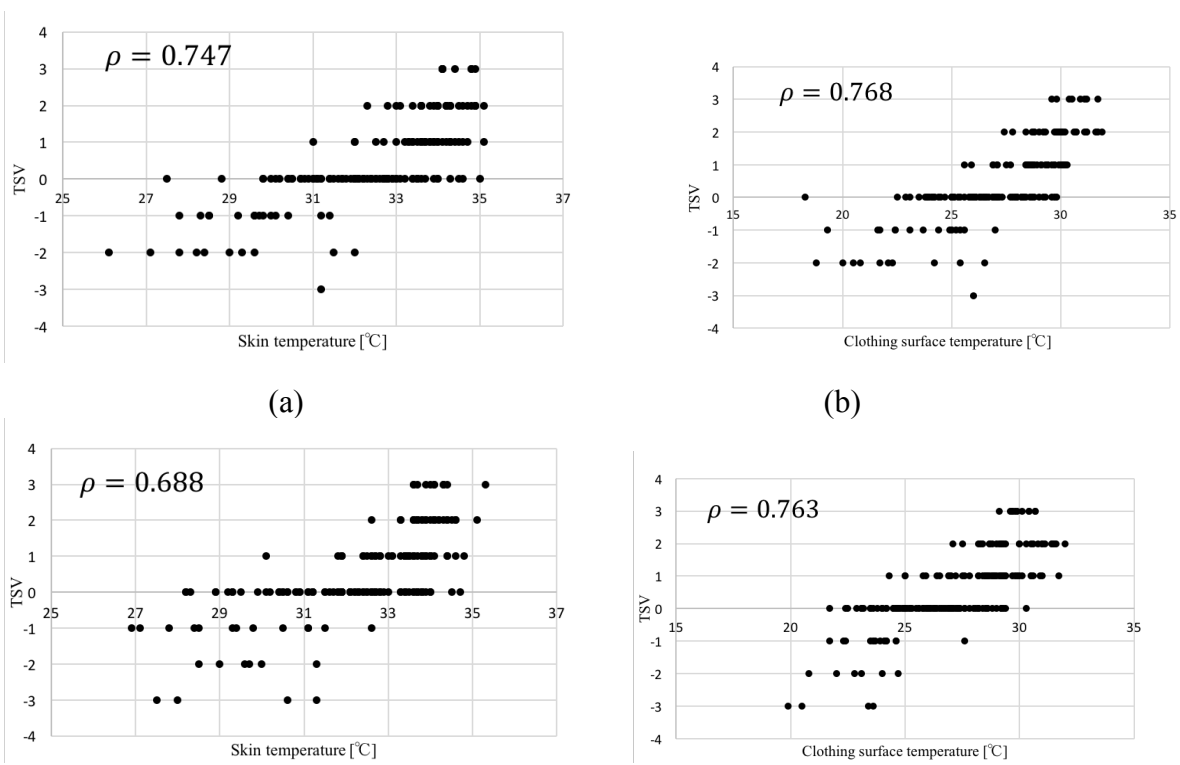

Figure 3-5 Relationships between thermal sensations and (a) skin temperature of female subject (b) clothing surface temperature of female subject (c) skin temperature of male subject (d) clothing surface temperature of male subject.

3.3.2 Classification:

Based on 5-fold cross-validation with both female and male data, Table 3-8 shows the recall scores with cross-validation based on different parameter values of SVM and RF, respectively. As shown in the table, in terms of SVM model configuration, SVM with linear kernel has much better performance than Gaussian kernel with feature set A while there are few differences among all SVM configurations with the base feature set and feature set B for both subjects. Meanwhile, in terms of RF model configuration, there are few differences among all combinations of RF configurations and features sets. Since larger penalty number will result in slower SVM model and larger tree depth and number of trees will also result in slower RF model, SVM with linear kernel and penalty number of 1 were selected as SVM best model configuration and RF with maximum depth of 3 and 50 trees were selected as RF best model configuration.

Table 3-8 Best parameters selected with model selection

Model configuration	**Average Recall score**					
	Female			Male		
	Base	A	B	Base	A	B
SVM, C=1, kernel = linear	0.65	0.98	0.65	0.62	0.96	0.57
SVM, C=1, kernel = Gaussian	0.62	0.68	0.57	0.61	0.78	0.59
SVM, C=10, kernel = linear	0.62	0.98	0.6	0.6	0.96	0.6
SVM, C=10, kernel = Gaussian	0.62	0.82	0.52	0.6	0.88	0.58
RF, Max_depth=3, number of tree=50	0.6	0.96	0.6	0.68	0.95	0.59
RF, Max_depth=3, number of trees=100	0.6	0.96	0.59	0.58	0.96	0.61
RF, Max_depth=4, number of tree=50	0.63	0.97	0.59	0.57	0.99	0.62
RF, Max_depth=4, number of tree=100	0.62	0.99	0.59	0.6	0.98	0.6

Meanwhile, Table 3-9 and Table 3-10 show the performance benchmark among the thermal models of the two subjects with the three feature sets trained by SVM, RF and PMV, respectively. As a result, for the female subject, precision, recall and F1 scores of PMV on test data are 48.6%, 48.6% and 48.3%, respectively. Compared to the baseline of PMV, SVM and RF have better performances with all three different feature sets. Among the three feature sets, feature set A comprised of indoor air temperature, relative humidity, side face skin temperature and clothing surface temperature has 100% recall, precision and F1 score with SVM, which significantly outperforms the baseline. This may be because the effect of clothing insulation on thermal comfort

has been taken into account since the dynamic clothing insulation can be estimated with clothing surface temperature and skin temperature, and the causal effect analysis also illustrates the clothing surface temperature has higher correlation with thermal sensations than the skin temperature. In addition, SVM performs better than RF with all three feature sets.

For the male subject, precision, recall and F1 score of PMV on test data is only 35%, 33% and 31.8%, respectively. Moreover, even if outperforming the baseline with recall score, both SVM and RF have much worse performances in predicting thermal sensation of the male subject with the base feature set and the feature set B than those of female subject. This indicates individual differences on thermal comfort such as gender, thus the personalized heating and cooling system being important to develop. However, for the feature set A, SVM still achieves high precision, recall and f1 scores which indicates that SVM can be the best classifier with the feature set consisting of indoor air temperature, relative humidity, skin temperature and clothing surface temperature for both the female and male subject. Therefore, such combination is recommended to be the thermal model for real-time prediction for automatic personalized heating and cooling system in open-plan offices.

Table 3-9 Performance benchmark among the thermal models of the female subject

	Base Feature set			**Feature set A**			**Feature set B**		
	P[%]	R[%]	F1[%]	P[%]	R[%]	F1[%]	P[%]	R[%]	F1[%]
SVM	62.3	62.9	62	**100**	**100**	**100**	69.2	64.7	65.1
RF	57.7	48.6	48.6	91.6	91.4	91	49	47	46.3
PMV	48.6	48.6	48.3	48.6	48.6	48.3	48.6	48.6	48.3

Table 3-10 Performance benchmark among the thermal models of the male subject

	Base Feature set			**Feature set A**			**Feature set B**		
	P[%]	R[%]	F1[%]	P[%]	R[%]	F1[%]	P[%]	R[%]	F1[%]
SVM	33.5	42.5	35.8	**97.5**	**95**	**96.1**	32.1	43.6	34.5
RF	28.8	40	33.1	90.4	92.5	91.4	26.8	38.5	30.7
PMV	35	33	31.8	35	33	31.8	35	33	31.8

Moreover, Figure 3-6 and Figure 3-7 show the normalized confusion matrices on test data with the three feature sets for the two subjects by using SVM and RF, respectively. The normalization equation is shown below:

$$x_{norm\_ij} = \frac{x_{ij}}{\sum_{k=1}^{k=m} x_{ik}} \tag{3-3}$$

where x_{norm_ij} is the normalized value of cell x_{ij}, which is the element in the ith row and jth column. In addition, m is the number of the column of the confusion matrix.

As to female subject, the test data with neutral label has the highest accuracy for each feature set. With both SVM and RF, for base feature set, the test data with cold (-2) label has the lowest accuracy while for feature set B, the test data with cool (-1) label has the lowest accuracy. As to male subject, same as female subject, the test data with neutral label has the highest accuracy for each feature set. Moreover, as shown in Table 5, the number of uncomfortable sensations is much smaller than that of neutral sensation. Therefore, it is more difficult to predict uncomfortable thermal sensations, including cold/hot (-2/2) and very cold/very hot (-3/3) than neutral sensation. However, as shown in the figures, SVM performs better on predicting uncomfortable thermal sensations than RF for both subjects.

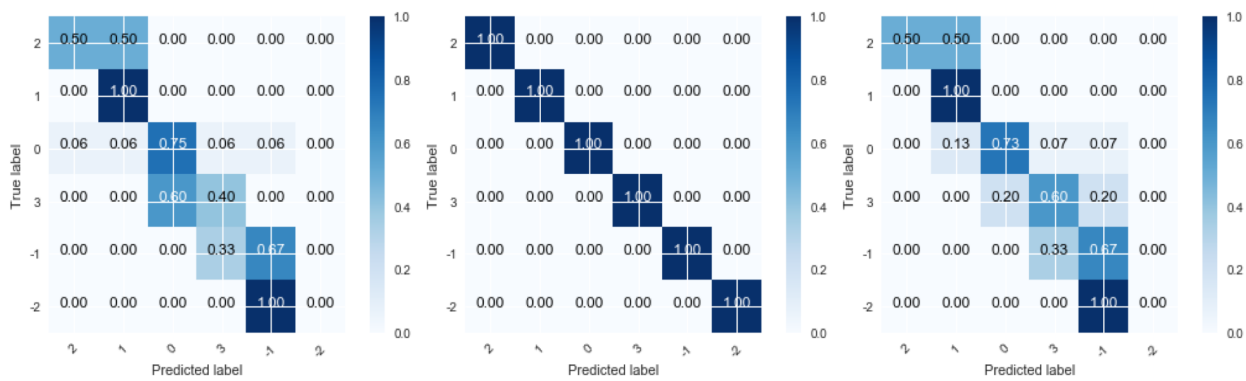

(a) Base Feature set with SVM (b) Feature set A with SVM (c) Feature set B with SVM

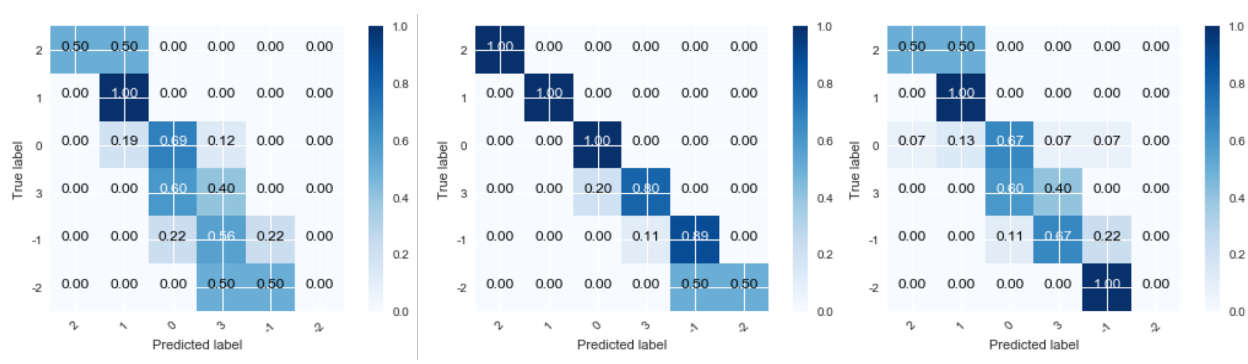

(d) Base Feature set with RF (e) Feature set A with RF (f) Feature set B with RF

Figure 3-6 Normalized confusion matrix of the female subject

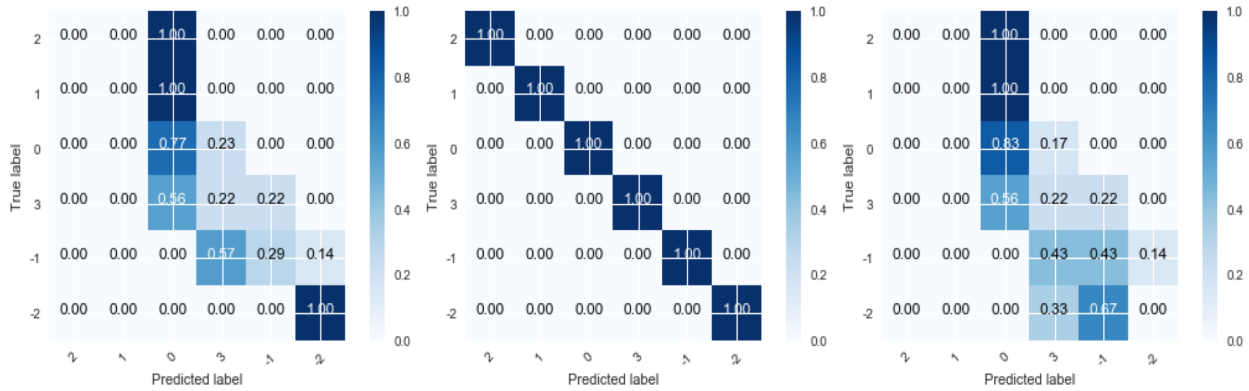

(a) Base Feature set with SVM (b) Feature set A with SVM (c) Feature set B with SVM

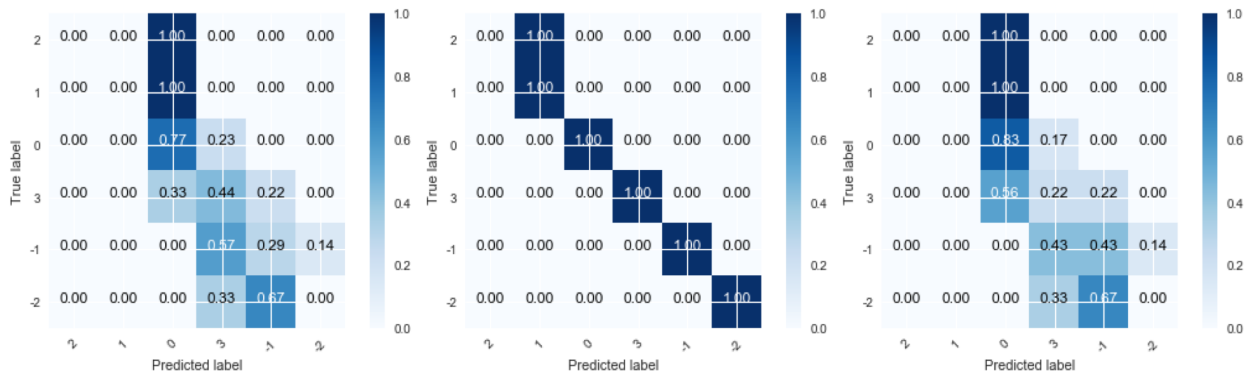

(d) Base Feature set with RF (e) Feature set A with RF (f) Feature set B with RF

Figure 3-7 Normalized confusion matrix of the male subject

3.4 Discussions of the preliminary study

In order to realize occupant-responsive system, it is of great significance to study individual thermal comfort. Compared to theoretical physical models, the data-driven approaches to studying thermal comfort have emerged to mitigate the difficulty in developing complex models and still maintain high accuracy. Meanwhile, compared to wearable sensing techniques, non-intrusive sensing technique has drawn more attention for occupant-related factors to thermal comfort. This paper proposes to use the non-intrusive infrared camera in combination with temperature and humidity sensors to infer individual thermal comfort in real-time with two classification algorithms of SVM and RF. The results have shown the model on testing data of the female subject performs much better than that of the male subject with the base feature set and the feature set B. This reveals individual differences on thermal comfort and indicates it is necessary to update the thermal models with more data in real-time when adapting new users.

Compared to existing methods, besides skin temperature, the proposed method also takes clothing surface temperature and skin temperature difference into consideration. Moreover, unlike ASHRAE RP884 where only a few instances were collected for each individual, the proposed experimental study collected over 300 instances for each individual so that the amount of data is enough for those classification algorithms. Additionally, besides using machine learning algorithms for thermal comfort inference like existing literature, this study also conducted a causal analysis with correlation coefficient to interpret the machine learning classification results. The results have shown the model with the feature set consisting of indoor air temperature, indoor relative humidity, side face skin temperature and clothing surface temperature perform best for both subjects. This can be explained by the fact that the correlation coefficient between clothing surface temperature and thermal sensation is higher than that between skin temperature and thermal sensation. Additionally, the model performance of female subject is much better than that of the male subject with the base feature set and the feature set B, which reveals individual differences and indicates it is necessary to update the individual thermal models with more data in real-time when adapting new users.

However, since the current infrared camera is expensive to use, it may not be ideal for the real application in terms of thermal comfort. Therefore, more cost-effective sensing technique shall be investigated. AMG8833 is an 8x8 temperature infrared sensor used for occupancy detection where each pixel measures a surface temperature. Since AMG8833 is not only much more cost-effective than the infrared camera but also more easily integrated with temperature and humidity sensor such as DHT22, it has great potential to be used as a non-intrusive sensing system for the personalized HVAC system in different scenarios in the open-plan office buildings.

3.5 Conclusions:

This chapter has conducted a non-intrusive sensing technique, which consists of temperature, humidity sensor called DHT22, and an infrared camera named FLIR B8400. Two statistical thermal models for female subject and male subject were developed with SVM and RF based on a 6-day experimental study conducted in Shanghai, respectively.

A total of three different feature sets were selected to develop individual thermal models with the labels based on 7-point thermal sensation scale. As a result, all proposed feature sets have achieved much better performances than the baseline of PMV model. In addition, the model trained with the feature set consisting of indoor air temperature, indoor relative humidity, side face skin

temperature and clothing surface temperature, and with linear kernel SVM has achieved the best performances. The precision, recall and f1 scores of the best model was 100% on test data of female subjects and 97.5%, 96.1%, 95% on that of male subjects, respectively. Besides classification, the causal analysis has also shown that clothing surface temperature has higher correlation coefficient with thermal sensations than side face skin temperature for both subjects, which explains why the individual thermal models with feature set containing clothing surface temperature has the best performances. Last but not least, the individual difference in thermal comfort indicates the importance of personalized heating and cooling systems. On top of that, the proposed sensing system could be improved further by using smaller-sized infrared sensor such as AMG8833 to realize large-scale real deployment in the open-plan office buildings.

Chapter 4 A case study of the interactive task-ambient conditioning cooling control in Shanghai

Table 4-1 Nomenclature

Abbreviation	Description
ASHRAE RP884	ASHRAE RP-884 Adaptive model project
ASHRAE 55	ASHRAE Thermal environmental conditions for human occupancy
ASH	ASHRAE thermal sensation scale
PMV	predicted mean vote
TAC	task ambient conditioning
SVM	support vector machine
RF	random forest
DHT22	temperature/humidity sensor
AMG8833	infrared temperature sensor
IR	infrared thermography
ESP8266	micro-controller with 2.4GHz WIFI module
Wemo	wireless plug
Ouimeaux	open source Wemo control
Thingspeak	cloud-based database

With the preliminary study regarding individual thermal models for two subjects, it is of significance to investigate further regarding thermal comfort in open-plan offices where multiple occupants are working at the same time. Moreover, since in the preliminary study, side face temperature was measured with infrared camera, which is expensive to use in reality, a more cost-effective infrared temperature sensor was proposed. Therefore, taking cost-effectiveness into account, this chapter aims to develop personal thermal models with SVM by collecting data from a sensing system consisting of an indoor air temperature and relative humidity sensor called DHT22, an infrared temperature sensor called AMG8833 and a micro-controller called ESP8266 with WIFI module. Moreover, the performance of the proposed personalized cooling system controlled with thermal comfort models was also enhanced in an open-plan office in Shanghai during the cooling season by optimization of the whole TAC system. Since the study aims to

evaluate the proposed TAC system has higher energy efficiency than baseline while maintaining personal thermal comfort, it contributes to the field of personalized thermal comfort by proposing a new cost-effective sensing system to develop adaptive thermal models, and further integrating the models into personalized system control as well as TAC system in the regular open-plan office building.

4.1 Overview of the proposed TAC system

Figure 4-1 shows the 3D visualization and the real field study testbed in an open plan office. As shown in the figure, each participant is provided with a personalized device while an air-conditioner is used to control the overall thermal environment. The proposed task conditioning system realizes the automatic adjustments of the local thermal environment around the occupants while still allows the user to override the automatic actions from the controller. Since the proposed system aims not only to improve occupant thermal comfort but also increase energy savings by widening the temperature set-point dead band with the centralized HVAC system, the proposed integrative system has higher energy efficiency than the centralized system.

Figure 4-1 The proposed TAC system in an open-plan office

The field study with a total of 14 sessions was conducted in a 2.56x3.5x4.3 m^3 office room in Shanghai from July to early September 2018 during the cooling season. In the office environment, an air-conditioner was operated when the space was occupied. Moreover, the radiation effect on thermal comfort was avoided by using curtains to prevent direct sunlit through windows. For each session, 5 participants attended the study for at least continuous 3 hours. Meanwhile, a total of 9 healthy female and 11 healthy male participants at the age between 20 to 40 attended the study.

4.2 Development of task conditioning system

4.2.1 Non-intrusive sensing system

In order to predict personal comfort in real-time, a personalized sensing system has been implemented for each individual. Table 4-2 shows the specification of each component in the sensing system. As shown in the table, inspired by advantages of contactless sensing device, a contactless temperature array called AMG8833 (Grideye) was used to measure the side face skin temperature.

Table 4-2 Components in the non-intrusive sensing system

Variable	Sensor	Unit	Resolution	Accuracy	Operating range
Air temperature	DHT22	℃	0.1℃	±0.5℃	-40-80℃
Relative humidity	DHT22	%	0.1%	±2%	0-100%
Skin temperature(calibrated)	AMG8833	℃	0.01℃	±0.5℃	0-80℃

AMG8833 is a temperature array sensor for temperature detection. It has two-dimensional area with 8x8 pixels. The typical application of the sensor includes occupancy detection, energy savings, digital signage and home appliances. However, it has potential to be used for skin temperature measurement. Compared to infrared camera like Lepton 2.5, AMG8833 has much lower price as $64. In addition, the accuracy of the sensor will be ±0.5℃ after calibration (Abbas M., 2015), which is higher than that of Lepton being ±2.5℃. Moreover, unlike infrared temperature sensor called MLX90614, AMG8833 measures temperature distribution of an area at a time instead of a single temperature spot. The calibration process of AMG8833 is shown as below:

Cool or warm the object covered with electric tape whose emissivity is 0.95 (the calibrated object needs have high emissivity close to 1) uniformly so that the object temperature can be distinguished from the environment temperature and the electric tape has the uniform surface temperature distribution.

1) Use Infrared camera to take the photo of the object (Figure 4-2(a)) and measure the average temperature T_{rad} of the tape surface with the camera at 0.5-meter distance.

2) Measure the temperature of the tape surface (Figure 4-2(b)) with AMG8833 at the same distance and make sure that all pixels ($T_{11}, T_{21} \ldots T_{88}$) only measure the surface temperature of the electric tape.

3) Calibrate the temperature of all pixels with T_{rad}. For instance, $\Delta t_{11} = T_{11} - T_{rad}$.

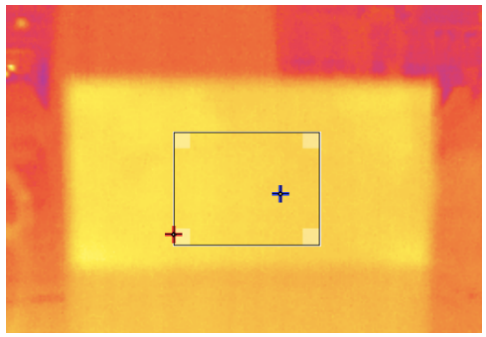

Figure 4-2(a) IR image of electric tapes (emissivity=0.95).

Figure 4-2(b) RGB image of electric tapes (emissivity=0.95).

Moreover, in order to measure side face temperature correctly, the sensor is designed to be installed 0.5 m away from the user so as to avoid the error due to distance. Since the view angle of AMG8833 is around 7.5° and the distance between the sensor and the user is 0.5 m, part of the pixels may measure the background temperature (i.e. temperature of the object surface behind the user) instead of side face temperature. Since in regular office buildings, the radiative surface temperature in the background is always lower than that of occupant face skin temperature, in order to ensure only the radiative temperature of the side face area is captured, a simple yet effective skin temperature extraction is proposed such that the side face temperature is estimated as the mean of 3x3 largest temperatures among these 64 pixels. Figure 4-3 shows an example of skin temperature detection.

```
[24.00, 24.25, 24.75, 24.75, 25.25, 25.00, 24.50, 26.25,
24.00, 24.50, 25.25, 25.00, 24.75, 25.25, 25.00, 26.00,
24.00, 24.75, 24.75, 25.50, 24.75, 25.25, 25.75, 25.75,
24.50, 24.50, 24.75, 25.25, 25.00, 24.75, 25.50, 25.50,
24.50, 25.25, 24.75, 25.25, 25.25, 26.00, 25.25, 25.75,
25.00, 24.50, 24.75, 25.25, 25.75, 26.00, 26.25, 25.75,
24.50, 24.25, 24.75, 25.25, 26.00, 26.00, 26.00, 25.25,
24.25, 24.50, 24.75, 25.50, 25.00, 25.00, 25.50, 25.00,
]
```

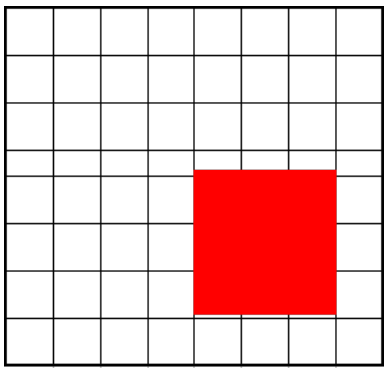

Figure 4-3 An example of skin temperature detection

In addition, a micro-controller called ESP8266 with WIFI module was used for data collection with sample frequency of 1 sample every 5 minutes so as to correspond the survey feedback interval described below. The sensing system and each part is shown in Figure 4-4.

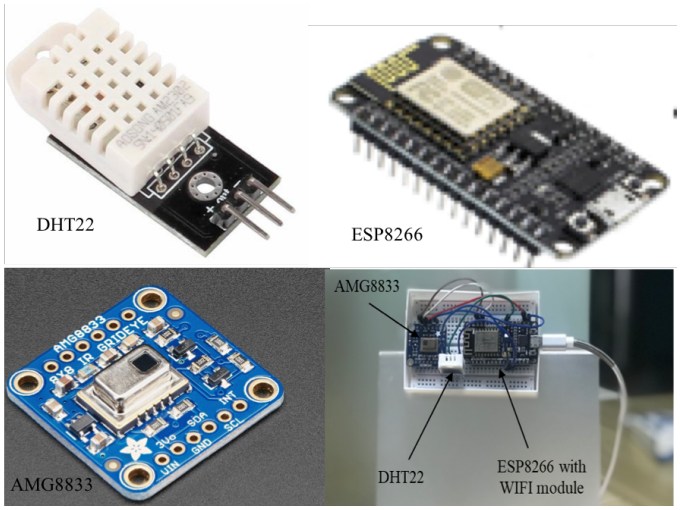

Figure 4-4 The non-intrusive sensor board

Besides sensing system, the personalized cooling system also includes an 8' desktop mini-fan (the supply direction can be adjusted so that the air velocity towards each occupant is controlled without draft risk by validating from participants' responses). Compared to conventional air-conditioning system, TAC system with fan has several advantages. Firstly, fans offer a straight-forward, economic, and independently operable technique to increase movement of air so as to ultimately improve thermal comfort in a room (S.C. Sekhar, 1995). Moreover, when operated with AC system, the downwash propelled by foil (rotating) drives the warm air downwards to blend with the cold air, countering the impacts of buoyancy (Li, W., 2016).

4.2.2 Development of personal comfort models

The development of personal comfort models consists of two phases. The first phase was to collect sensor data used as features and thermal comfort feedback used as labels from various participants. Personal comfort models were trained by varying the temperature set-point from 22℃ to 30℃ slowly. However, it was not guaranteed that same people would attend all the sessions in both phases. During each session, they were asked to report their thermal sensation and thermal satisfaction with 7-point thermal sensation and 5-point thermal satisfaction scale every 5 minutes, as shown in Table 4-3.

Table 4-3 Thermal sensation scale and thermal satisfaction scale

Thermal sensation vote	**Meaning**	**Thermal satisfaction vote**	**Meaning**
-3	very cold	4	unsatisfactory
-2	cold	3	A bit unsatisfactory
-1	cool	2	A bit satisfactory
0	neutral	1	satisfactory
1	warm	0	Very satisfactory
2	hot		
3	very hot		

Figure 4-5 describes the development of personal comfort models in the first phase. The classification follows the standard machine learning pipeline, including feature extraction, feature selection, classification and validation. Even if the baseline uses the same machine learning pipeline, only air temperature is used for thermal sensation and thermal satisfaction prediction, respectively. Since the study was conducted in a real shared office, parameters such as metabolic rate, clothing insulation, mean radiant temperature are difficult to measure. Hence, PMV model may not be suitable to be used as baseline. Since models trained with SVM in Chapter 2 have achieved the best performances, in this study, SVM was used for developing personal comfort models, including thermal sensation and thermal satisfaction prediction in the first phase. Moreover, same as Chapter 2, recall score was also used to evaluate the performances of personal comfort models.

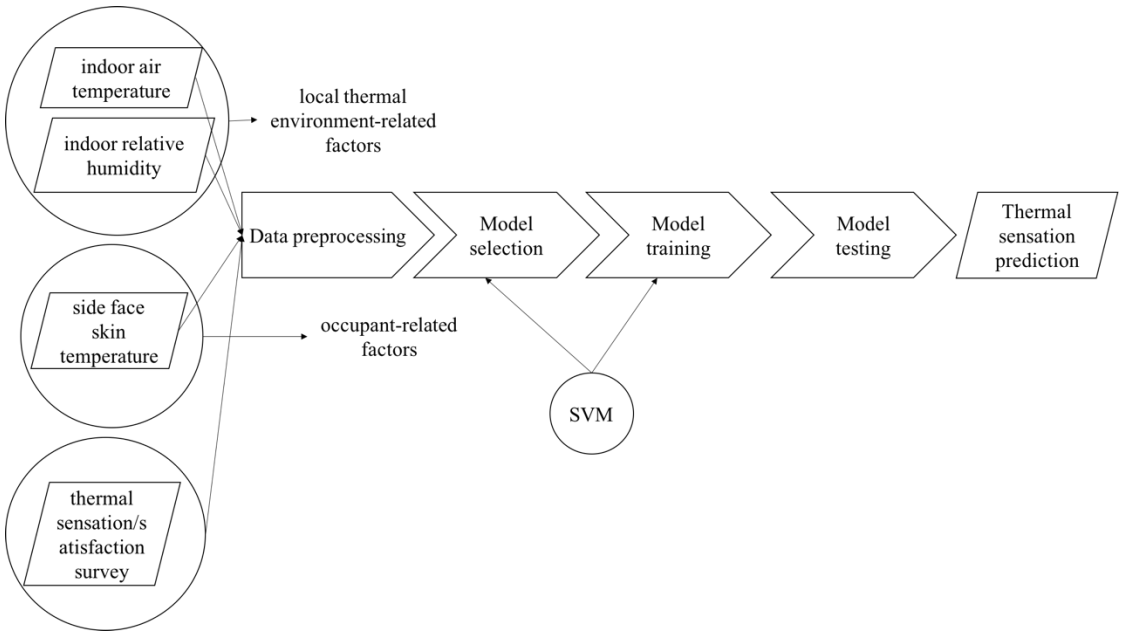

Figure 4-5 Personal comfort model pipeline in the first phase

The second was to update personal comfort models by observing the thermal environment when individuals overrode the actuations of the fan controlled with personal comfort models. Due to the fact that some participants in the first phase did not attend the second phase and some participants in the second phase had insufficient data from the first phase to get well-developed personal comfort models, the initialized personal comfort model for each female individual participating in the second phase was developed with all female data, and so was the initialized personal comfort model for males. The second phase was conducted with a group of five participants for a two-day comparison study at the end of August. For each of the two days, a total of 18 fan actuations based on thermal sensation predictions were made.

In addition, in this study, the task conditioning system was designed to control the duration of the mini-fan operation based on personal comfort model predictions by wireless plug called Wemo insight with an open source Wemo control package called Ouimeaux (McCracken I., 2014). Based on performance benchmark between thermal satisfaction models and thermal sensation models in the first phase, the mini-fan was controlled based on thermal sensation predictions in the second phase. Since the plug can only be controlled on/off, the fan was designed to be turned off when the sensation prediction was negative (uncomfortably cool) or neutral while being turned on when it was positive (uncomfortably warm). However, the user still had the right to override the control, and the system recorded the overridden actuations. During all of these phases, data from all participants, including sensor data and plug status were stored in a remote server using an open-

source platform called ThingSpeak (Mathworks, 2015). The proposed close-loop task conditioning system diagram used in the second phase is shown in Figure 4-6.

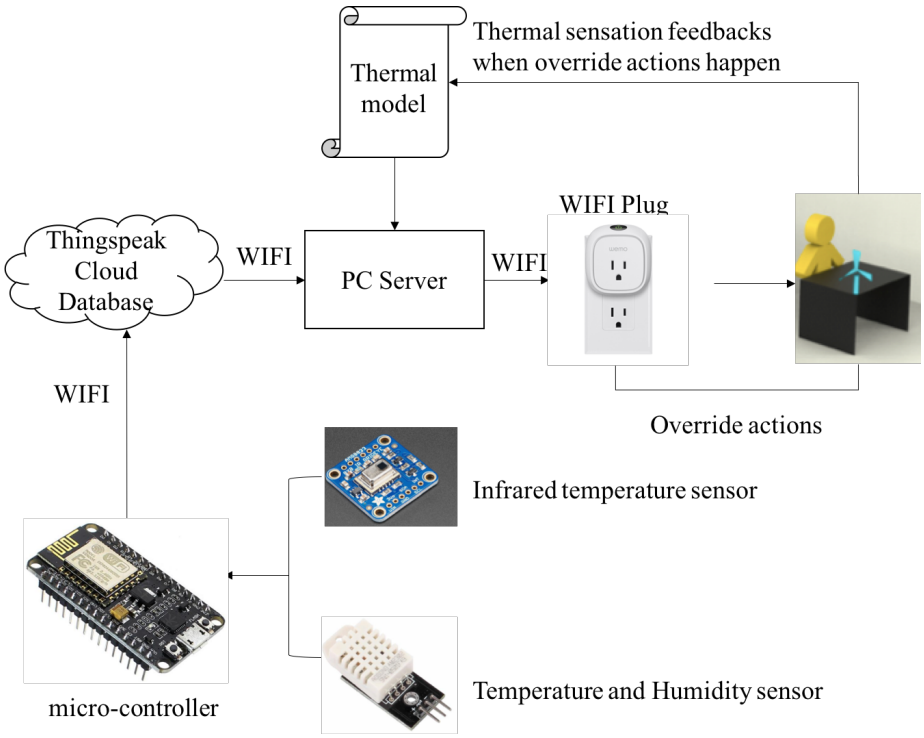

Figure 4-6 Closed-loop task system diagram of the task conditioning system

Moreover, instead of interrupting occupants by asking them to respond surveys in the second phase, personal comfort models were updated with dynamic rule-based logics by taking override actions into account so as to construct a closed-loop task conditioning system. The reason for that was because it took a long time to get enough amount of data for retraining personal comfort models since the override actions happened infrequently. Figure 4-7 shows an example updating the personal comfort model with the rule-based control logics. The example assumes the participant overrides the fan actuation from turning on into turning off on the first day with the indoor air temperature t_0 and skin temperature t_{sk}.

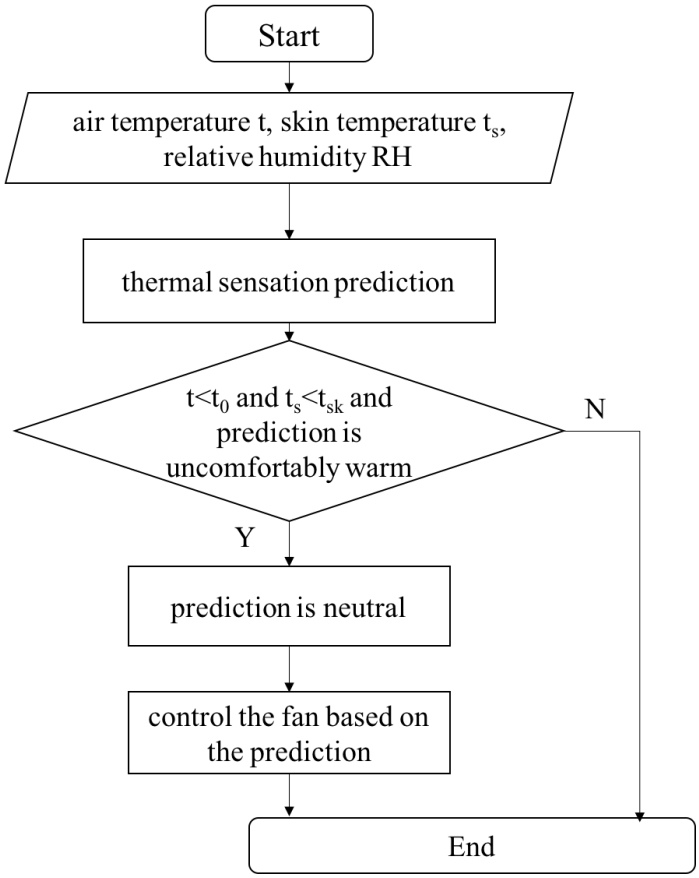

Figure 4-7 An example updating the personal comfort model

4.2.3 Development of ambient conditioning system

For ambient conditioning system, since widening the set-point dead band reduces sensible loads, the energy consumption can be reduced. Therefore, besides personal comfort model experiments for task conditioning system evaluation, a five-day experiment was conducted at the end of July and the beginning of September for ambient condition system evaluation. In order to conduct energy consumption benchmark, two energy meters with the resolution of 0.001 kWh were used for measuring energy consumption between the room with the proposed system and the room with the baseline at the same time for five sessions. Meanwhile, the energy consumption of the fans as well as the fan statuses were also monitored by Wemo insight. In addition, the outdoor temperature was measured with the average of three Type K thermocouples, as shown in Figure 4-8. Lastly, based on participant feedback in the first phase as well as the fact that the effect of the mini-fan on personal comfort is much faster than that of temperature set-point due to thermal mass, the interval for the personalized cooling control is 10 minutes while that for the temperature set-point control is 15 minutes.

The system diagram of the proposed TAC system is shown in Figure 4-8. As shown in the figure, the initial temperature set-point is 22℃. Moreover, the coordinator controller is designed with the objective of minimizing temperature difference between the outdoor temperature and the average indoor air temperature with the constraints of the thermal sensation prediction of each participant and the number of fans operated. The baseline was created in an office room next to the occupied test room with the same orientation, the same floorplan, and the same type of air-conditioner whose temperature set-point is always 22℃. The two office rooms were separated by a well-insulated door so that there was little heat transfer between these two rooms.

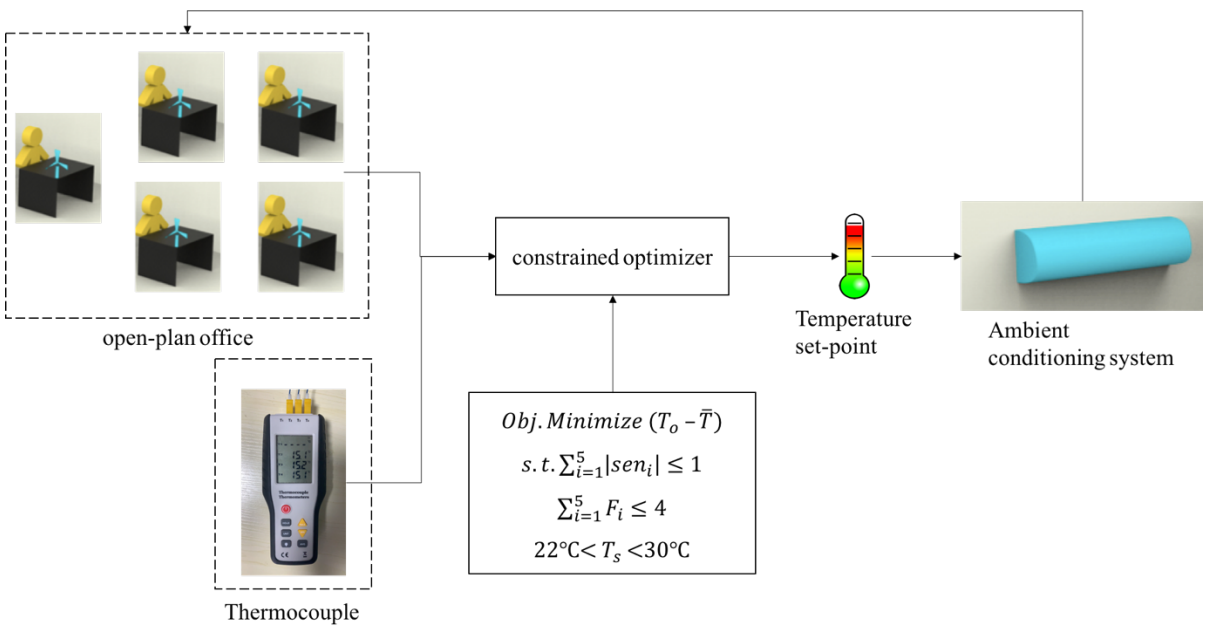

Figure 4-8 The overall TAC system diagram

The state space includes local indoor air temperature T_{it}, local indoor relative humidity RH_{it}, individual skin temperature $T_{is,}$ individual thermal sensation prediction sen_{it}, personalized fan status F_{it} where i=1,2,3,4,5, outdoor air temperature T_{ot}, and average indoor air temperature $\bar{T}$. On the other hand, the action space includes the actuation of the local fan (on/off based on prediction or overriding events) as well as temperature set-point T_s control of the ambient conditioning system (increasing/no change/decreasing the set-point).

As to control law of the temperature set-point, instead of developing a group thermal model, this study implements a multi-agent control system with the constrained optimization on ambient conditioning system, as shown in the following equations.

$Objective$:

$$Minimize\ (T_{ot} - \bar{T}) \quad (4\text{-}1)$$

$subjective\ to$:

$$\sum_{i=1}^{5} |sen_{it}| \leq 1 \quad (4\text{-}2)$$

$$\sum_{i=1}^{5} F_{it} \leq 4 \quad (4\text{-}3)$$

$$22℃ < T_s < 30℃ \quad (4\text{-}4)$$

The reason for using temperature difference between the average indoor air temperature and the outdoor air temperature as objective function is because the major part of the sensible cooling loads is caused by the temperature difference between the outdoor air temperature and indoor air temperature. Since in summer, compared to sensible cooling loads, latent cooling loads can be negligible in regular open-plan offices in Shanghai. Moreover, without direct radiation, sensible cooling loads monotonously decrease as the temperature difference decreases. Therefore, minimization of the objective function will minimize sensible cooling loads globally, thus reducing energy consumption.

The constraints are designed based on the sum of individual thermal sensation predictions. However, since the prediction may not be accurate, the actual number of fans operated shall not be more than four so that at least 80% of occupants feel thermally comfortable. Moreover, since fans help reduce air stratification so that the supply air could flow into the occupied zone and mixes with the warm air more quickly, it brings about cooler environment for occupants. However, if the temperature set-point is too high, the fan may increase the discomfort since the fan cannot reduce the actual amount of heat indoors. Therefore, besides constraints due to thermal comfort requirements, the temperature set-point shall not be higher than 30℃.

4.3 Result analysis

4.3.1 Analysis between objective thermal environment conditions and subjective thermal comfort

Even if 20 participants attended the study in the first phase, some of them did not have enough amount of data for training. Therefore, only 12 personal comfort models were developed. Hence, throughout the field study, a total of 488 instances collected from female subjects and a total of 770 instances collected from male subjects were used for developing thermal models. Figure 4-9(a) shows the distribution among neutral sensation and non-neutral sensation votes. Moreover, Figure 4-9(b) shows the distribution among satisfaction and dissatisfaction votes. As shown in the figure, among all feedbacks from the first phase, the number of votes for neutral sensation is much

larger than that for non-neutral sensation. Similarly, the number of votes for satisfaction is much larger than that for dissatisfaction. This indicates that in regular office environment, it is more difficult to detect discomfort states than comfort states. Moreover, in order to realize more fine-grained thermal comfort management, it is of great significance to operate localized and personalized control so as to reduce individual discomfort as much as possible.

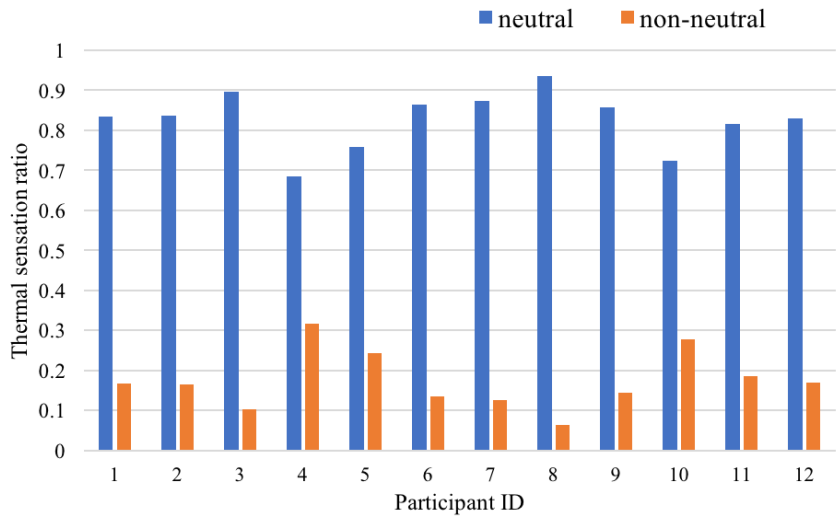

Figure 4-9(a) Comparison between votes for neutral and non-neutral sensation

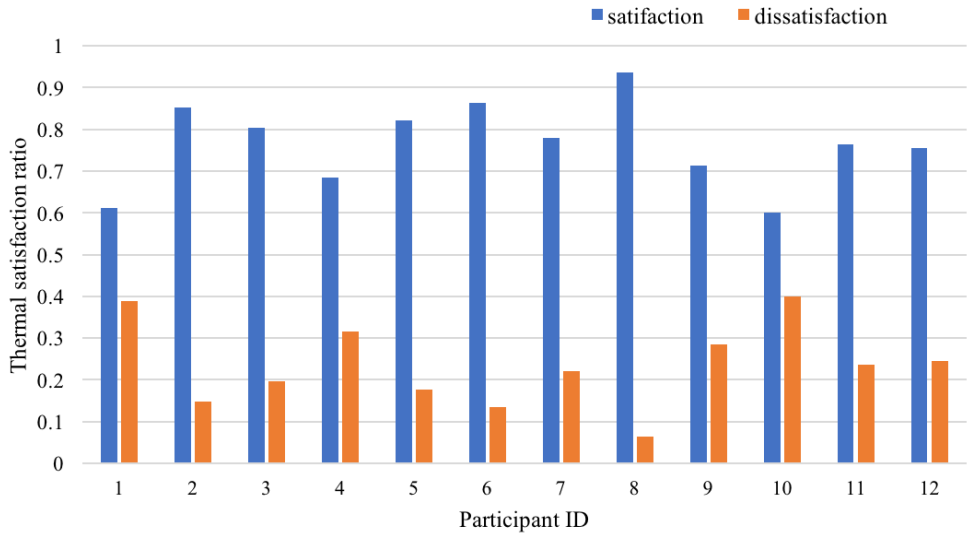

Figure 4-9(b) Comparison between votes for satisfaction and dissatisfaction

Moreover, Figure 4-10(a)-(h) show the boxplots between thermal environment conditions and thermal sensation and thermal satisfaction. Figure 4-10(a)-(b) show the box plots of indoor air temperature to thermal sensation of the female and male subjects. As shown in the figures, both

female and male subjects perceive warmer as the indoor air temperature increases. Meanwhile, the air temperature is 29°C when participants feeling neutral, which indicates it has potential to save energy consumption by increasing standard indoor air temperature of 26°C in such climate [42].

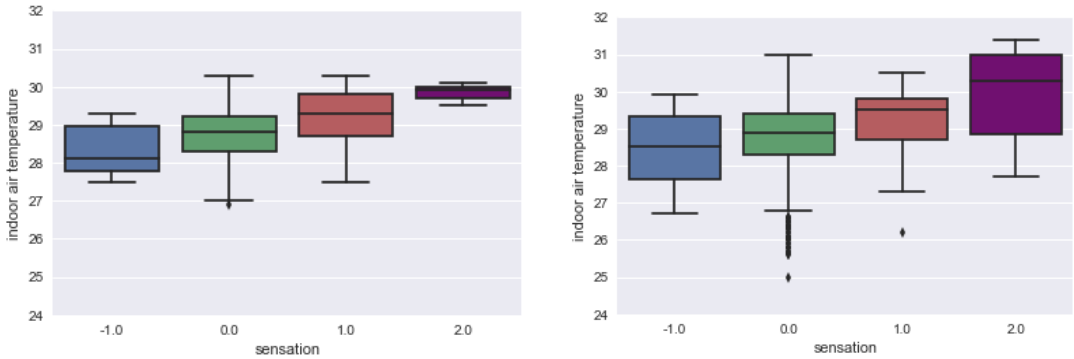

(a) air temperature vs sensation of females (b) air temperature vs sensation of males

Figure 4-10(c)-(d) show the box plots of skin temperature to thermal sensation of the female and male subjects. Unlike the relation between air temperature and thermal sensation, the relation between skin temperature and thermal sensation of female subjects differ from that of male subjects. As to female subject, the median skin temperatures are 31.31°C, 31.11°C, 31.52°C and 31°C, respectively, which vary little among different thermal sensations while as to male subjects, the median skin temperatures are 31.47°C, 31.53°C, 32.22°C, 32.88°C, which vary over 1°C when thermal sensation is above 0. This indicates that female subjects are more sensitive than male subjects. Moreover, since relative humidity was not strictly controlled, the thermal sensation of participants is likely to be affected by skin wetness.

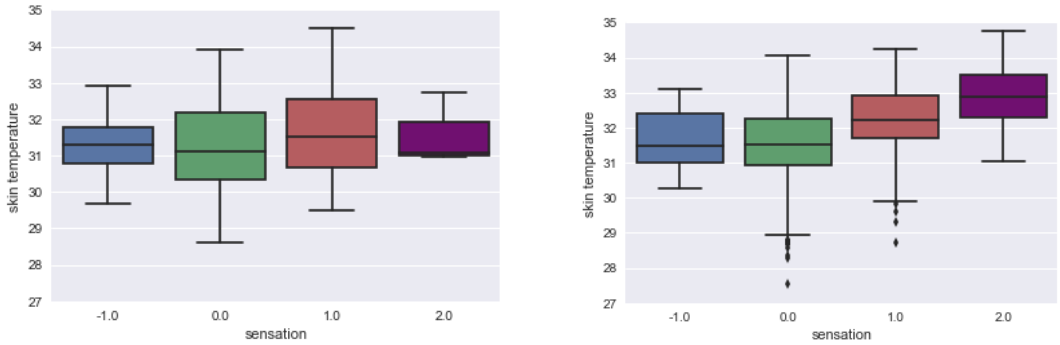

(c) skin temperature vs sensation of female (d) skin temperature vs sensation of males

Figure 4-10(e)-(f) show the box plots of indoor air temperature to thermal satisfaction of the female and male subjects. As shown in the figures, the air temperature differences among different thermal sensations of female subjects is much smaller than those of male subjects. Moreover,

compared to male subjects, the female subjects are more satisfied under the thermal environment with higher air temperature than the male subjects. In addition, considering thermal sensation distribution, the female subjects prefer warm environment while the male subjects prefer cold environment, which indicates even if thermal sensation is the precondition of thermal satisfaction (Auliciems, A, 1997), it may not be the same as thermal satisfaction all the time.

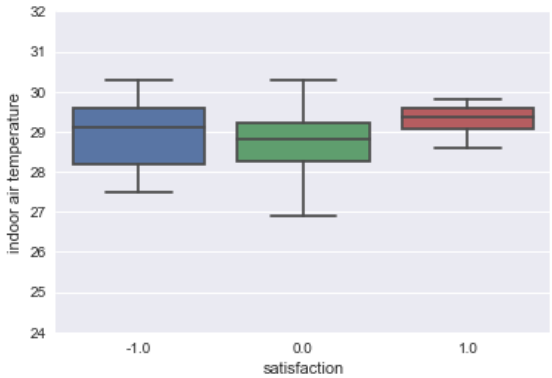

(e) Air temperature vs satisfaction of females

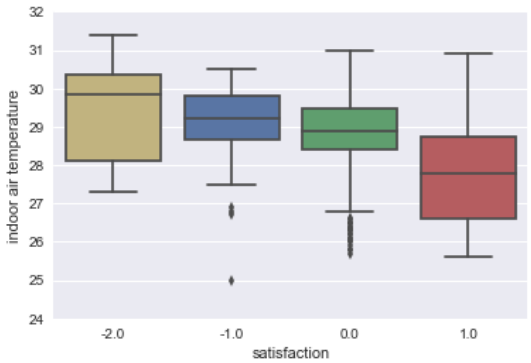

(f) Air temperature vs satisfaction of males

Lastly, Figure 4-10(g)-(h) show the box plots of skin temperature to thermal comfort of the female and male subjects. The results also illustrate the female subjects are very satisfied thermally with higher skin temperature while male subjects are very satisfied thermally with lower skin temperature. Moreover, similarly to thermal sensation, thermal satisfaction is also likely to be affected by skin wettedness.

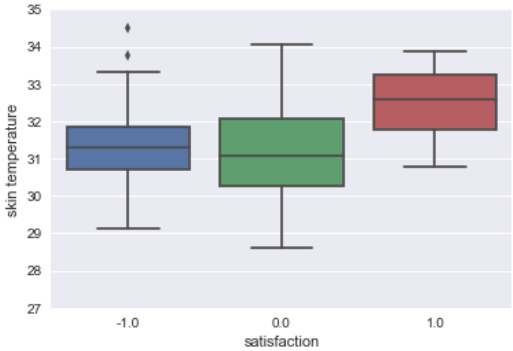

(g) skin temperature vs satisfaction of females

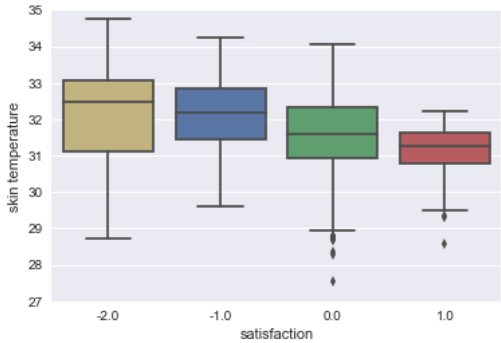

(h) skin temperature vs satisfaction of males

Figure 4-10 Relations between air/skin temperature and thermal sensation/satisfaction

3.2 Performances of personal comfort models

Table 4-4 shows the performance benchmark of the personal thermal sensation and satisfaction models with recall score. As shown in the table, compared to baseline models, the personal thermal sensation models and the thermal satisfaction models developed with data of all female subjects

outperform by 2% and 3%, respectively. In addition, thermal sensation models and thermal satisfaction models developed with data of all male subjects have similar performances to the baseline models. However, performances vary from 61.5% to 100% among different individuals and the highest recall score improvement was 25% for both sensation and satisfaction predictions.

Moreover, among all personal comfort models for female subjects, 80% of thermal sensation models and 100% of thermal satisfaction models with the proposed features has no worse performances than those with baseline features, respectively. Meanwhile, for male subjects, all thermal sensation and thermal satisfaction models with proposed features have no worse performances than those with baseline features. Therefore, personal comfort models with air temperature, skin temperature and relative humidity outperform those with air temperature only. Moreover, compared to thermal satisfaction predictions, 11 out of 12 subjects have better performances in thermal sensation predictions. Therefore, thermal sensation models were applied into task conditioning control for each participant.

Table 4-4 Performance benchmark of the thermal models with recall scores

Gender	**Sensation prediction with baseline model**	**Sensation prediction with proposed model**	**Satisfaction prediction with baseline model**	**Satisfaction prediction with proposed model**
All_female	82.65%	84.7%	73.5%	76.5%
All_male	87%	87%	81.2%	82.5%
F	93.0%	88.0%	83.0%	84.0%
F	90.9%	91.0%	63.6%	77.3%
F	84.6%	85.0%	84.6%	84.6%
F	50.0%	75.0%	50.0%	75.0%
F	61.5%	61.5%	84.6%	84.6%
M	92.3%	94.9%	82.1%	82.0%
M	86.7%	90.0%	80.0%	87.0%
M	83.3%	83.3%	83.3%	83.3%
M	94.7%	94.7%	89.5%	90.0%
M	100.0%	100.0%	100.0%	100.0%
M	100.0%	100.0%	100.0%	100.0%
M	61.5%	61.5%	46.1%	46.1%

Moreover, Figure 4-11 shows the comparison regarding the proportion of the override actions among all actuations between the two days in the second phase. Since both experiments were conducted under the same outdoor climates with same type of air-conditioner, the override actions can be used to indicate if fans make occupants thermally comfortable. As shown in the figure, 60% of the subjects have fewer override actions with the updated thermal sensation models than the initialized personal comfort models. Moreover, for those participants providing override actions on the first day achieved a reduction of 11-27% based on override actions. This indicate the rule-based updating mechanism does help improve the performances of personal comfort models.

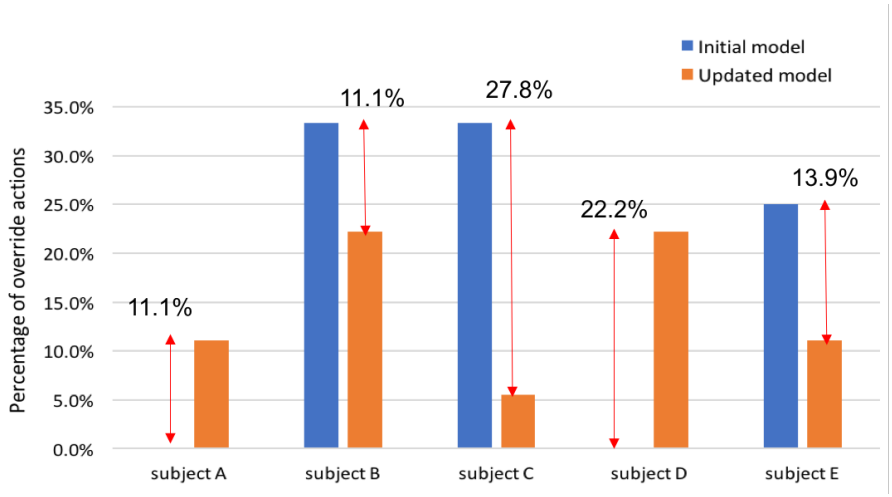

Figure 4-11 The comparison between initial and updated thermal comfort models

Last but not least, Figure 4-12 shows the energy performance benchmark between the proposed optimization framework and the baseline. As shown in the figure, the proposed system can save energy consumption 9.6% on average while maintaining individual thermal comfort. Moreover, the savings are varied among the five comparative tests due to different outdoor climates as well as the individual usage of the personalized fans.

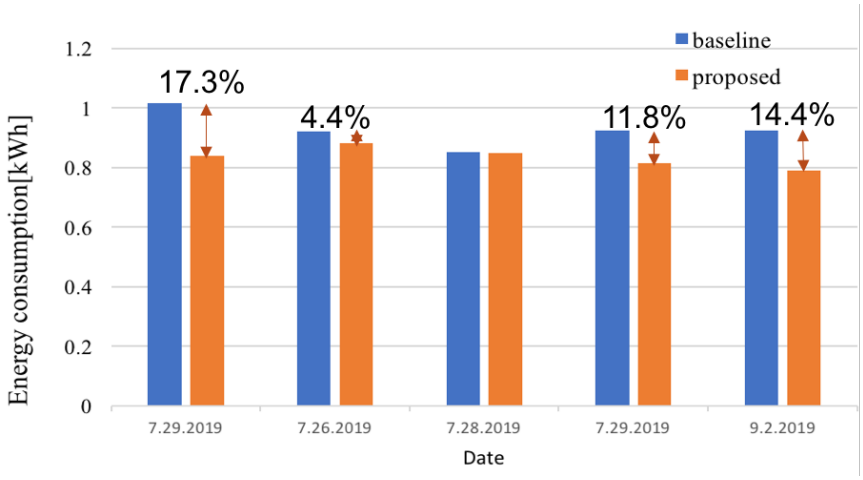

Figure 4-12 Energy performance benchmark between the proposed system and the baseline

4.4 Discussions of the proposed task-ambient conditioning system

In order to evaluate the proposed inter-connected TAC system under the constrained optimization framework, this study has conducted a field study showing the energy savings while maintaining individual thermal comfort with the proposed TAC system in an open-plan office. In addition, instead of using expensive IR camera, this study has proposed a cost-effective sensing system featuring non-intrusive infrared temperature array called AMG8833 as well as air temperature and relative humidity sensor called DHT22 to develop personal comfort models, including individual thermal sensation and thermal satisfaction predictions. Moreover, personal comfort models were further updated with the feedback mechanism by collecting the override actions of the personalized fans.

As one of the key components in the system, personal comfort models are proposed and evaluated for real-time task conditioning control. As shown in the results, even if the recall scores of the initialized comfort models developed with data from all female subjects or all male subjects are above 80%, the performances of personal comfort models developed with individual data only vary among different individuals. This is not only because individual differences but also because the amount of data from some individuals are not sufficient enough to train personal comfort models. Therefore, an initialized personal comfort model with large amount of data from various occupants is a good start point and the individual thermal models can be updated continuously via the interactions with the personalized cooling system in real-time. Besides personal comfort models for task conditioning systems, the current optimization framework of the ambient system is designed to optimize the energy savings while maintaining individual thermal comfort by

maximizing the cooling set-point. As a consequence, the proposed TAC could achieve up to 14% energy savings than baseline. In addition, the current sensing system for personal comfort prediction consists of DHT22 and AMG8833. With non-intrusive infrared temperature array, occupants no longer need to wear any devices to measure skin temperature. Moreover, compared to existing non-intrusive skin temperature measurement method, the proposed AMG883 is more cost-effective.

However, there still exists some limitations to be improved. Firstly, since the objective function is based on the simplification that latent cooling loads shall be neglected, it may not be applicable in other climates. Therefore, the decision variable shall be further decided to take both sensible cooling loads and latent cooling loads into account. Secondly, even if the current experimental testbed consists of only a split air-conditioner in a thermal zone and occupants can interacted with personal fans with only on/off operation, since the system is only for temperature set-point control and task devices can be designed with more options for personal comfort control, the proposed framework can also be easily implemented in more complex HVAC systems such as VRF.

4.5 Conclusions

This study has conducted a field study to evaluate an integrative TAC system featuring non-intrusive sensing technique and automatic control with personal comfort models developed with SVM in an open-plan office room. The temperature set-point of ambient conditioning system was then maximized with constraints of individual thermal sensations and the number of operated fans. This study also evaluates the feedback collection mechanism to calibrate personal comfort models by observing interactions between personalized systems and occupants instead of interrupting occupants with surveys. As a result, the performances of personal comfort models with features consisting of indoor air temperature, relative humidity and face skin temperature were better than those with baseline feature consisting of indoor air temperature only. Moreover, the performances of thermal sensation models were better than satisfaction models. Moreover, five 3-hour sessions have shown that the proposed system could achieve average 9.6% of energy savings compared with the baseline. The study contributes to the development of TAC system to maximize energy performances while maintaining individual thermal comfort in the regular shared office space. In the future, the proposed TAC system shall be applied into larger open-plan office buildings with multiple thermal zones and the personalized cooling of task systems shall be developed with more

fine-tuned thermal comfort management for individuals. However, since field studies have limited scenarios, more comprehensive and detailed studies shall be conducted with CFD simulations as well as energy simulations.

Chapter 5 Data-driven personal comfort models combined with CFD simulator for the local fan-induced air conditioning system

Table 5-1 Nomenclature

Abbreviation	Description
SVM	support vector machine
RF	random forest
DHT22	temperature/humidity sensor
AMG8833	infrared temperature sensor
IR	infrared thermography
ESP8266	micro-controller with 2.4GHz WIFI module
comfort database	Global thermal comfort database
CFD	computational fluid dynamics
kw SST	K-omega SST turbulence model
SIMPLE	Semi-implicit method for pressure linked equations

5.1 Overview of CFD simulation for the local fan-induced air-conditioning system

Even if recent studies on adaptive and personal thermal comfort benefit a lot from field studies by developing adaptive and personal thermal comfort models with various machine learning algorithms, it is still necessary to study thermal comfort in CFD simulations since they provide more theoretical explanations on effects of proposed air-conditioning system on individual thermal comfort in terms of airflow patterns, temperature and humidity distributions. However, most studies on adaptive and personal thermal comfort have utilized field studies and simulations separately. Therefore, in order to evaluate effects of the proposed TAC system, which can also be referred as local fan-induced air-conditioning system, on individual thermal comfort more realistically, CFD simulations have been conducted with the best personal thermal comfort models developed with support vector machine (SVM) and random forest (RF) based on the data from both comfort database II as well as an empirical study in an open-plan office at the end of August in Tongji University, Shanghai.

This research mainly has two contributions. The first contribution is to use machine learning algorithms to develop adaptive and personal thermal comfort models based on comfort database II as well as an empirical study where real-time monitoring was realized with the non-intrusive

sensing system described in chapter 4. The second contribution is to propose and evaluate effects of the integrated local fan-induced air-conditioning system on thermal comfort with CFD simulation. In addition, instead of conducting field studies and CFD simulations separately, this research proposes to apply personal thermal comfort models from field studies into CFD simulations so as to get more insights into individual thermal comfort differences and system design optimization such as ambient conditioning cooling set-point.

Figure 5-1 shows the diagram of the simulation and empirical study. As shown in the figure, the personal thermal comfort models with SVM and RF were developed based on a six-day empirical study in an open-plan office in Shanghai. Meanwhile, a CFD simulation with the same building configurations, including floorplan, envelopes, air-conditioning system and occupancy schedules as the test bed used in the empirical study were conducted to analyze airflow patterns, thermal stratifications as well as effects of increasing temperature set-point dead band on individual thermal comfort with the personal thermal comfort models.

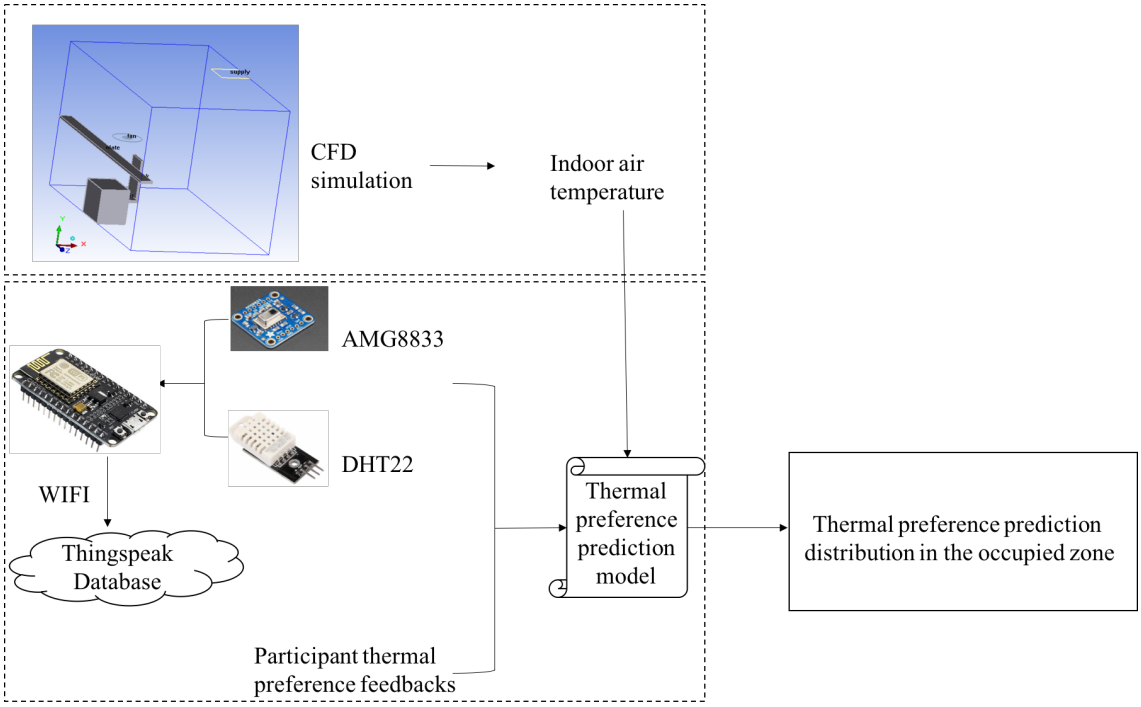

Figure 5-1 The diagram of the method for the proposed local fan-induced air-conditioning

5.2 Development of adaptive and personal thermal comfort models

5.2.1 Adaptive thermal comfort with Global Thermal comfort database II

The classification follows the standard machine learning pipeline, including feature selection, model selection, model training and prediction. The dataset used is the subset of comfort database

II, which was collected from the air-conditioned office buildings during summer season. The total number of instances of the subset is 4664. In addition, similar to chapter 1, since most of features have large amount of missing data and lack of consistency, including physical factors such as gender and age, common environment-related and occupancy-related were extracted from the original codebook is shown in Table 5-2. Moreover, the tree-based estimator was also implemented to rank the importance of the extracted features (Guyon & Elisseeff, 2003).

Table 5-2 The feature extracted from comfort database II

Feature name	Description
Air temperature	Average air temperature [℃]
Relative humidity	Relative humidity [%]
Air velocity	Average air velocity [m/s]
Clo	Clothing insulation [clo]
Radiant temperature	Mean radiant temperature [℃]
Met	Metabolic rate [met]

Additionally, instead of thermal sensation scale, thermal preference scale is used as labels, including cooler, warmer and no change. Moreover, SVM and RF with 5-fold cross-validation were also implemented to develop adaptive thermal comfort models with comfort database II and personal comfort model from the empirical study. Table 5-3 shows the parameters of SVM and RF tuned with cross-validation. Meanwhile, the thermal comfort models were also evaluated based on recall, precision and F1 scores.

Table 5-3 Parameters tuned in the algorithms

Algorithms	Parameters	Values
SVM	Penalty parameter C	1,10
	Kernel type	Gaussian, linear
RF	Tree depth	3,4
	Number of trees	50,100

5.2.2 Personal thermal comfort with the empirical study

As mentioned before, the comfort database is not suitable for developing personal thermal comfort models since the number of instances of each individual is limited. Therefore, in order to develop personal thermal comfort models capturing the fine-tuned differences among different individuals, a six-day empirical study were conducted to collect certain amount of data for each of the two healthy subjects in their mid-twenties (one male and one female) between 8/21/2018 and

8/27/2018 in an open-plan office building in Tongji University, Shanghai. A total of 171 instances were collected from a male subject and 151 instances were collected from a female subject. Last but not least, the models were developed with Python and the data collection system were written in C++.

5.2.2.1 Experimental setup

Figure 5-2 shows the 4.8 x 3 x 3.2 m^3 test bed setup and the correspondent interior 3D model where an air-conditioner is used to control the thermal environment. In addition, since the whole study was conducted in the evening, the effects of solar radiation is avoided. Moreover, in order to create different thermal environment conditions, the overhead air conditioner was controlled where the air temperature increases no more than 0.04°C/min on average. Before each session, the participants were asked to be seated for half an hour so as to ensure they have neutral thermal sensation in the beginning. Moreover, they were also asked to change the location to avoid draft risk due to supply air.

Figure 5-2 The open-plan office in the empirical study

Same as chapter 3, the experiment used the calibrated AMG8833 to measure the side face skin temperature as well as DHT22 for air temperature and relative humidity. Meanwhile, the micro-controller called ESP8266 with WIFI module was used to transmit data to a remote database platform called Thingspeak. The interval of data sampling from the sensor board is 5 minutes, which corresponds with the occupant feedback responses. In addition, even if the initial votes were collected with 7-point thermal sensation scale, in order to compare performances of the adaptive thermal comfort models developed with thermal comfort database II, thermal sensation votes were

converted to thermal preferences votes, including cooler, no change and warmer were collected. According to participants' responses, thermal sensation votes larger than 1 are cooler while thermal sensation votes less than -1 are warmer. Moreover, Figure 5-3(a) shows a participant status in the empirical study where there was a desktop fan on the shelves in the occupied zone. The fan was operated with on/off actions and can be rotated before the experiments started so as to avoid draft risk in the occupied zone. In addition, Figure 5-3(b) shows the proposed sensor board.

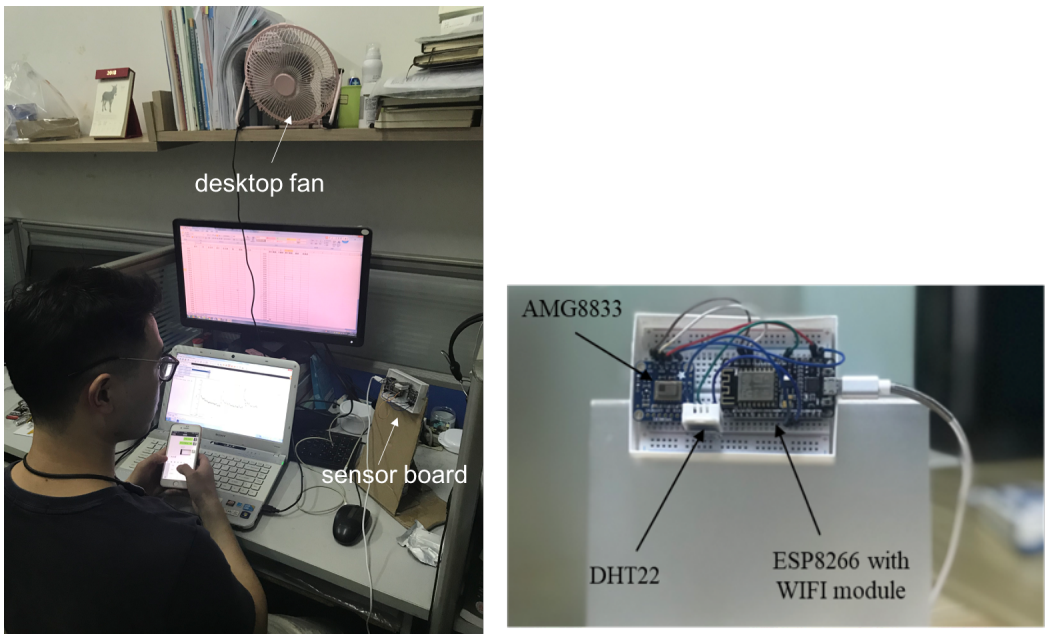

(a) participant status (b) the proposed sensor board

Figure 5-3 An experiment in the empirical study and the proposed sensor board

In addition, there were a total of 6 different sessions and each session last for at least 2 hours. Table 5-4 shows the temperature changes from the sensors during each session. Since the participants attended the study for all sessions, all levels of thermal sensations were reported at least once by participants and the majority vote belonged to "no change".

Table 5-4 Indoor air temperature change during each session

Date	**Start time**	**End time**	**Start temperature (℃)**	**End temperature (℃)**
8/21	19:45	22:00	23	30
8/23	19:35	22:00	24	30

8/24	19:45	22:00	25	30
8/25	19:00	22:00	24	30
8/26	20:00	22:00	25	30
8/27	19:00	22:00	24	30

5.2.2.2 Adaptive and personal thermal comfort models

In order to validate the two subjects are not outliers and their personal thermal comfort models can be representative, the data collected in the experiments were used as test set of the model trained with the comfort database II before classification. Since the thermal environment conditions in the experiment were within the range of those collected in the comfort database II where the climate is selected as "Humid subtropical", if test performances with the field data are similar to that achieved with the test set of comfort database II, it means the model trained with comfort database II is not overfitting or under-fitting on the field dataset. In other words, the two subjects have similar patterns among large group of occupants in the open-plan office buildings collected in the comfort database II. However, since skin temperature is not included as one of the features in the comfort database II, indoor air temperature and relative humidity are used for performance benchmark between the comfort database II and the field data. Last but not least, the same model configurations were used for developing individual thermal comfort models with field data where the feature set consists of indoor air temperature, indoor relative humidity and side face skin temperature. Additionally, in order to evaluate the adaptive individual thermal comfort models, the field dataset was also split into 80% for training and 20% for testing. Figure 5-4 describes the development of adaptive thermal comfort model with comfort database II and data from the empirical study.

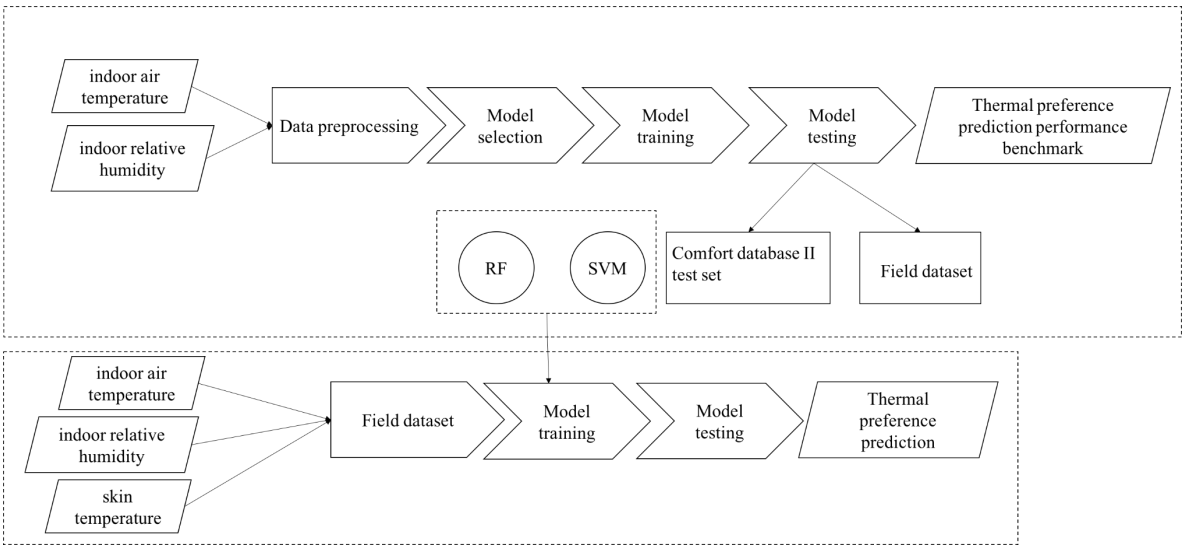

Figure 5-4 The adaptive thermal comfort model development pipeline

5.3 Development of Computational Fluid Dynamic Simulation

In order to analyse effects of the personalized cooling system on the overall indoor thermal environments and individual thermal comfort, a computational fluid dynamic (CFD) simulation was conducted to study airflow patterns and thermal stratification with the proposed fan-induced air-conditioning system in an open-plan office. The simulation was conducted with Ansys Icepak 18.2, which provides powerful electronic cooling solutions utilizing ANSYS Fluent solver for thermal and fluid flow analyses. Figure 5-5 shows the 4.8 x 3 x 3.2 m^3 3D model where a fan is located on the plane above the occupant while the overall thermal environment was controlled with the supply air and the workstation is built in the middle of the room left side.

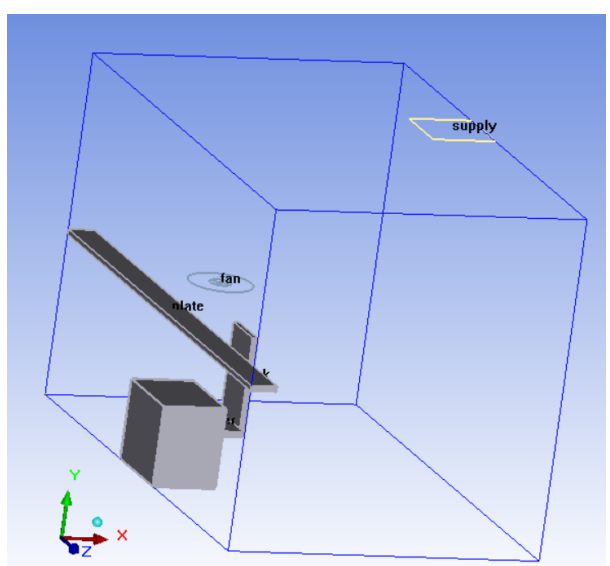

Figure 5-5 3D model in the CFD simulation

As mentioned before, a personalized fan disturbs airflow around the occupant, thus increasing forced convection between the indoor and outdoor as well as evaporation from human skin. As a consequence, the local indoor air temperature and skin temperature decrease and the occupant feels cooler with the operation of the fan. However, if the supply air temperature of the air-conditioning system is too high, it also results in discomfort since the temperature difference between indoor and outdoor is too small so that the forced convection may even increases the warm air flows into the local occupied zone. Therefore, the supply air temperature set-point shall not be too high so as to increase energy savings while compromise occupant thermal comfort. In Icepak, the object of a 2D internal circular fan with the diameter of 30 cm is installed 1.8 m above the floor with the fixed air velocity being 2.5m/s in order to avoid draft risk in the occupied zone, which is defined as the region within an occupied space between 75 and 1800 mm above the floor and more than 600 mm from the walls or fixed air-conditioning equipment. Additionally, the air temperature set-point changes from 24℃to 30℃ so as to analyze the changes of air flow patterns and thermal stratifications inside the room. In addition, the boundary conditions were designed based on the empirical study so that the simulations can be validated, as shown in Table 5-5. Lastly, Figure 5-6 and Figure 5-7 show the cross-sections where the temperature distributions and the thermal preference predictions were compared, respectively.

Table 5-5 The boundary conditions

Boundary conditions	**Values**
Supply air velocity	5 m/s
Supply air temperature	24℃, 26℃, 28℃, 30℃
Relative humidity	50%
Internal heat rate	100 W
Outdoor air(Ambient) temperature	30 ℃
Wall	Adiabatic
Window	Opening with ambient temperature
Fan velocity	2.5 m/s

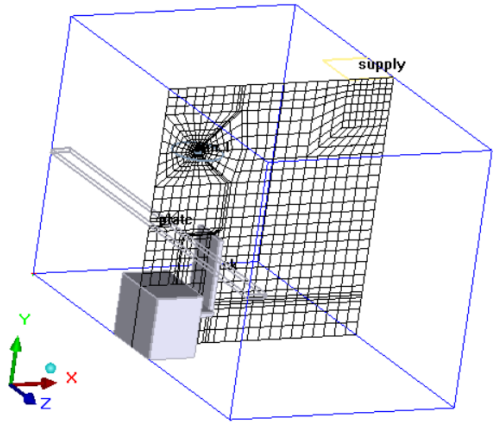

Figure 5-6 z=2.4 m

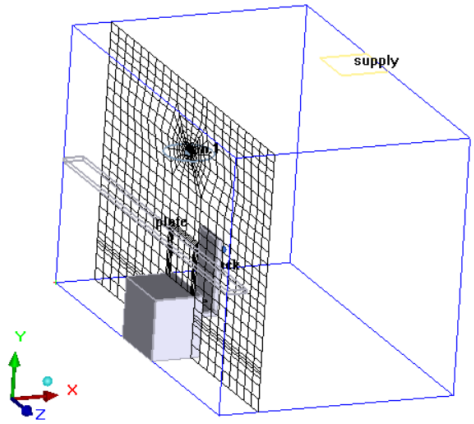

Figure 5-7 x=0.5 m

Moreover, *k-w* SST turbulence model and Semi-Implicit Method for Pressure Linked Equations (SIMPLE) algorithm was used to solve Navier-Stokes equations. Meanwhile, the hexahedral unstructured mesh was generated. Meanwhile, the mesh quality was evaluated with skewness, which is defined as how close the face or cell is to be equilateral or equiangular. Besides CFD simulation, with the individual thermal comfort models developed with the empirical study, the thermal comfort distribution with or without fans in the occupied zone can be simulated and compared. However, since the skin temperature cannot be simulated in the model and the relative humidity is set to be constant, the adaptive thermal comfort models used in the post-processing analysis of CFD simulation were developed with the air temperature only. Moreover, the simulation was validated with the empirical study by averaging the steady air velocities after continuous measurement for 1 minute with Swema EMP3500 anemometer around 0.8 m above the floor in several spots behind the seats without the fan operation when the temperature set-point was 24℃. In addition, the spot measurement map is shown in Figure 5-8. Among all spots, spot 2 and 3 were the workstations where the two participants were seated.

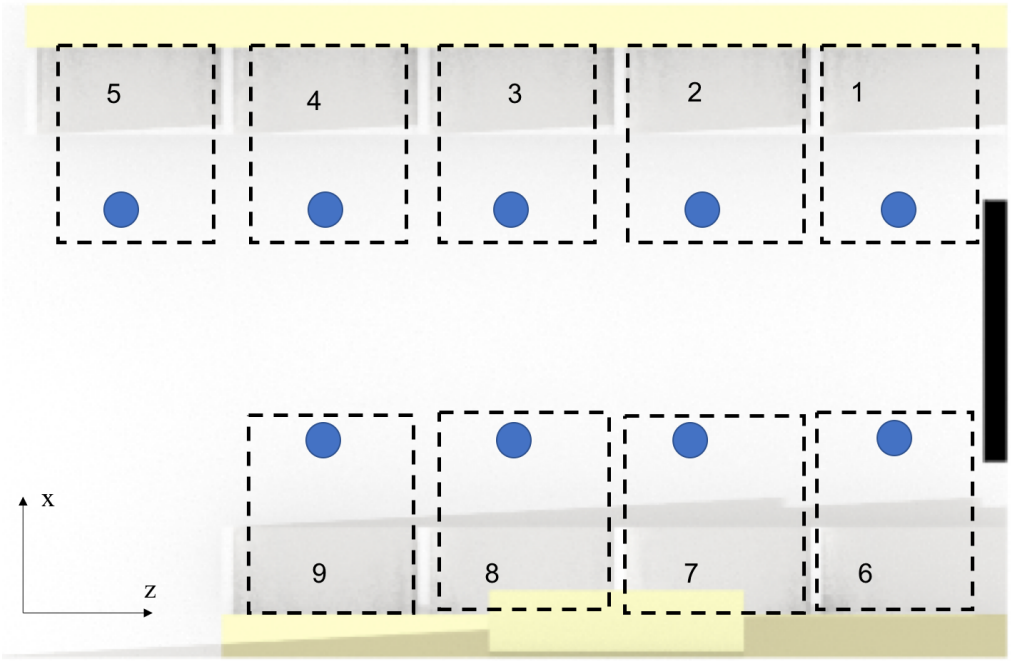

Figure 5-8 The spot measurement map for velocity

5.4 Result analysis

5.3.1 Adaptive and personal thermal comfort model performances

In terms of feature importance ranking, Table 5-6 shows the ranking score of all features in the comfort database II. As shown in the table, top three features are indoor air temperature, indoor mean radiant temperature, relative humidity. Since the empirical study was conducted in the evening, mean radiant temperature can be estimated to be the same as air temperature, the top features except clothing insulation related to thermal preferences are measured with the sensor board in the empirical study.

Table 5-6 Ranking score of all features

Air temperature	**Radiant temperature**	**Relative humidity**	**Clo**	**Air velocity**	**Met**
0.187	0.175	0.172	0.172	0.153	0.141

Meanwhile, Table 5-7 shows the average scores with cross-validation based on different parameter values of SVM and RF, respectively. As shown in the table, SVM with Gaussian kernel and the penalty number of 10 have the best performance. In addition, the prediction performance of the best model trained with training set of the comfort database II shows that the recall score on

the test set of comfort database II and the field data from the female and male subjects are 65.5%, 66%, 66%, respectively. Therefore, the performances with field dataset is similar to those with the comfort database II. In other words, the two subjects participating in the empirical study can be seen as representative subjects in the open-plan office buildings.

Table 5-7 Cross-validation benchmark among different model configurations

Model configuration	**Average recall score**
SVM, C=1, kernel = linear	66.4%
SVM, C=1, kernel = Gaussian	66.7%
SVM, C=10, kernel = linear	66.5%
SVM, C=10, kernel = Gaussian	67.8%
RF, Max_depth=3, number of tree=50	66.8%
RF, Max_depth=3, number of trees=100	66.8%
RF, Max_depth=4, number of tree=50	67.4%
RF, Max_depth=4, number of tree=100	66.5%

Moreover, Table 5-8 shows the performance benchmark between the individual thermal comfort models with the proposed feature set for both male and female subjects in the empirical study. As a result, models achieve high performances for both subjects with the proposed feature set. However, since the majority thermal preference vote in the empirical study is “no change”, most of the predictions are “no change”, which results in false positive classifications. Therefore, even if it is less regular to have thermal preference of “cooler” or “warmer” in the real air-conditioned open-plan office than “no change”, it is necessary to collect “cooler” or “warmer” preference feedbacks from occupants by expanding temperature range in the empirical study so as to collect a balanced dataset for the development of adaptive individual thermal comfort. Moreover, since such data-driven approach heavily relies on the data quality, it is better to develop semi data-driven adaptive thermal comfort models by combining the prediction results with machine learning algorithms and the results with domain knowledge (i.e. ASHRAE standards).

Table 5-8 Prediction performance with test set of field data

	Precision	**Recall**	**F1**
Female	81%	90%	85.3%
Male	94.2%	97%	95.6%

5.3.2 Results of CFD simulation

Figure 5-9 shows the validation results of the average air velocities between simulations and measurements. The standard deviation of the spot measurement and the simulation result

difference is 0.04, which indicates the simulated indoor thermal environment matches the empirical study and the thermal environment can be used to predict individual thermal comfort. Moreover, compared to ASHRAE Handbook-Fundamental that the velocity in the occupied zone should be lower than 0.25m/s so as to avoid discomfort due to draft risk (ASHRAE, 2013). However, even if the fan-induced air-conditioning system used in the study has higher velocity than 0.25 m/s in the occupied zone, since participants reported that they did not have draft discomfort during each session, the empirical study was still focused on the development of adaptive thermal comfort models with indoor air temperature, relative humidity and skin temperature only.

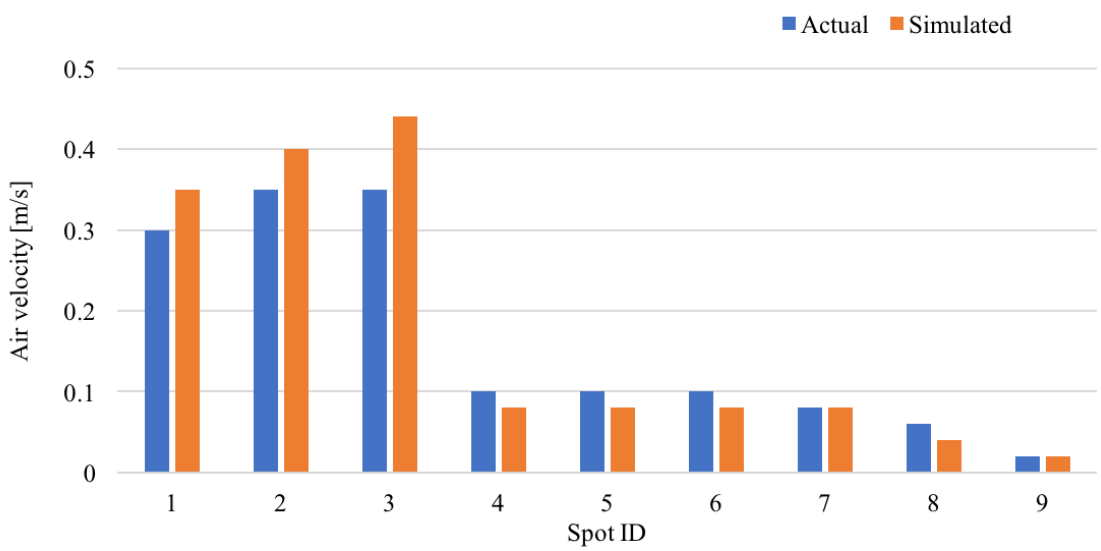

Figure 5-9 Velocity validation between the actual measurement and simulation values

Figure 5-10(a)-(h) show the air temperature distribution of the cross-section at z=2.4 m with or without the fan operation under different temperature set-points of supply air. As shown in the figures, the air temperature in the occupied zones increases as the temperature set-point increases. Moreover, when the air temperature set-point is no more than 28℃, the supply air is induced in the occupied zone so as to overcome thermal plumes with the help of the fan. However, when the temperature set-point increases further, there is no difference in the air temperature distribution with or without fan. Therefore, with the operation of the fan, the temperature set-point dead band can be increased so that more energy savings can be achieved by increasing temperature set-point without the compromise of individual thermal comfort.

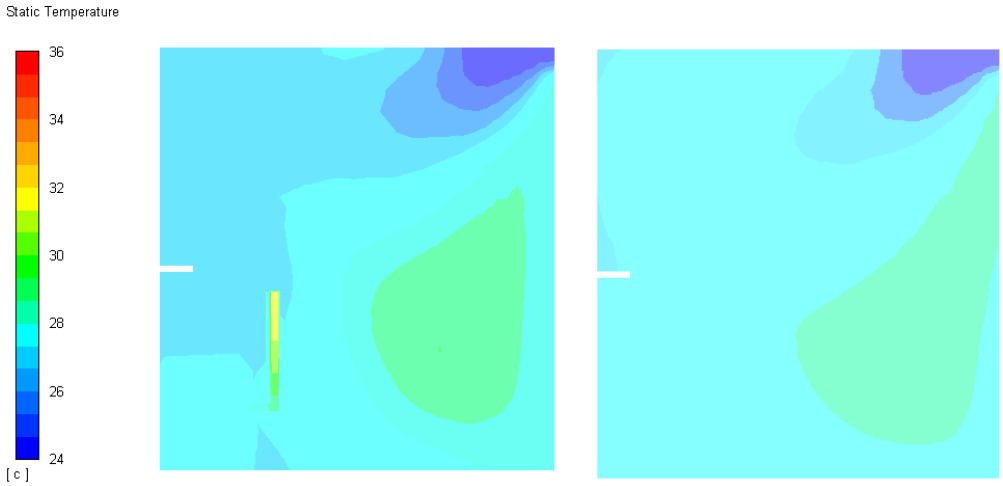

(a) fan = on, set-point = 24°C (b) fan = off, set-point = 24°C

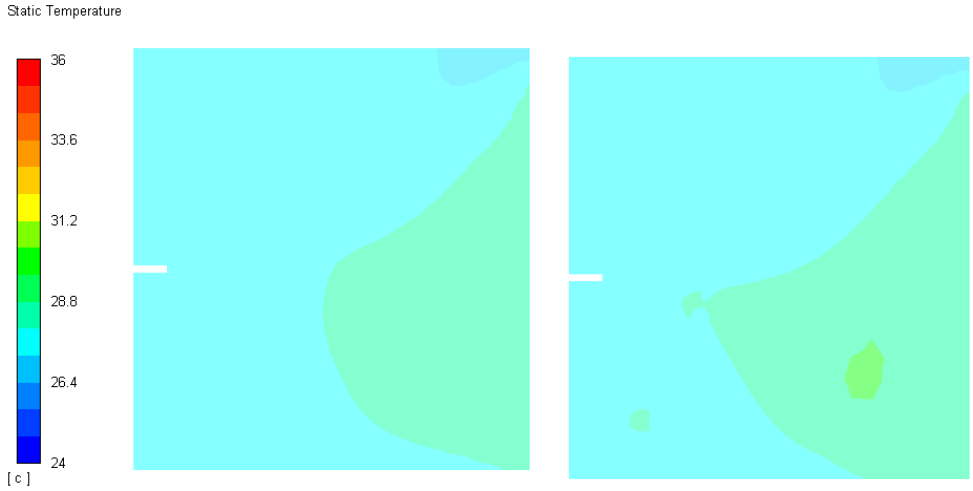

(c) fan = on, set-point = 26°C (d) fan = off, set-point = 26°C

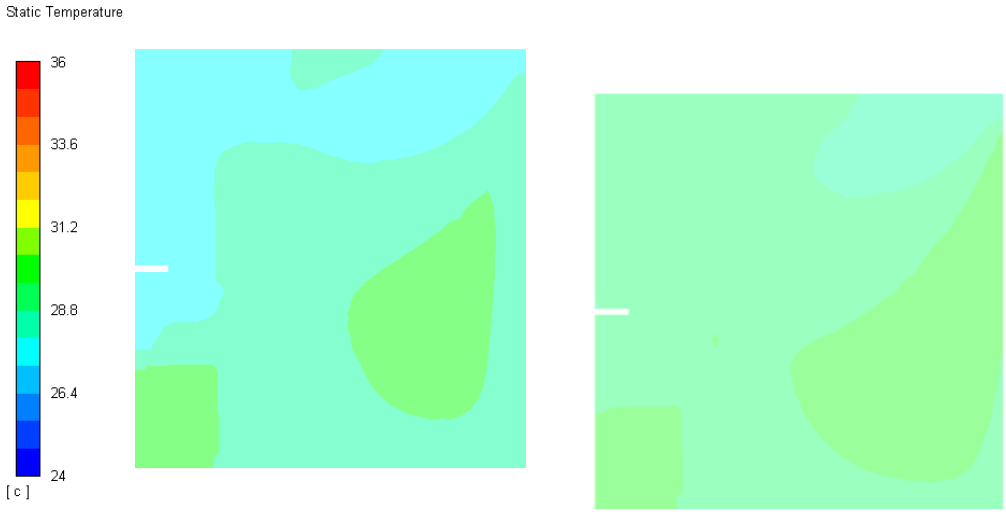

(e) fan = on, set-point = 28°C (f) fan = off, set-point = 28°C

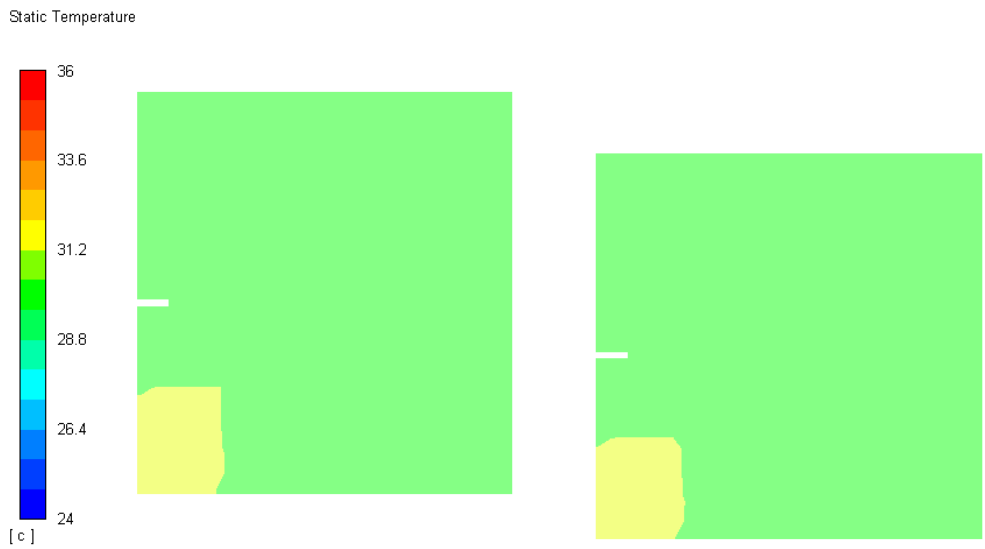

(g) fan = on, set-point = 30℃ (h) fan = off, set-point = 30℃

Figure 5-10 The air temperature distribution with or without the fan operation under different temperature set-points of supply air

Figure 5-11 shows the air temperature change along the fan axis from 0 to 1.5m height in the occupied zone, which further validates the advantage of using personalized fan. As shown in the figure, when the height is larger than 0.75 m and the temperature setpoint is no more than 28℃, under the same temperature setpoint, the air temperature without fan operation is higher than that with fan operation at the same height level. Moreover, the temperature difference with or without fan increases as the temperature setpoint decreases. As a result, there is little difference with or without fan operation when the temperature setpoint increases to 30℃. Moreover, the temperature differences between the ankle and neck under different temperature set-points are all less than 3℃ to ensure thermal comfort while the temperature gradient increases suddenly at the height of 0.8 m due to the heat generation of occupants.

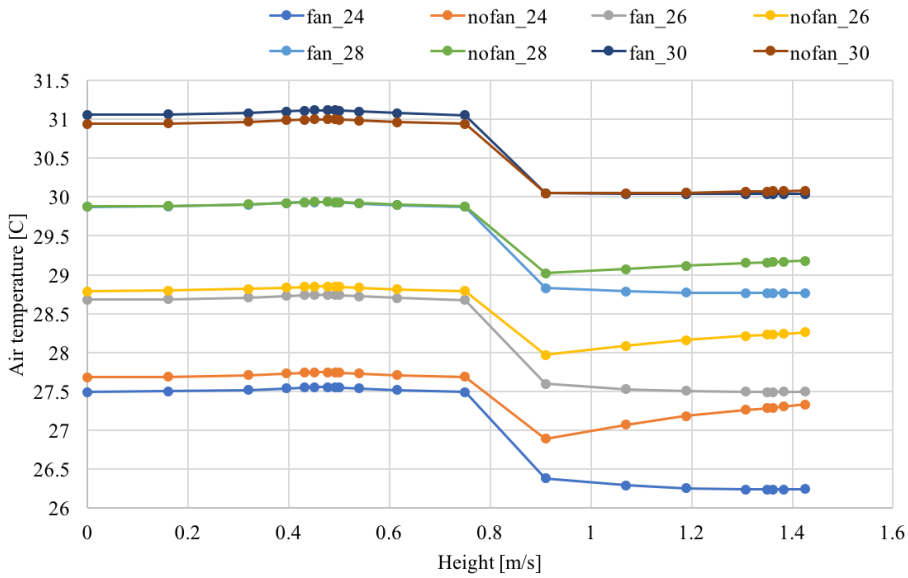

Figure 5-11 The air temperature change along the fan axis from 0 to 1.5m height in the occupied zone

In addition, Figure 5-12 (a)-(h) show the thermal preference distribution in the occupied zone for both female and male subjects. As mentioned before, even if the accuracy of both adaptive individual thermal comfort models is high, most of the prediction results are "no change" due to imbalanced dataset in the empirical study. According to Nie et al. (2011), when the clothing insulation is 0.3 clo and subjects have sedentary activity, the upper limit of thermal neutral temperature is 29 ℃. Therefore, a combination of the data-driven approach and rule-based approach was implemented as follow:

$$\text{Thermal preference} = \left(\begin{cases} \text{cooler} & \text{if temperature} < 24 \text{ or pred} = \text{cooler} \\ \text{no change} & \text{if } 23 < \text{temperature} < 29 \text{ or pred} = \text{no change} \\ \text{warmer} & \text{temperarture} > 28 \text{ or pred} = \text{warmer} \end{cases}\right) \quad (5\text{-}1)$$

As a result, when the temperature setpoint is lower than 28℃, even if the temperature distribution differs with various setpoints, there is little difference with or without fan operation. Moreover, most of the area in the occupied zone is classified as "no change", which means the occupants are satisfied with the thermal environment. In addition, when the temperature setpoint increases to 28℃, the area in the occupied zone classified as "cooler" with fan operation is smaller than that without fan operation. However, there is no difference with or without fan operation

when the temperature setpoint is 30℃. Therefore, in terms of individual thermal preferences, the temperature setpoint can be increased to 28℃ but no more than 30℃ in order to maintain individual thermal comfort.

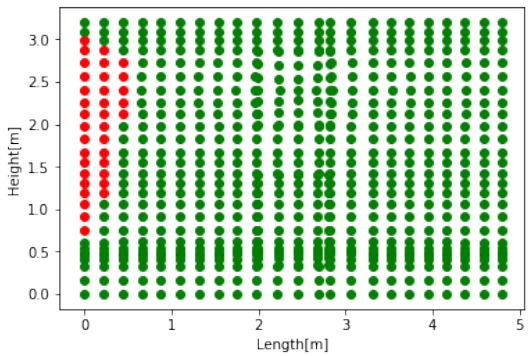

(a) fan = on, set-point = 24℃

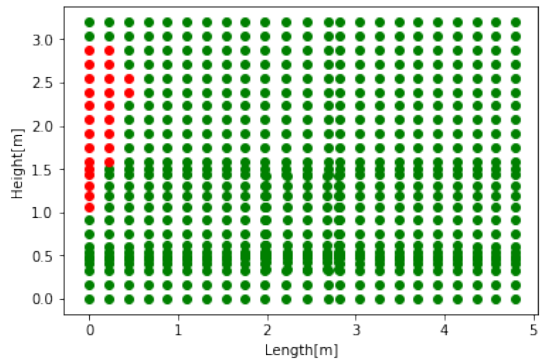

(b) fan = off, set-point = 24℃

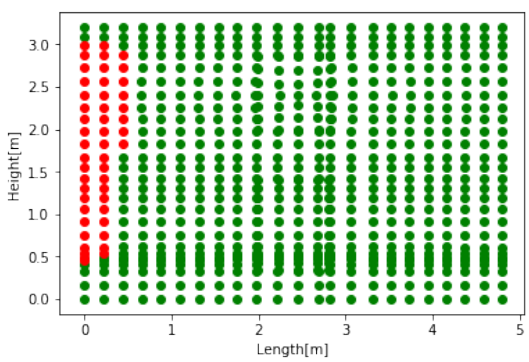

(c) fan = on, set-point = 26℃

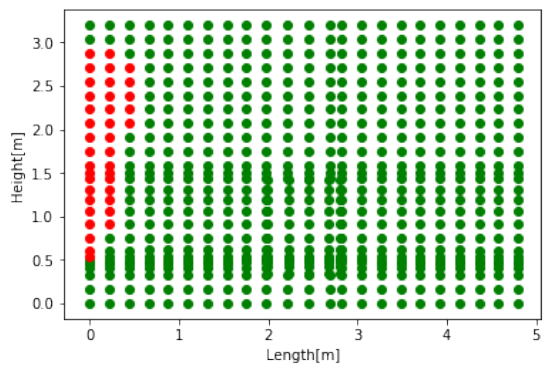

(d) fan = off, set-point = 26℃

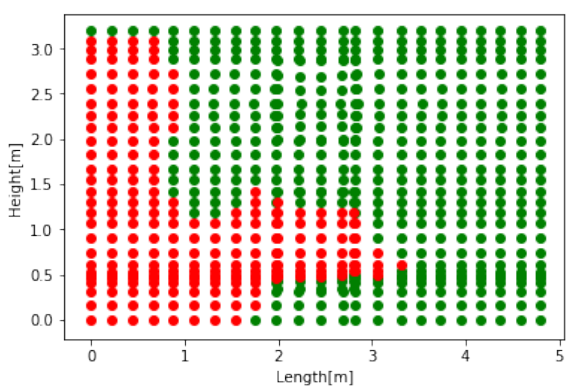

(e) fan = on, set-point = 28℃

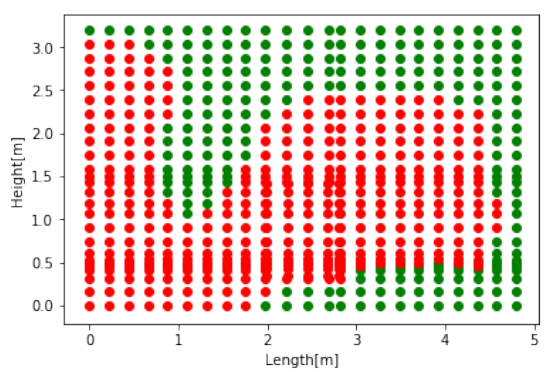

(f) fan = off, set-point = 28℃

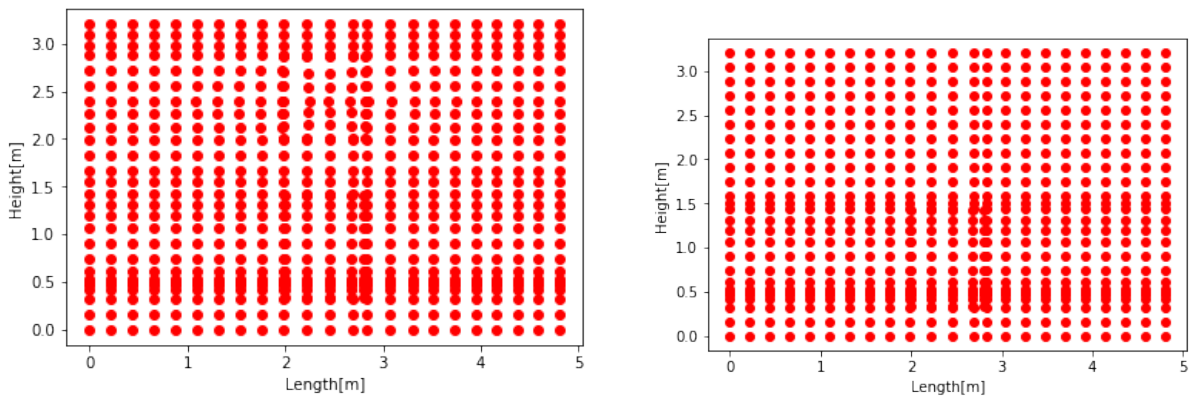

(g) fan = on, set-point = 30℃ (h) fan = off, set-point = 30℃

Figure 5-12 the thermal preference distribution in the occupied zone

5.5 Discussions

This research aims to evaluate the benefits of thermal comfort improvements with the proposed local-fan induced air-conditioning system by applying data-driven adaptive thermal comfort models into a CFD simulation. In addition, two machine learning classification methods: SVM and RF were implemented to develop adaptive thermal comfort models with comfort database II as well as the data collected from an empirical study conducted in an open-plan office in Shanghai. As a result, with comfort database II, the adaptive thermal comfort models developed with SVM outperform those developed with RF. Moreover, since the local fan helps induce the supply air into the occupied zone, the thermal preference prediction being “no change” has larger proportion in the occupied zone with fan operation than that without fan operation when the supply air temperature set-point is increased to 28℃. However, there is no significant difference between the thermal preference distribution with or without the fan operation when the supply air temperature set-point has increased to the same as the outdoor air temperature. The proposed method could be further applied to study adaptive thermal comfort of different individuals under different HVAC systems.

The combination of data-driven approach and simulation used in the study realizes the thermal preference distribution analysis in the occupied zone with different temperature set-points. Even if CFD simulation is slow to converge with complex models, it provides an opportunity to do parametric analysis spatially and temporally in a more fine-grained way. In addition, compared to static thermal comfort models implemented with CFD simulations in the previous work such as

PMV, adaptive thermal comfort models are more realistic to describe thermal comfort. However, since the empirical study was conducted with the temperature set-point range between 24℃ and 30℃, the dataset collected based on the empirical study was very imbalanced where the majority vote is "no change". As a result, the predictions misclassify other thermal preferences. Hence, the empirical study should be conducted with larger temperature set-point range to make the dataset more balanced and the combination of the data-driven model and the domain knowledge shall be integrated to enhance prediction performances. Moreover, since effects of radiation and velocity on thermal comfort are not investigated in the study, the models can only be used to predict thermal comfort in the core zone of the space with acceptable air velocity. Therefore, future study could also be conducted to take radiation and velocity into account.

5.6 Conclusions

In order to evaluate the benefits of thermal comfort improvements with the proposed local-fan induced air-conditioning system, this study has conducted a six-day empirical study in an open-plan office in Shanghai. Additionally, the machine learning algorithms of SVM and RF were used for the development of adaptive thermal preference models with the comfort database II and the field data. Moreover, the models were applied into a CFD simulation for performance benchmark on thermal preference distribution in the occupied zone with or without the fan operation.

As a result, with the feature set of indoor air temperature, indoor relative humidity and skin temperature, the precision, recall and F1 score of the prediction models for the female subject are 81%, 90% and 85.3%, respectively. Meanwhile, the precision, recall and F1 score of the prediction models for the female subject are 94.2%, 97% and 95.6%, respectively. In addition, based on CFD simulation results, since the fan helps induce the supply air into the occupied zone when the supply temperature set-point is no more than 28℃, the proportion of the area in the occupied zone where the thermal preference prediction is "no change" with fan operation is larger than that without fan operation. In future, more balanced dataset for the development of thermal preference prediction models should be collected. Meanwhile, the proposed method of combining data-driven models and simulation models could be applied into developing different individuals and evaluating effects of different HVAC systems on thermal comfort in future.

Chapter 6 Energy co-simulation study of the task-ambient cooling control based on synthetic thermal preference distributions

Table 6-1 Nomenclature

Abbreviation	Description
GMM	Gaussian mixture model
KDE	Kernel density estimation
BIC	Bayesian information criterion
comfort database	Global thermal comfort database
CFD	Computational fluid dynamics
DX cooling coil	Direct expansion cooling coil unit

6.1 Overview of energy simulation for the task-ambient cooling system

The CFD simulation has illustrated that the proposed task-ambient cooling system could benefit from energy savings while still maintaining thermal comfort when temperature set-point is no more than 28℃. Besides CFD simulation, energy simulation of the proposed task-ambient cooling system was conducted with adaptive thermal comfort models developed with the comfort database. Unlike CFD simulation focused only on a single person, the energy co-simulation aims to evaluate energy savings based on the optimization of the ambient conditioning system with constraints of thermal comfort levels in an open plan office room. Moreover, same as CFD simulation, thermal preferences were used for describing occupant thermal comfort.

6.2 The development of thermal preference distribution used in Energyplus

Even if individuals have different thermal preferences under the same thermal environment in air-conditioned open-plan offices, most of the thermal preference distributions can be approximated as Gaussian distributions where the majority are satisfied while only a few of occupants vote for either being uncomfortably warmer or uncomfortably cooler. Therefore, in order to simulate different thermal preferences in a shared space, Figure 6-1 shows the diagram of developing the synthetic thermal preference distributions with the comfort database. As shown in the figure, the pipeline is comprised of clustering of the thermal environments in the database, thermal preference distribution synthesis and sampling.

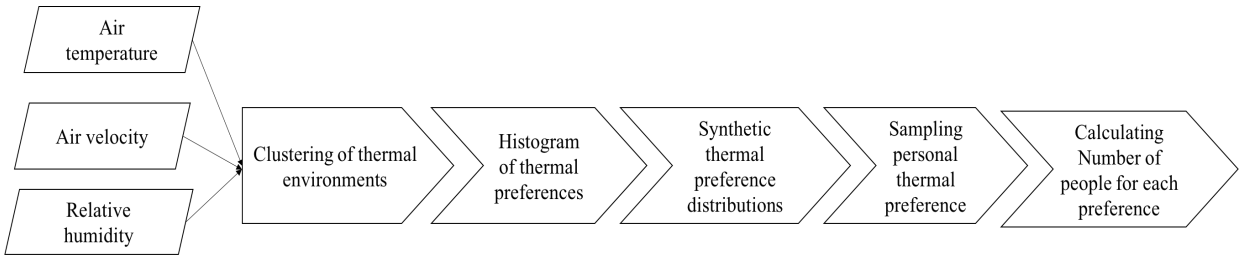

Figure 6-1 The diagram of developing the synthetic thermal preference distributions

The subset of the comfort database was used where a total of 2354 instances were collected. In the subset, both the task-ambient cooling system consists of ceiling fans and the centralized cooling and the conventional centralized cooling system were operated. Among them, 815 instances were collected with the task-ambient cooling system while 1539 instances were collected with the conventional centralized cooling system.

Since the indoor environments is expected to vary a bit in the database, the unsupervised clustering is implemented so as to cluster the similar thermal environments into a single cluster and see the histogram of thermal preference in each cluster. Moreover, same as clustering method in chapter 2, similar thermal environment conditions, including air velocity, air temperature and relative humidity were clustered with GMM where the number of clusters were selected based on BIC score. After clustering, the histogram of thermal preference under each cluster was developed so that in the energy model, the number of occupants for each thermal preference can be sampled from the synthetic thermal preference distribution with kernel density estimation (KDE) under the given cluster. Moreover, since Energyplus cannot simulate the thermal environment changes after fans were operated, the subset without fan operations and the subset with fan operations were clustered, respectively.

6.2.1 Thermal preference synthesis algorithms:

As mentioned before, the synthetic thermal preference distributions were approximated with Gaussian distribution. Therefore, kernel density estimation (KDE) was implemented based on the dataset. Kernel *K(x; h)* is a function controlled by the bandwidth parameter h, which can be seen as smoothing parameter controlling the tradeoff between bias and variance in the result. Given the kernel form, the density estimate at a point y within a group of points x_i; *i=1..N* is given by

$$\rho_K(y) = \sum_{i=1}^{N} K\left(\frac{y-x_i}{h}\right) \quad (6\text{-}1)$$

where *h* is bandwidth.

Same as previous chapter, the bandwidth is tuned with 5-fold cross-validation from 5 candidate values between 0.1 and 1.

6.3 Co-simulation with the proposed optimization framework

The energy simulation was implemented with the co-simulation between energyplus and python. The one-story small office building was simulated in Shanghai from July 1st to August 31st. The total ground floor area is 512 m^2 and 5 thermal zones are built. Moreover, the cooling is supplied with packaged DX cooling coil and the heating is supplied with gas heating coil. The 3D rendering and floor plan are shown in Figure 6-2 and Figure 6-3. The co-simulation framework was developed in (Zhang et al., 2018).

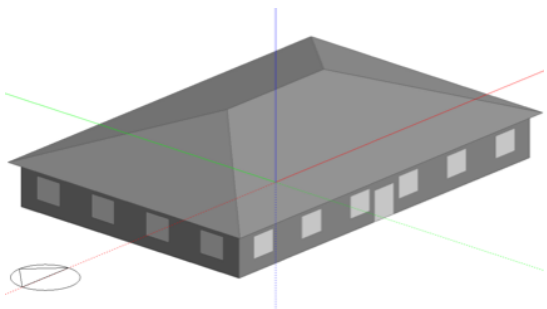

Figure 6-2 3D rendering of the reference building

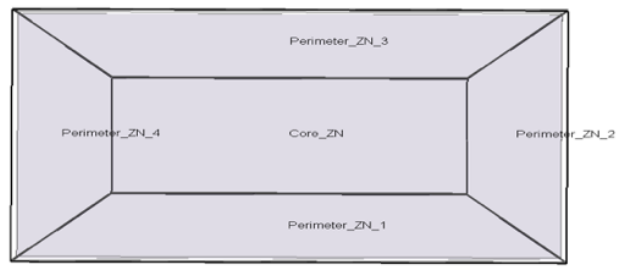

Figure 6-3 Thermal zones of the building

The baseline simulation and optimized simulation were both conducted with dual setpoint schedule where the heating set-point is constant to be 21 ℃ while the cooling set-point differs over a day. The baseline cooling set-point schedule is the default schedule where the cooling set-point is predetermined and fixed to be 22℃ (Figure 6-4) while the proposed cooling set-point schedule is based on the optimization framework. Moreover, Figure 6-5 shows the occupancy schedules used in the simulations.

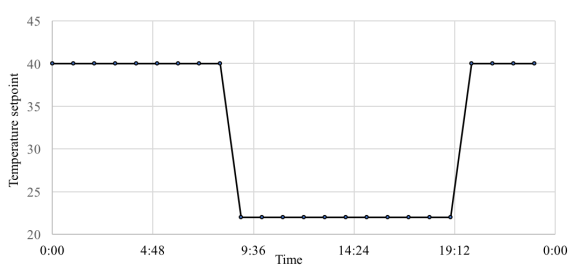

Figure 6-4 The fixed temperature set-point schedule

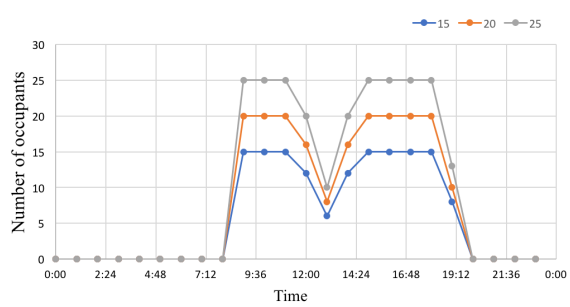

Figure 6-5 The occupancy schedules

Besides baseline set-point schedule, Figure 6-6 shows the flow diagram of the proposed optimization framework. As shown in the diagram, two histogram models were implemented to simulate the conditions when the personalized fan is operated or not, respectively. Moreover, the initial cooling set-point is 24℃ and the setpoint is increased by 1℃ or no change when the space is occupied at each time step. However, it is assumed that the reason for turning on fans is only because of feeling warm. Meanwhile, it is also assumed that all the fans will be turned off when determining a new set-point.

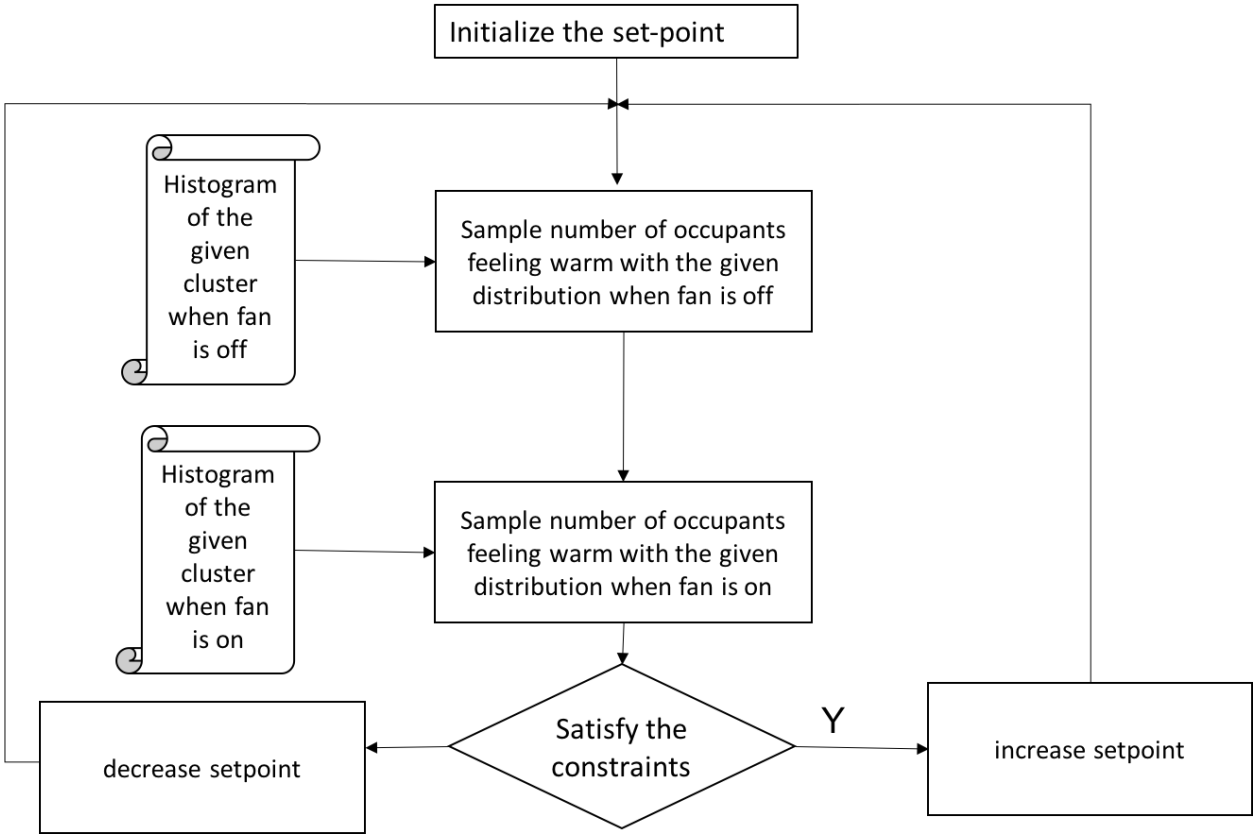

Figure 6-6 Flow diagram of the proposed optimization framework

Meanwhile, the control law of the proposed optimization framework is shown below:

Objective function:

$$min.\ Sensible\ cooling\ loads$$

subjective to:

$$\%\ of\ occupants\ feeling\ warm < \delta \quad (6\text{-}2)$$

$$20\ ℃ < cooling\ set\text{-}point\ t < 30\ ℃ \quad (6\text{-}3)$$

As shown in the control law, the cooling set-point is controlled every 30 minutes since the indoor air temperature and relative humidity always change slower than set-points due to thermal mass. In addition, since the objective function of sensible cooling loads is monotonously decreasing when cooling set-point is increasing, it will reach the optimal state under the constraints after several time steps in the end. Meanwhile, if constraints are not satisfied that the number of occupants feeling warm exceeds the threshold or the setpoint exceeds the boundary, the updating will decrease 1℃ for this time step. The threshold can be tuned with benchmark of multiple simulations.

6.4 Result analysis

6.4.1 Synthetic thermal preference distributions

With comfort database, 7 clusters were selected for the subset without fans and 6 clusters were selected for the subset with fans on according to the lowest BIC scores. Table 6-1 shows the mean of each cluster and the correspondent best bandwidth for KDE. Figure 6-7 shows the histogram of thermal preference distribution within each cluster for the subset without fans, respectively. As shown in the table, except cluster 1, different clusters have similar indoor air temperature and indoor air velocity. Since no fans were deployed for the system, the air velocity is smaller than 0.2 m/s. However, relative humidity varies a lot among different clusters. This may result from lack of humidity control in common office buildings. In addition, except cluster 1, thermal preference histograms have shown that the majority vote is “no change” in different clusters. Moreover, compared to thermal preference vote of “want cooler”, all clusters but cluster 1 have more votes for “want warmer”. This may be because of low air temperature. Therefore, there is a potential to increase cooling set-point to save energy while maintaining occupant thermal comfort.

Table 6-2 The centroid of each cluster and the correspondent optimal bandwidth

Velocity[m/s]	Temperature [°C]	Relative humidity [%]	Optimal bandwidth
0.56	25.78	58.65	1
0.11	23.76	63.34	0.18
0.16	23.96	56.12	0.56
0.12	22.59	67.19	0.56
0.13	23.7	38.1	1
0.12	23.91	58.6	0.18
0.12	23.13	48.85	0.18

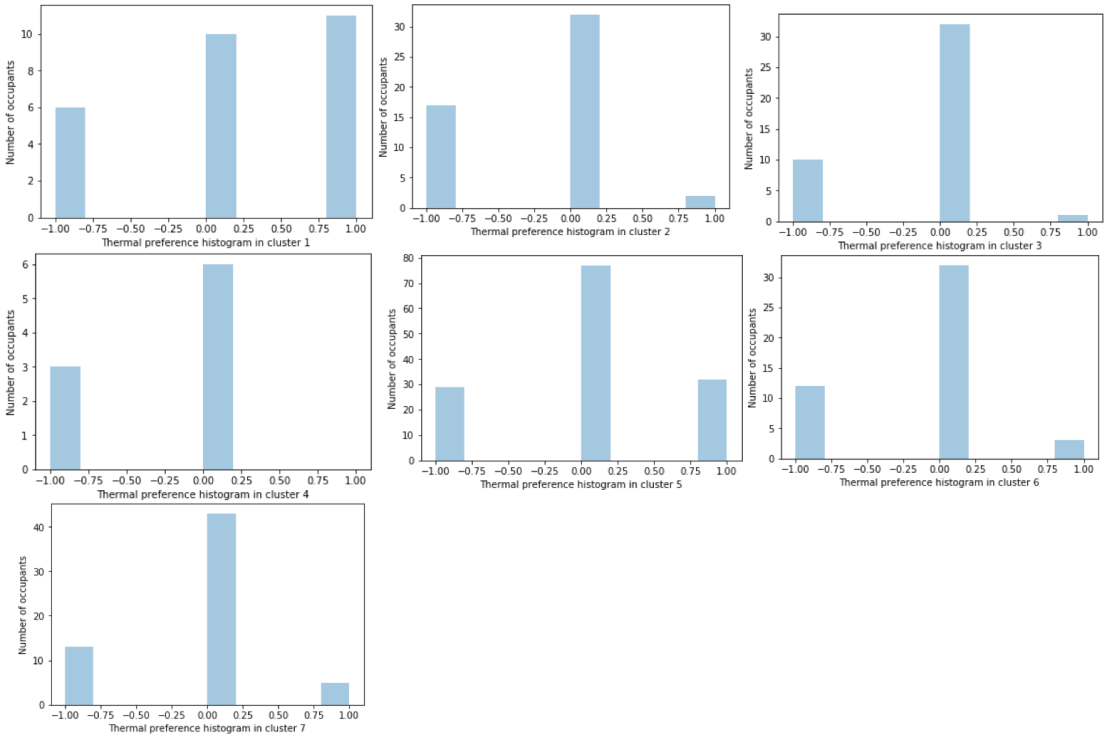

Figure 6-7 The histogram of thermal preference distribution

In addition, Table 6-3 shows the means of the clusters and Figure 6-8 shows the histograms of the thermal preference distribution within each cluster for the subset with fans on, respectively. As shown in the table, the mean air velocity of each cluster is higher than those in most of clusters without fans, which is because of the operation of fans. Meanwhile, the table has illustrated the average value of the mean air temperature in each cluster with fans on is larger than that without fans. In addition, the figure has illustrated that the majority votes within each cluster is “no change”, which means such task-ambient cooling system has potential to increase air temperature to save energy while still maintaining high thermal comfort level.

Table 6-3 The centroid of each cluster and the correspondent optimal bandwidth

Velocity[m/s]	Temperature [°C]	Relative humidity [%]	Optimal bandwidth
0.31	25.98	66.24	0.56
0.34	26.72	58	0.32
0.47	25.85	63.09	0.32
0.28	24.83	75.68	0.32
0.17	23.5	44.54	0.56
0.19	25.36	63.27	0.32

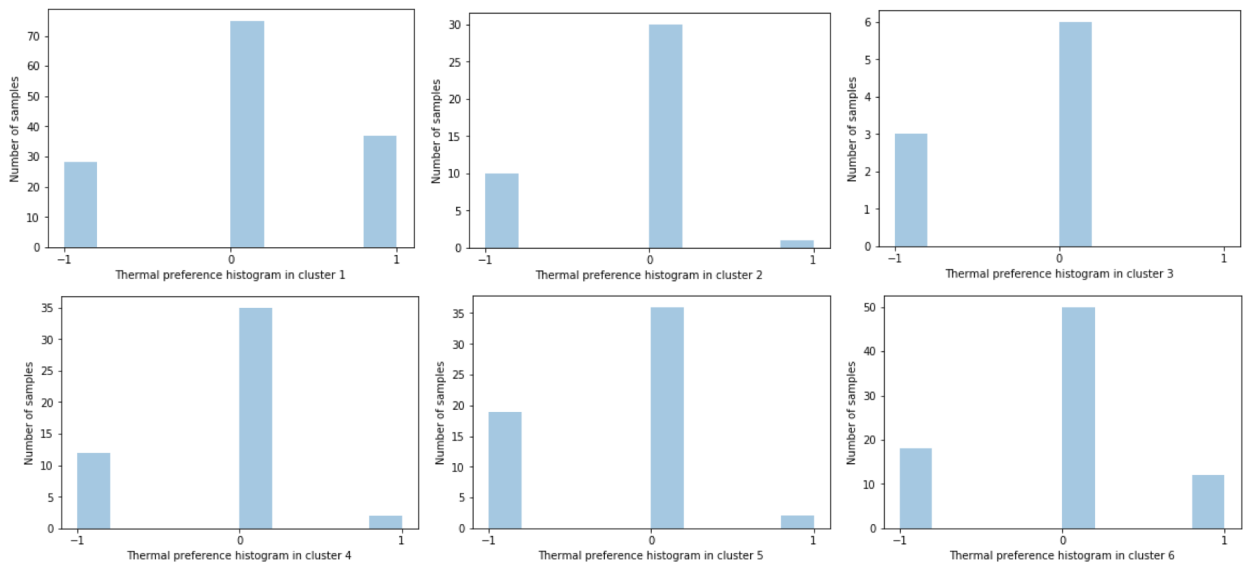

Figure 6-8 The histogram of thermal preference distribution

6.4.2 Energy benchmark of the proposed optimization framework

In terms of energy benchmark between baseline control and the proposed control framework, HVAC electric demand power was used to evaluate the energy performances. Meanwhile, the percentage of occupants feeling warm is controlled within 10%. As a result, Figure 6-9 shows the comparisons of HVAC electric demand power between baseline models and the proposed models with different occupancy schedules. As shown in the figure, the proposed framework has achieved 5%, 5.3% and 5.6% demand power reduction compared to baseline models with 90% of occupants are comfortable when the number of occupants are 15, 20 and 25, respectively. Therefore, it is meaningful to develop the task-ambient system which not only creates comfortable local environment for each occupant but also improves the overall energy performance.

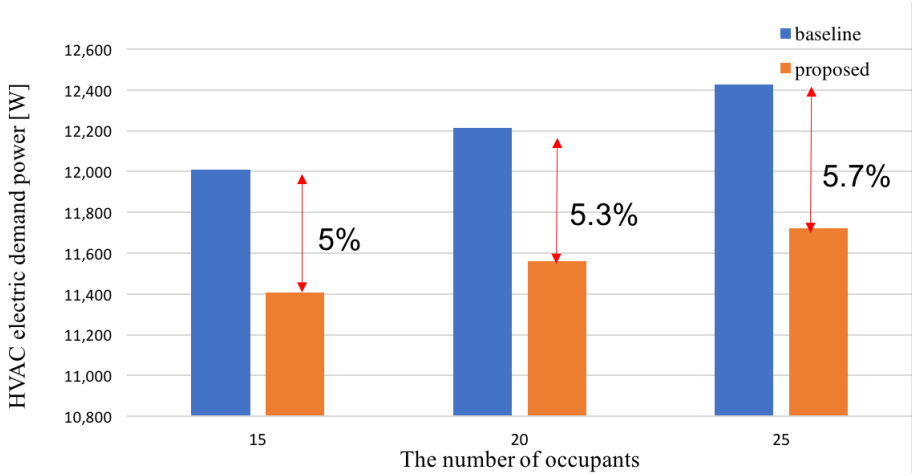

Figure 6-9 HVAC electric demand power between baseline and the proposed models

6.5 Discussions of the proposed framework through energy models

The simulation study has evaluated the energy performances of the task-ambient cooling system consisting of ceiling fans and the centralized cooling system. In order to simulate individuals, have different thermal preferences in a shared office space, the synthetic thermal preference distributions have been developed so as to generate "virtual" occupants with various thermal preferences in the same thermal environments. The results have validated that the proposed optimization framework could achieve 5.3% of HVAC electric demand power savings on average without the compromise of occupant thermal comfort. However, there are still limitations in the energy models. Firstly, due to lack of data, instead of local fans such as desktop fans, this energy simulation has applied comfort database where the task-ambient cooling system is comprised of ceiling fans and the ambient conditioning system. Since ceiling fans cannot be seen as task conditioning system, the thermal preference distributions based on comfort database may be different from those based on the experiments. In addition, same as the experimental study, the objective function may be improved to not only take sensible cooling loads but also take latent cooling loads into consideration.

6.6 Conclusions

This chapter has conducted an optimized framework to maximize the energy efficiency and thermal comfort with the local fan-induced air-conditioning system by updating the cooling set-point. In order to evaluate energy performances with the proposed optimization framework, a co-simulation of a typical office building was conducted with Energyplus. In order to simulate the

fact that different people have different thermal preferences in Energyplus, synthetic thermal preference distributions were generated with kernel density estimation in each cluster based on GMM clustering of the thermal environment given in the comfort database. The results have shown that with the proposed framework, the proposed framework has achieved 5%, 5.3% and 5.6% demand power reduction compared to baseline models with 90% of occupants are comfortable when the number of occupants are 15, 20 and 25, respectively. In future, more work could be done to optimize the energy performances in the simulation by updating other parameters such as relative humidity.

Chapter 7 Conclusions and future work

This dissertation has proposed and evaluated a new integrative task-ambient cooling control system featuring personal thermal comfort models with non-intrusive sensing techniques for open-plan office spaces with two comfort databases, two experimental studies, one field study, one CFD simulation study and one energy simulation study. All of these studies have proved the main hypothesis as well as sub-hypotheses. Moreover, some future work was proposed so as to enhance the performances of the interactive task-ambient conditioning system controlled with personal comfort models with the non-intrusive sensing systems in real open-plan office buildings.

7.1 Contributions

This dissertation has mainly three contributions. One of the major contributions is the introduction to an interactive and automatic task-ambient cooling system consisting of task conditioning system and an ambient conditioning system. The task conditioning system is controlled with the personal thermal comfort model for each individual. Moreover, the ambient conditioning is controlled with the optimization of the sensible cooling loads under the constraints of multiple fan statuses as well as individual thermal comfort predictions. With the task conditioning system, each occupant has access to adjusting their own local thermal environment without interrupting others'. The second contribution is the development of the non-intrusive sensing system for personal thermal comfort inference, including the infrared temperature sensor called AMG8833 and the indoor air temperature and relative humidity sensor called DHT22. Compared to existing products in the market such as infrared cameras and wrist bands, the proposed sensing system is much more cost-effective while still maintaining the merits of non-intrusiveness and high accuracy. Another major contribution is to implement various machine learning algorithms into the real system and the simulation, including adaptive and personal thermal comfort models and Q-learning based temperature set-point control. Compared to baseline such as PMV, the proposed system has higher prediction performances on the same dataset and can adapt individual thermal preferences better than the conventional prediction model. Meanwhile, the proposed adaptive and personal thermal comfort models can be applied into different simulation tools, including data-driven simulator, CFD simulator, Energyplus simulator, etc. These three major contributions have been dedicated to thermal comfort research and provided insights into future work on adaptive and personal thermal comfort-based HVAC system control in the real open-plan office environments.

7.2 Summary of findings

This dissertation has mainly demonstrated a newly data-driven task-ambient cooling system with adaptive and personal thermal comfort models and non-intrusive sensing techniques in an open-plan office. The findings here are summarized into five categories which corresponding to each chapter. These findings are useful for future study on similar topics.

Chapter 2 has conducted a data-driven simulation of comfort-based temperature set-point control system with tabular Q-learning has been conducted. In addition, the thermal comfort model is a classification model with machine learning methods of KNN, SVM and RF to predict thermal sensation and indicate thermal comfort. Compared to baseline of PMV, the recall of the thermal comfort model with the tree algorithms has increased 6.3%, 5.4% and 5.4%, respectively. Besides the statistical thermal comfort models, the reinforcement learning-based controller with tabular Q-learning control can reach the optimal comfort state after training with 100 episodes and generate the optimal policy from whatever start state in terms of indoor thermal environment.

Chapter 3 has conducted a non-intrusive sensing technique, which consists of temperature, humidity sensor called DHT22, and an infrared camera named FLIR B8400. Two statistical thermal comfort models for female subject and male subject were developed with SVM and RF based on a 6-day experimental study conducted in Shanghai, respectively. As a result, the models trained with the feature set consisting of indoor air temperature, indoor relative humidity, side face skin temperature and clothing surface temperature, and with linear kernel SVM have achieved the best performances. The precision, recall and f1 scores of the best model was 100% on test data of female subjects and 97.5%, 96.1%, 95% on that of male subjects, respectively.

Chapter 4 has conducted a field study to evaluate an integrative TAC system featuring non-intrusive sensing technique and automatic control with adaptive thermal models developed with SVM in an open-plan office room. The temperature set-point of ambient system was then maximized with constraints of individual thermal sensations and the number of operated fans. As a result, the recall scores of the thermal sensation model and satisfaction model with the data from all female subjects are 84.7% and 76.5%, respectively. Meanwhile, the recall scores of the thermal sensation and satisfaction models with the data from all male subjects are 87% and 82.5%, respectively. However, the performances of individual thermal models vary among different individuals. Moreover, five 3-hour sessions have shown that the proposed system could achieve 9.6% of HVAC energy savings on average compared with the baseline.

Chapter 5 has conducted a six-day empirical study in an open-plan office in Shanghai. Additionally, the machine learning algorithms of SVM and RF were used for the development of adaptive thermal preference models with the comfort database II and the field data. Moreover, the models were applied into a CFD simulation for performance benchmark on thermal preference distribution in the occupied zone with or without the fan operation. As a result, with the feature set of indoor air temperature, indoor relative humidity and skin temperature, the precision, recall and F1 score of the prediction models for the female subject are 81%, 90% and 85.3%, respectively. Meanwhile, the precision, recall and F1 score of the prediction models for the female subject are 94.2%, 97% and 95.6%, respectively. In addition, based on CFD simulation results, since the fan helps induce the supply air into the occupied zone when the supply temperature set-point is no more than 28℃, the proportion of the area in the occupied zone where the thermal preference prediction is "no change" with fan operation is larger than that without fan operation, which demonstrates the potential to reduce energy by increasing the cooling set-point.

Chapter 6 has conducted an optimized framework to maximize the energy efficiency and thermal comfort with the local fan-induced air-conditioning system by updating the cooling set-point. In order to evaluate energy performances with the proposed framework, a co-simulation of a typical office building was conducted. Meanwhile, the synthetic thermal preference prediction distributions were generated with kernel density estimation based on GMM clustering of given the thermal environment given in the comfort database II. The results have shown that with the proposed framework, the average HVAC electric demand power decreases by 5.3% compared to the baseline while at least 90% of occupants feel comfortable without cooling set-point change.

7.3 Hypotheses revisit

Main hypothesis: An interactive task and ambient cooling system will provide higher energy savings than a conventional air-conditioning (ambient only) system, while maintaining thermal comfort in open-plan office buildings.

- Sub-hypothesis 1: Task conditioning system can be operated automatically based on the personal thermal comfort models.
- Sub-hypothesis 2: Personal thermal comfort model can be continuously improved by collecting occupant override actions.
- Sub-hypothesis 3: An interactive task-ambient cooling system can be optimized by minimizing sensible cooling loads with the constraints of personal thermal comfort.

The main hypothesis has been tested to be true with the field study in the test office room in Shanghai as well as energy co-simulations. The results have illustrated that HVAC energy savings could achieve 9.6% on average in the field study and 5.3% on average in the simulations with the proposed task-ambient controls. In addition, since one of the constraints for the ambient conditioning system optimization ensures that at least 80% and 90% of occupants feel thermally comfortable with the operation of the personalized fans in the field study and co-simulations, respectively. In addition, the sub-hypothesis 1 has been tested with the field study and identified that it is possible to provide task conditioning automatically to individual occupants with the initial personal comfort models and wireless task conditioning system, which consists of the non-intrusive sensing system as well as the WIFI plug. Moreover, in terms of sub-hypothesis 2, it has been proved true based on the phase 2 of the field study where participants who provided override actions saw better improvements in their correspondent personal comfort models. Last but not least, as mentioned in the discussion on main hypothesis, sub-hypothesis 3 have both been tested to be true with the experimental study as well as the energy simulation.

Besides the findings to support hypotheses, another interesting finding is that the majority votes for thermal sensation and thermal preference are neutral and no change in the typical open-plan office buildings, respectively. This illustrates that the thermal comfort difference between different people is limited and only a few occupants are not neutral or satisfied in the open-plan office buildings. Therefore, in order to improve fine-tuned thermal comfort management, the personalized/task heating and cooling system is of great significance to be developed.

7.4 Limitations and future work

This research contributes to innovations in adaptive and personal thermal comfort research to realize higher energy savings and thermal comfort improvements. Even if the findings have proved the advantages of the proposed task-ambient cooling system, some limitations have also pointed to the future research directions:

- Deployment in a large-scale office buildings with multiple thermal zones

  In the field study, only one thermal zone equipped with a simple split air-conditioner has been tested with the proposed system. Therefore, the proposed task-ambient cooling system shall be implemented in a multi-zone open-plan office area with more complex centralized air-conditioning systems such as VAV system. Moreover, since personal thermal comfort is affected by other factors such as radiation and air velocity, it could be more comprehensive if

the field study was conducted in different conditions with different scenarios so as to evaluate the performances of the interactive task-ambient cooling system. In addition, the analysis of cost benefit shall be conducted to evaluate the savings in a large-scale open office building.

- Implementation with a more complex optimization control algorithm

In this study, only one constrained single objective function was implemented in the optimization of the ambient conditioning system both in the field study and the energy simulations. However, since the current optimization function only contains sensible cooling loads, the performances of energy savings and thermal comfort improvements may not be optimal. Future work should be conducted to develop a constraint-free multi-objective optimization or reinforcement learning control with a reward function based on both energy savings and thermal comfort. Moreover, in the field study, it was assumed that only more than 80% of fans were turned on, the ambient temperature cooling set-point needs decreasing. However, the threshold of the percentage needs more experiments for fine-tuning and it could be better if occupants are provided with feedback access so that they could give more detailed thermal comfort responses.

- Continuous collection of new data to improve performances of personal comfort models

In the field study, performance benchmark between the initial thermal comfort models and the updated thermal comfort models were limited with only 2-day comparison for 5 subjects. In order to evaluate the performances of the updating mechanism, more data from override actions shall be collected. Therefore, continuous collection shall be conducted for a longer period. Moreover, the current updating mechanism is rule-based since the override action with a personalized fan is only on/off. Such rule-based updating mechanism could be improved with more override options besides on/off (i.e. change of fan speed).

References

Abbas M. (2015). Frequently asked questions: Infrared Grideye sensor. Panasonic Inc. Retrieved from https://cdn.sparkfun.com/assets/2/0/3/f/b/faqs_grideye_v1.0.pdf

Abdallah, M., Clevenger, C., Vu, T., & Nguyen, A. (2016). Sensing occupant comfort using wearable technologies. *In Construction Research Congress* 2016 (pp. 940-950).

Altman, N. S. (1992). An introduction to kernel and nearest-neighbor nonparametric regression. *The American Statistician*, *46*(3), 175-185.

Andersen, M. P., Fierro, G., Kumar, S., Chen, M., Truong, L., Kim, J., Arens E.A., Zhang H., Raftery P., & Culler, D. E. (2015). Well-connected microzones for increased building efficiency and occupant comfort. *In Proceedings of the 2nd ACM International Conference on Embedded Systems for Energy-Efficient Built Environments* (pp. 121-122). ACM.

ASHRAE, A. S. (2013). Standard 55-2013. *Thermal environmental conditions for human occupancy*, 12.

Auffenberg, F., Stein, S., & Rogers, A. (2015, June). A personalised thermal comfort model using a Bayesian network. In *Twenty-Fourth International Joint Conference on Artificial Intelligence*.

Auliciems, A., & Szokolay, S. V. (1997). Thermal comfort. PLEA.

Bauman, F. S., & Arens, E. A. (1996). Task/ambient conditioning systems: engineering and application guidelines.

Bratman, G. N., Hamilton, J. P., & Daily, G. C. (2012). The impacts of nature experience on human cognitive function and mental health. *Annals of the New York Academy of Sciences*, *1249*(1), 118-136.

Choi, J. H. (2010). CoBi: bio-sensing building mechanical system controls for sustainably enhancing individual thermal comfort. Thesis.

Cosma, A. C., & Simha, R. (2018). Thermal comfort modeling in transient conditions using real-time local body temperature extraction with a thermographic camera. *Building and Environment*, 143, 36-47.

Cosma, A. C., & Simha, R. (2019). Machine learning method for real-time non-invasive prediction of individual thermal preference in transient conditions. *Building and Environment*, 148, 372-383.

Dai, C., Zhang, H., Arens, E., & Lian, Z. (2017). Machine learning approaches to predict thermal demands using skin temperatures: Steady-state conditions. *Building and Environment*, 114, 1-10.

Dalamagkidis, K., Kolokotsa, D., Kalaitzakis, K., & Stavrakakis, G. S. (2007). Reinforcement learning for energy conservation and comfort in buildings. *Building and environment*, 42(7), 2686-2698.

D'Oca, S., Hong, T., & Langevin, J. (2018). The human dimensions of energy use in buildings: A review. Renewable and Sustainable Energy Reviews, 81, 731-742.

Dounis, A. I., & Caraiscos, C. (2009). Advanced control systems engineering for energy and comfort management in a building environment—A review. *Renewable and Sustainable Energy Reviews*, *13*(6-7), 1246-1261.

Faber, V. (1994). Clustering and the continuous k-means algorithm. *Los Alamos Science*, *22*(138144.21).

Fanger, P. O. (1970). Thermal comfort. Analysis and applications in environmental engineering. *Thermal comfort. Analysis and applications in environmental engineering.*

Földváry, V., Cheung, T., Zhang, H., de Dear, R., Parkinson, T., Arens, E., ... & Li, P. (2018). Development of the ASHRAE Global Thermal Comfort Database II. *Building and Environment*.

Gao, G., Li, J., & Wen, Y. (2019). Energy-Efficient Thermal Comfort Control in Smart Buildings via Deep Reinforcement Learning. *arXiv preprint arXiv:1901.04693*.

Ghahramani, A., Jazizadeh, F., & Becerik-Gerber, B. (2014). A knowledge based approach for selecting energy-aware and comfort-driven HVAC temperature set points. *Energy and Buildings*, 85, 536-548.

Ghahramani, A., Castro, G., Karvigh, S. A., & Becerik-Gerber, B. (2018). Towards unsupervised learning of thermal comfort using infrared thermography. *Applied Energy*, 211, 41-49.

Ghahramani, A., Castro, G., Becerik-Gerber, B., & Yu, X. (2016). Infrared thermography of human face for monitoring thermoregulation performance and estimating personal thermal comfort. *Building and Environment*, *109*, 1-11.

Guo, J., & Niedermeier, R. (2007). Invitation to data reduction and problem kernelization. *ACM SIGACT News*, *38*(1), 31-45.

Guyon, I., & Elisseeff, A. (2003). An introduction to variable and feature selection. *Journal of machine learning research*, *3*(Mar), 1157-1182.

Han, D., Li, R., Wang, F., Sun, Z., Moon, S., Gong, Z., & Zhang, Y. (2017). Study on indoor thermal environment control based on thermal sensation prediction. *Procedia Engineering*, 205, 3072-3079.

Hasan, M. H., Alsaleem, F., & Rafaie, M. (2016). Sensitivity study for the PMV thermal comfort model and the use of wearable devices biometric data for metabolic rate estimation. *Building and Environment*, 110, 173-183.

Huang, C. C. J., Yang, R., & Newman, M. W. (2015). The potential and challenges of inferring thermal comfort at home using commodity sensors. *In Proceedings of the 2015 ACM International Joint Conference on Pervasive and Ubiquitous Computing* (pp. 1089-1100). ACM.

Jain, M., Kalaimani, R. K., Keshav, S., & Rosenberg, C. (2018). Using personal environmental comfort systems to mitigate the impact of occupancy prediction errors on HVAC performance. *Energy Informatics*, *1*(1), 60.

Jazizadeh, Farrokh, and Wooyoung Jung. "Personalized thermal comfort inference using RGB video images for distributed HVAC control." Applied Energy 220 (2018): 829-841.

Kohavi, R. (1995, August). A study of cross-validation and bootstrap for accuracy estimation and model selection. In Ijcai (Vol. 14, No. 2, pp. 1137-1145).

Kim, J., Schiavon, S., & Brager, G. (2018). Personal comfort models–A new paradigm in thermal comfort for occupant-centric environmental control. *Building and Environment*, *132*, 114-124.

Klein, L., Kwak, J. Y., Kavulya, G., Jazizadeh, F., Becerik-Gerber, B., Varakantham, P., & Tambe, M. (2012). Coordinating occupant behavior for building energy and comfort management using multi-agent systems. *Automation in construction*, *22*, 525-536.

Lee, J. H., Kim, Y. K., Kim, K. S., & Kim, S. (2016). Estimating clothing thermal insulation using an infrared camera. Sensors, 16(3), 341.

Lee, S., Bilionis, I., Karava, P., & Tzempelikos, A. (2017). A Bayesian approach for probabilistic classification and inference of occupant thermal preferences in office buildings. *Building and Environment*, *118*, 323-343.

Li, D., Menassa, C. C., & Kamat, V. R. (2018). Non-intrusive interpretation of human thermal comfort through analysis of facial infrared thermography. *Energy and Buildings*, *176*, 246-261.

Li, W., Zhang, J., Zhao, T., & Liang, R. (2018). Experimental research of online monitoring and evaluation method of human thermal sensation in different active states based on wristband device. *Energy and Buildings*.

Li, W. (2016). Numerical and Experimental Study of Thermal Stratification in Large Warehouses (Doctoral dissertation, Concordia University).

Liaw, A., & Wiener, M. (2002). Classification and regression by randomForest. *R news*, *2*(3), 18-22.

Liu, W., Lian, Z., & Deng, Q. (2015). Use of mean skin temperature in evaluation of individual thermal comfort for a person in a sleeping posture under steady thermal environment. *Indoor and Built Environment*, 24(4), 489-499.

Lu, S., Wang, W., Lin, C., & Hameen, E. C. (2019). Data-driven simulation of a thermal comfort-based temperature set-point control with ASHRAE RP884. *Building and Environment*.

Lu, S., Wang, W., Wang, S., & Cochran Hameen, E. (2019). Thermal Comfort-Based Personalized Models with Non-Intrusive Sensing Technique in Office Buildings. *Applied Sciences*, *9*(9), 1768.

Lu, S., Wang, S., Cochran Hameen, E., Shi, J., & Zou, Y. Comfort-based integrative HVAC system with non-intrusive sensing in office buildings. Computer-aided Architectural design research in Asia, CAADRIA 2019, Wellington, New Zealand, April 2019.

Lu, S., Cochran Hameen, E., Zou, Y. An interactive building control for the integrative HVAC system featuring personalized cooling in office buildings. ASHRAE annual conference, Kansas City, Missouri, June 2019.

Lu, S., Cochran Hameen, E. Simulation Study of Individual Thermal Comfort with the Integrated Personalized Fan and VAV System. Building simulation, Rome, Italy, September 2019.

Makhoul, A., Ghali, K., & Ghaddar, N. (2013). Desk fans for the control of the convection flow around occupants using ceiling mounted personalized ventilation. *Building and Environment*, *59*, 336-348.

Mathworks. (2015). ThingSpeak Communication Library for Arduino, ESP8266 and ESP32. Retrieved from https://github.com/mathworks/thingspeak-arduino

McCracken I. (2014). Ouimeaux: Open Source WeMo Control. Retrieved from https://github.com/iancmcc/ouimeaux

Nie, C., Gao, Y., Li, B., & Tan, M. (2011, June). Research of summer comfortable temperature in Air-conditioning Room in Chongqing, China. In *2011 International Conference on Remote Sensing, Environment and Transportation Engineering* (pp. 4318-4321). IEEE.

Pedregosa *et al.*, Scikit-learn: Machine Learning in Python, JMLR 12, pp. 2825-2830, 2011.

Reynolds, D. (2015). Gaussian mixture models. *Encyclopedia of biometrics*, 827-832.

Schwarz, G. (1978). Estimating the dimension of a model. *The annals of statistics*, *6*(2), 461-464.

Roelofsen, P. (2011). Evaluation of draught in surgical operating theatres: proposed revision to (NEN)-EN-ISO-7730. Journal of Facilities Management, 9(1), 64-70.

Ranjan, J., & Scott, J. (2016). ThermalSense: determining dynamic thermal comfort preferences using thermographic imaging. *In Proceedings of the 2016 ACM International Joint Conference on Pervasive and Ubiquitous Computing* (pp. 1212-1222). ACM.

Sekhar, S. C. (1995). Higher space temperatures and better thermal comfort—a tropical analysis. *Energy and Buildings*, *23*(1), 63-70.

Sekhar, C., & Zheng, L. (2018, August). Study of an integrated personalized ventilation and local fan-induced active chilled beam air conditioning system in hot and humid climate. In *Building Simulation* (Vol. 11, No. 4, pp. 787-801). Tsinghua University Press.

Shetty, S. S., Hoang, D. C., Gupta, M., & Panda, S. K. (2019). Learning desk fan usage preferences for personalised thermal comfort in shared offices using tree-based methods. *Building and Environment*, *149*, 546-560.

Sim, S. Y., Koh, M. J., Joo, K. M., Noh, S., Park, S., Kim, Y. H., & Park, K. S. (2016). Estimation of thermal sensation based on wrist skin temperatures. *Sensors*, 16(4), 420.

Smola, A. J., & Schölkopf, B. (2004). A tutorial on support vector regression. *Statistics and computing*, *14*(3), 199-222.

Sutton, R. S., & Barto, A. G. (2018). *Reinforcement learning: An introduction*. MIT press.

Kohavi, R. (1995). A study of cross-validation and bootstrap for accuracy estimation and model selection. In IJCAI.

Wang, Z., Parkinson, T., Li, P., Lin, B., & Hong, T. (2019). The Squeaky wheel: Machine learning for anomaly detection in subjective thermal comfort votes. *Building and Environment*, *151*, 219-227.

Zhang, H., Arens, E., Kim, D., Buchberger, E., Bauman, F., & Huizenga, C. (2010). Comfort, perceived air quality, and work performance in a low-power task–ambient conditioning system. *Building and Environment*, 45(1), 29-39.

Zhang, Z., Chong, A., Pan, Y., Zhang, C., Lu, S., & Lam, K. P. (2018). A deep reinforcement learning approach to using whole building energy model for hvac optimal control. In 2018 Building Performance Analysis Conference and SimBuild.

Zhao, J. (2015). Design-build-operate energy information modeling for occupant-oriented predictive building control. Thesis.

Zhao, Q., Cheng, Z., Wang, F., Jiang, Y., & Ding, J. (2014, August). Experimental study of group thermal comfort model. In *2014 IEEE international conference on automation science and engineering (CASE)* (pp. 1075-1078). IEEE.

Appendices

Appendix A: Codes & Metadata

- Chapter 2 : https://github.com/lusiliang93/thermal_model_rp884.git
- Chapter 3 : https://github.com/lusiliang93/personalized-cooling-fan.git
- Chapter 4 : https://github.com/lusiliang93/bae_personal_comfort.git
- Chapter 5 : https://github.com/lusiliang93/cfd_task-ambient_cooling.git
- Chapter 6 : https://github.com/lusiliang93/energyplus_task-ambient_cooling.git

Appendix B: Experimental data for chapter 3 and 5

Chapter 3: Thermal comfort data from male subject

temperature	humidity	skin	clothing	comfort	sensation
17.4	37.9	28.2	21.7	0	0
17.3	40.2	28.9	22.4	0	0
23.5	35.2	31.8	26.9	-1	1
26.8	33.1	33	27.8	-1	1
26.9	31.4	33.7	28.4	-2	2
27.8	32.1	33.7	28.7	-2	2
28.7	30.4	34.3	29.7	-3	3
29.3	29.6	35.3	30.7	-3	3
28.1	30.8	33.9	29.2	-2	2
25.3	33.1	34.8	28.2	-1	1
24	34.4	33.4	26.5	0	0
22.6	32.7	32.8	25.1	0	0
22.2	27.6	31.9	25	-1	1
22.5	26.8	31.9	24.7	0	0
22.4	27.2	31.9	25.3	0	0
22.5	28.3	31.8	25.6	0	0
22.7	30	32.3	26.1	0	0
26.6	28.3	33.4	28.6	-1	1
29.6	26.3	33.6	30.4	-3	3
28	26.9	33.6	29	-1	1
26.9	28.1	33.8	28.8	1	0
26.5	28.6	33.5	28.5	-1	1
26.2	29	33.8	28.4	-1	1
26	25	33.8	28.2	0	0
25.2	24	33.6	26.9	1	0
25	22.4	33.8	26.9	1	0
24.6	25	33.8	26.6	1	0
24.3	26.1	33.4	25.9	1	0
19.3	34.5	30.9	23.1	1	0
19.2	34.9	30.9	22.9	1	0
19.1	35.3	31.2	22.5	0	0
19.9	35.1	31.2	24	0	0

21.5	34.2	31.9	25	-1	1
23.1	32.3	33.3	26.5	-1	1
23.7	31.7	32.4	25.9	-1	1
25.2	30.8	32.8	26.9	-1	1
26.1	29.9	33.6	27.1	-2	2
27.5	29	34.6	29.3	-2	2
27.6	29.1	34.1	29.6	-3	3
28.2	29.5	34.1	29.8	-3	3
26.1	30.4	33.9	28.8	-2	2
24.9	32.3	33.8	28.7	-2	2
22.5	32.4	32.8	25.6	0	0
20.9	32.2	32.5	25	1	0
17.7	40.5	28.4	22.4	-1	-1
19.6	39.5	29.2	23.1	0	0
20.6	38.6	30.1	24.3	-1	1
23.8	34.4	31.9	27.2	-1	1
26.4	31.5	32.6	28.2	-2	2
27.8	30.2	33.7	29.1	-3	3
28.9	29.5	34.4	30.4	-3	3
27.6	30	34.1	29	-2	2
20.7	36.1	31.7	23.8	1	0
22	36.5	31.9	25.2	0	0
23.6	34.7	32.4	25.8	-1	1
27.1	30.7	33.3	28.3	-2	2
28	30.6	33.6	29.2	-2	2
28.4	30	34	29.7	-3	3
25	32.6	33.5	27.5	-1	1
24.4	31.4	34.4	28.5	0	1
19.2	51.3	29.9	24.2	0	0
19.4	51.3	30.2	23.5	0	0
20.2	49.6	30.6	24.9	1	0
21.9	45	32.1	26	1	0
22.3	44.3	32.1	26	0	0
23.4	43	32.5	26.4	-1	1
25.3	39.5	33.9	28.6	-1	1
26.7	39.1	33.6	29.1	-1	1
27.4	36.9	33.6	30	-2	2
28.3	35.9	34.1	29.4	-2	2
28.9	36	34.4	30.5	-2	2
27.5	37.1	34.1	28.9	-1	1

26.1	38.8	33.6	27.3	0	0
24.7	41	33.3	26.3	1	0
29.6	34	33.9	30.7	-3	3
25.9	38.7	34.5	30.3	0	0
25.6	39.5	33.1	28.9	-1	1
24	38.6	32.6	27.6	-1	-1
24.6	42.1	32.7	28.1	0	0
24.7	39.3	32.7	27.4	0	0
21	35.1	31.3	24.7	-2	-2
19.8	35.9	31.3	23.4	-3	-3
18.7	36.1	30.6	23.6	-3	-3
25.2	35.3	32.8	27.6	1	0
25	35.8	33.4	28.2	1	0
27	34.1	33.9	29.3	-1	1
28.1	34.5	33.8	29.4	-1	1
28.5	33.1	34.4	30.1	-1	1
26.5	35	34	28.6	0	0
25.1	37.3	33.7	28	1	0
24.3	38.9	33.5	27	1	0
21.4	51.2	31.1	24.2	1	0
21.2	52	31.8	24.7	1	0
22.2	48.7	31.9	25	0	0
22.9	47.1	32.6	27	-1	1
24.6	43.2	32.7	27	-1	1
25.6	41.2	33.3	27.5	-2	2
27.8	39	33.6	29.9	-3	3
28.5	37.6	34.3	30.1	-3	3
25.4	42	34	28.2	-1	1
24	45.1	33.7	27.1	0	0
23	47.3	32.7	26.4	1	0
22.1	51	32.6	26.9	1	0
22	50.6	32.6	25.8	1	0
20.9	49.6	31.5	23.9	-1	-1
18.7	54.3	31.1	23.7	-1	-1
20	58	31.1	24.6	-1	-1
20.4	57.6	32.1	24.8	0	0
21	61.2	30.4	24.5	1	0
21.3	59.7	30.4	26.1	1	0
24.7	54.1	32.5	27.3	0	0
26.8	49.8	33.4	28.8	-1	1

28.4	46.9	33.4	29.9	-1	1
29.2	44.7	33.8	30.5	-1	1
30	42.4	34.2	31.6	-2	2
30.6	40.5	34.1	31.4	-2	2
29.9	41.1	33.8	31	-1	1
27.9	43.7	33.7	29.3	0	0
27.1	45.3	33.9	29.2	0	0
26.5	45.7	34.7	29.4	1	0
17.3	43.4	28.5	20.8	-2	-2
16.6	41.6	28	20.5	-3	-3
15.7	41.1	27.5	19.9	-3	-3
17.9	48.6	29	23.1	-2	-2
19	51.7	29.3	23.5	-1	-1
19	54.8	29.4	24.1	-1	-1
19.8	54.5	29.8	24.2	-1	-1
20.1	54.1	29.3	24.6	0	0
20.4	54.2	30.1	26.3	0	0
20.5	54.5	29.5	24	0	0
20.5	53.8	30.5	25.2	0	0
21	53.5	30.5	24.9	1	0
22.3	50.6	31.2	26.2	1	0
23.5	48	31.5	26.8	1	0
25.7	45	33.3	29	0	0
27.1	42.3	32.6	27.6	-1	1
28	41.8	32.8	29.2	-1	1
28.7	40.3	33.1	30.5	-1	1
29.1	40	33.4	30.9	-1	1
28.2	40.6	33.5	30	-1	1
26.7	43.4	33.4	29.2	-1	1
25.7	45	33	28.4	0	0
22.7	63.3	31.6	27.8	0	0
26.5	55	32.7	29.2	0	0
28.9	52	33.7	30.6	-1	1
29.8	48.8	34.5	31.5	-2	2
30.3	47.1	34.6	32	-2	2
28.6	50.3	34.1	31	-2	2
27.7	52	35.1	30.8	-2	2
27.2	52.5	34	29.3	-1	1
25.4	55.6	34	28.6	0	0
24.4	57.4	33.7	28.2	1	0

23.7	55.9	32.4	25.2	1	0
20.9	58.6	32.4	25.5	0	0
18.5	52.3	30	22	-2	-2
18.7	53.8	29.7	22.8	-2	-2
19.6	71.6	30.8	24.5	1	0
19.9	71.3	30.8	24.6	1	0
22.3	63.2	31.5	26.7	0	0
23.8	59.2	32.2	27	0	0
24.5	57.5	32.9	28.5	0	0
26.1	54.8	34	29.4	-1	1
26.8	53.8	32.7	29.2	-1	1
28.8	49.8	34.3	31.4	-2	2
29.5	48	33.7	31	-2	2
28.3	51.4	33.8	30.3	-2	2
26.7	52	34.6	29.7	-1	1
24.9	55.9	32.6	27.2	0	0
21.5	62	31.9	26.3	1	0
21.6	62	31.1	26.1	1	0
23	59.2	32.3	27.1	1	0
24.8	56.7	32.3	27.4	0	0
27.2	51.7	33.6	29.8	-1	1
29.5	48.2	33.9	31.7	-1	1
29.4	48.5	34.4	31.1	-2	2
28.7	50	34	30.6	-2	2
27.4	52	34.2	30	-2	2
26	53.6	33.5	28.5	-1	1
25	55.5	33.8	27.6	0	0
22.6	57.1	31.9	26	1	0
22.5	64.9	32.2	25.8	1	0
20.6	56.1	30.5	22.3	-1	-1
18.7	52.5	29.6	24	-2	-2
16.1	47.1	28.2	23.2	0	0
15.7	50.8	28.3	23.5	0	0
14.4	53.4	26.9	21.7	-1	-1
15	54.6	27.1	23.6	-1	-1
15.6	55.7	27.8	24.6	-1	-1
16.1	54.1	28.5	24.2	-1	-1
16.5	53.2	28.9	23.6	0	0
16.6	52	29.3	24	0	0
21.3	47.7	30.6	25.8	0	0

22.5	45.1	32.1	27.1	0	0
23	40.9	32.8	28.8	-1	1
24.5	40.1	33.4	28.7	-1	1
26.2	36.2	33.7	29.1	-2	2

Chapter 3: Thermal comfort data from female subject

temperature	humidity	skin	clothing	sensation	comfort
17.4	37.9	28.5	21.7	-1	0
17.3	39.5			-1	0
17.3	40.2	29.2	22.4	-1	0
18.5	39			0	0
23.5	35.2	31	26.9	1	-1
26.4	32.1			2	-2
26.8	33.1	32.8	27.8	2	-2
26.7	31.4			2	-2
26.9	31.4	32.3	28.4	2	-2
27.2	33.7			2	-2
27.8	32.1	33.6	28.7	2	-2
28	31.6			2	-2
28.7	30.4	34	29.7	2	-2
29.1	30			2	-2
29.3	29.6	34.8	30.7	2	-2
28.9	30.1			1	-1
28.1	30.8	33.7	29.2	0	0
26.5	31.2			0	0
25.3	33.1	34	28.2	0	1
24.4	33.7			0	1
24	34.4	32.7	26.5	0	1
23.5	33.3			0	1
22.6	32.7	32.2	25.1	0	1
22.3	32.6			0	1
22.2	27.6	32	25	0	0
22.3	27.2			0	0
22.5	26.8	32.2	24.7	0	0
22.4	26.6			0	0
22.4	27.2	32.1	25.3	0	0
22.4	27.8			0	1
22.5	28.3	32.4	25.6	0	1
22.7	28.7			0	1
22.7	30	32	26.1	0	1
22.8	22.9			0	1
26.6	28.3	33.6	28.6	1	-1
28.4	26.9			2	-2
29.6	26.3	34.1	30.4	3	-3
29	26.5			2	-2

28	26.9	34	29	2	-2
27.2	28.2			1	-1
26.9	28.1	34.2	28.8	1	-1
26.7	28.4			1	-1
26.5	28.6	33.6	28.5	1	-1
26.4	28.6			1	-1
26.2	29	34	28.4	1	-1
26.2	29			1	-1
26	25	33.5	28.2	0	0
25.6	24.1			0	0
25.2	24	33.6	26.9	0	0
25.1	23.3			0	0
25	22.4	33.4	26.9	0	0
24.8	23.8			0	0
24.6	25	33.4	26.6	0	0
24.4	26			0	0
24.3	26.1	32.8	25.9	0	0
19.3	34.7			0	1
19.3	34.4			0	1
19.3	34.5	30.8	23.1	0	1
19.2	34.7			0	1
19.2	34.9	31.2	22.9	0	1
19.1	35			0	1
19.1	35.3	30	22.5	0	1
19.2	35.7			0	1
19.9	35.1	30.4	24	0	1
20.4	35.1			0	0
21.5	34.2	31.4	25	0	0
22.5	33			0	0
23.1	32.3	33	26.5	0	0
23.4	32.2			0	0
23.7	31.7	32	25.9	1	-1
24.1	32.1			1	-1
25.2	30.8	32.5	26.9	1	-1
25.7	30.1			1	-1
26.1	29.9	32.7	27.1	1	-2
26.5	29.4			2	-2
27.3	29.2			2	-2
27.5	29	34.3	29.3	2	-2
27.3	29.2			2	-3

27.6	29.1	34.1	29.6	3	-3
28.5	29.1			3	-3
28.2	29.5	34.1	29.8	3	-3
27.6	29.5			3	-3
26.1	30.4	33	28.8	2	-2
25.3	31.4			2	-2
24.9	32.3	34.1	28.7	1	-1
24.1	32.3			1	-1
22.5	32.4	32	25.6	1	-1
21.7	32.7			0	0
20.9	32.2	31.4	25	0	0
17.7	40.3			0	0
17.7	40.5	28.8	24.1	0	0
17.8	40.7			0	0
19.6	39.5	29.8	23.8	0	1
20.2	38.9			0	1
20.6	38.6	30.2	23.9	0	1
21.9	36.2			0	0
23.8	34.4	31.7	26.5	0	0
25.6	32.3			0	0
26.4	31.5	32.5	27.7	0	0
27.2	31			1	-1
27.8	30.2	33.3	28.5	1	-1
28.4	29.7			1	-1
28.9	29.5	33.6	28.8	2	-2
29.5	29.1			2	-2
27.6	30	33.4	27.1	1	-1
25.3	32.6			0	0
21.2	35.1			0	1
21	35.2			0	1
20.8	35.7			0	1
20.7	36.1	30.5	25.1	0	1
20.8	36.6			0	1
22	36.5	31.5	26	0	0
23	35.6			0	0
23.6	34.7	32.2	27.3	0	0
24.5	33.7			1	-1
26.6	31.4	33.3	28.9	1	-1
27.1	30.7			1	-1
27.7	30.7	33.9	29.8	2	-2

28	30.6			2	-2
28.1	30	33.8	30	2	-2
28.4	30			2	-2
25.5	31.7			0	0
25	32.6	33.9	28.2	0	0
24.6	32.2			0	0
24.4	31.4	34.5	29	0	0
19	52.5			0	1
19.2	51.3	29.8	23.9	0	1
19.3	51.3			0	1
19.4	51.3	30.1	24.2	0	1
20.2	49.6	30.7	24.2	0	1
20.8	49.1			0	1
21.9	45	31.6	25.4	0	1
22.3	44.5			0	1
22.3	44.3	32	25.8	0	1
22.8	43.3			0	0
23.4	43	32.7	26	0	0
24.5	40.9			0	0
25.3	39.5	32.4	28.2	0	0
26.1	38.4			0	0
26.7	39.1	33.7	29.3	1	-1
27.1	37.2			1	-1
27.4	36.9	33.8	29.1	1	-1
27.9	36.1			2	-2
28.3	35.9	34.3	30	2	-2
28.7	35.3			2	-2
28.9	36	34.2	29.9	2	-2
28.2	36.9			1	-1
27.5	37.1	33.7	29.7	1	-1
27	37.9			0	0
26.1	38.8	33.5	28	0	0
25.2	39.4			0	0
24.7	41	32.7	27.2	0	0
24.5	41			0	0
24.1	41.3			0	0
29.9	33.3			3	-3
29.6	34	33.8	30	1	-1
27.5	35.9			0	0
26.5	38.1			0	0

25.9	38.7	34.6	29.6	0	0
25.6	39.5			0	0
25.6	39.5	32.9	29.8	0	0
25.5	40.2			0	1
24	38.6	32.8	28.4	0	0
24	42.4			0	0
24.6	42.1	32.8	29.3	0	0
25	41.8			0	1
24.7	39.3	33	28.3	0	0
23.2	37.7			-1	-1
22.4	36.5			-1	-1
21.5	35.5			-2	-2
21	35.1	31.5	25.4	-2	-2
21.3	34.8			-2	-2
19.8	35.9	32	26.5	-2	-2
19	37			-3	-3
18.7	36.1	31.2	26	-3	-3
18.5	36.1			-3	-3
20.8	63			0	0
21	61.2	31.2	24.5	0	0
21.1	60.7			0	0
21.3	59.8			0	0
21.3	59.7	32	26.5	0	0
21.7	59.2			0	0
23.5	56.4			0	0
24.7	54.1	33.1	27.1	0	0
25.3	52.9			0	0
25.8	51.9			0	0
26.8	49.8	34.3	28.4	1	-1
27.9	48.1			1	-1
28.4	46.9	34.5	30.2	1	-1
28.7	45.8			1	-1
29.2	44.7	34.6	29.7	1	-1
29.6	43.4			2	-2
30	42.4	34.9	31.2	2	-2
30.3	41.2			2	-2
30.6	40.5	35.1	31.1	2	-2
30.7	39.6			2	-2
29.9	41.1	34.7	30.1	1	-1
29	42.6			1	-1

27.9	43.7	34.3	29.7	0	0
27.1	45.3	34	28.3	0	0
26.7	46.1			0	0
26.5	45.7	35	28.7	0	0
17.3	43.4	29.3	22.3	-2	-2
17	42.1			-2	-2
16.6	41.6	29	21.7	-2	-2
16.3	41.4			-2	-2
15.7	41.1	28.2	20	-2	-2
16.6	44.4			-2	-2
17.9	48.6	30.4	24.9	-1	-1
18.6	52			-1	-1
19	51.7	29.7	23.7	-1	-1
18.2	55.2			-1	-1
19	54.8	29.6	24.4	-1	-1
19.5	54.6			-1	-1
19.8	54.5	31	25	0	0
19.9	54.3			0	0
20.1	54.1	30.7	26.4	0	0
20.2	54.8			0	0
20.4	54.2	30.5	24.4	0	0
20.4	54.3			0	0
20.5	54.5	30.9	26.3	0	0
20.5	53.9			0	1
20.5	53.8	31.1	23.5	0	1
20.5	53.8			0	1
21	53.5	32	25.1	0	1
21.8	52.4			0	1
22.3	50.6	32.3	27.1	0	0
22.7	49.8			0	0
23.5	48	32.8	27.1	0	0
24.4	46.7			0	0
25	46	33	27.5	1	-1
25.5	45.7			1	-1
25.7	45	34.3	29.6	1	-1
26.5	43.1			1	-1
27.1	42.3	34	30	2	-2
27.6	42.2			2	-2
28	41.8	34.6	30.6	2	-2
28.4	40.8			2	-2

28.7	40.3	34.5	29.9	2	-2
29	40.4			2	-2
29.1	40	34.8	30.5	3	-3
29.3	40.2			3	-3
28.2	40.6	33.4	30.2	2	-2
27.2	42.5			1	-1
26.7	43.4	34.3	29.9	1	-1
26.5	43.9			1	-1
25.7	45	33.4	28.7	1	-1
25	46.7			1	-1
24.5	48.4			1	-1
24.2	49.1			1	-1
23.8	51.6			1	-1
20.9	67.5			0	0
22.7	63.3	32.6	28	0	-1
25.4	56.6			0	-1
26.5	55	33.5	30.1	1	-1
27.6	52.6			1	-1
28.3	51			1	-1
28.9	52	33.9	29.4	1	-2
29.5	49.4			1	-2
29.8	48.8	34.9	31.6	2	-2
30.3	47.1	34.7	31.9	2	-3
29.3	49.4			2	-3
28.6	50.3	34.1	30.9	3	-2
28	51.5			3	-2
27.7	52	34.9	30.7	2	-2
27.6	52.8			2	-2
27.2	52.5	34.2	29.8	2	-1
26.4	54			2	-1
25.4	55.6	33.2	29.1	1	0
25	56.1			1	0
24.4	57.4	33.2	28.6	0	0
24.2	57.6			0	1
23.7	55.9	31.9	26.1	0	0
21.2	54.2			0	0
20.9	58.6	30.4	25.8	0	0
21.5	60.9			0	0
21.2	58			0	0
19.4	54.7			-1	-1

18.5	52.3	29.6	23.1	-1	-1
18.7	55.6			-2	-2
18.7	53.8	29.6	24.2	-2	-2
19.5	71.9			-1	-1
19.6	71.9			-1	-1
19.6	71.6	29.8	25.4	-1	-1
19.8	70.9			-1	-1
19.9	71.3	30	25.6	-1	-1
20.9	67.7			-1	-1
22.3	63.2	31.4	27	-1	-1
23.2	61.8			0	0
23.8	59.2	32.1	28	0	1
24.1	58.3			0	0
24.5	57.5	32.7	28.8	0	0
25.1	56.6			1	-1
26.1	54.8	33.7	30.1	1	-1
26.4	54.1			1	-1
26.8	53.8	33.1	29.2	2	-2
27.7	51.9			2	-2
28.8	49.8	33.6	31.7	2	-2
29.3	48.5			2	-2
29.5	48	34.2	31.2	2	-2
29.2	49.4			1	-1
28.3	51.4	34	30.3	1	-1
28.2	50.6			1	-1
26.7	52	35.1	30.2	1	-1
25.5	54.7			0	0
24.9	55.9	32.8	27.9	0	0
24	57.8			0	0
21.5	63.3			0	1
21.5	62	31.1	26.5	0	1
21.7	61.9			0	1
21.6	62	31.1	26.5	0	1
22.2	61.8			0	0
23	59.2	31.7	27	0	0
23.8	59.1			0	0
24.8	56.7	32.4	27.8	0	0
25.5	55.5			0	0
25.9	54.2			0	0
26.5	52.9			1	-1

27.2	51.7	33.6	29.4	1	-1
27.7	51			1	-1
28.2	50.2			2	-2
28.7	49.5			2	-2
29.5	48.2	34.4	31.2	3	-3
30	47.4			3	-3
29.4	48.5	34.9	31.7	3	-3
28.8	50.5			3	-3
28.7	50	34.8	31.1	3	-3
28	50.4			2	-3
27.4	52	34.3	30.1	2	-2
27	52.3			1	-1
26	53.6	34.4	29.4	1	-1
25.4	54.6			1	-1
25	55.5	33.9	27.7	1	-1
24.5	57.8			0	0
22.6	57.1	31.8	26.3	0	1
22.3	63.1			0	1
22.4	64			0	1
22.5	64.9	32.5	26.9	0	1
22	60.5			0	0
20.6	56.1	31.2	25.2	-1	-1
19.3	53.5			-1	-1
18.7	52.5	30.1	25	-1	-1
18.1	50.6			-1	-1
16.1	47.1	27.5	18.3	0	0
15.7	50.8	28.3	19.3	-1	-1
14.4	53.4	27.1	18.8	-2	-2
15	54.6	27.8	20.8	-2	-2
15.6	55.7	26.1	20.5	-2	-2
16.1	54.1	28.4	22.1	-2	-2
16.5	53.2	27.8	21.6	-1	-1
16.6	52	28.5	22.4	-1	-1
18.4	51.2			-1	-1
19	50			-1	-1
20	47.5			0	-1
20.6	47.8			0	-1
21.3	47.7	31	24.1	0	-1
22.5	45.1	32.1	26.1	0	0
23	40.9	32.9	6.2	0	0

24.5	40.1	33.5	26.7	0	0
25	36.8			1	-1
25.6	36.5			1	-1
26.2	36.2	33.6	27.4	2	-2

Chapter 5: Thermal comfort data for male subject

time	temperature	humidity	skin	sensation
2018-08-21 11:55:04 UTC	25.6	52.7	27.86	-1
2018-08-21 12:00:15 UTC	25.9	57.9	28.64	-1
2018-08-21 12:05:14 UTC	24.4	65.4	30.69	-1
2018-08-21 12:10:07 UTC	24.7	62.1	27.61	-1
2018-08-21 12:15:14 UTC	24.7	69.5	30.97	-1
2018-08-21 12:20:01 UTC	23.9	64.2	29.36	-1
2018-08-21 12:25:15 UTC	25.7	71.3	31.78	-1
2018-08-21 12:30:04 UTC	25.2	64.1	28.92	-1
2018-08-21 12:35:09 UTC	26	69	30.67	-1
2018-08-21 12:40:15 UTC	25.9	74.4	30.36	-2
2018-08-21 12:45:17 UTC	25.9	72.2	31.06	-2
2018-08-21 12:50:11 UTC	26.7	74.5	31.11	-1
2018-08-21 12:55:11 UTC	26.9	77.4	30.69	-1
2018-08-21 13:00:06 UTC	27.5	77.1	32.14	0
2018-08-21 13:05:13 UTC	27.8	77.3	31.19	0
2018-08-21 13:10:07 UTC	28	78.5	31.28	0
2018-08-21 13:15:16 UTC	28.2	77.7	31.33	0
2018-08-21 13:20:09 UTC	28.4	77.7	31.64	0
2018-08-21 13:25:00 UTC	28.6	77.5	30.92	0
2018-08-21 13:30:09 UTC	28.7	78	31.36	0
2018-08-21 13:35:00 UTC	29	76.2	31.56	0
2018-08-21 13:40:14 UTC	29	76.2	31.67	0
2018-08-21 13:45:11 UTC	29.3	75.4	31.81	0
2018-08-21 13:50:02 UTC	29.5	74.8	31.47	0
2018-08-21 13:55:08 UTC	29.4	74.5	31.11	0
2018-08-21 14:00:15 UTC	29.4	74.8	31.47	0
2018-08-23 11:35:15 UTC	24.3	58.8	29.47	-1
2018-08-23 11:40:09 UTC	23.9	56.9	29.61	-1
2018-08-23 11:45:04 UTC	23.5	56.7	29.81	-1
2018-08-23 11:50:13 UTC	25.6	64.2	31.83	0
2018-08-23 11:55:04 UTC	25.4	65.7	32.42	0
2018-08-23 12:00:14 UTC	25	66	31.69	0
2018-08-23 12:05:07 UTC	26.6	68.9	32.08	1
2018-08-23 12:10:13 UTC	26.2	64.4	28.75	0
2018-08-23 12:15:11 UTC	26.7	72.3	31.56	0
2018-08-23 12:20:06 UTC	26.2	66.2	29.17	0
2018-08-23 12:25:14 UTC	26.8	72.8	30.92	0
2018-08-23 12:30:06 UTC	27.3	73.4	31.11	0

2018-08-23 12:35:14 UTC	27.8	73.4	31.5	0
2018-08-23 12:40:04 UTC	28.2	73.1	31.5	0
2018-08-23 12:45:17 UTC	27	74.3	30.19	-1
2018-08-23 12:50:11 UTC	27.7	75.8	30.97	-1
2018-08-23 12:55:06 UTC	28.3	74.3	31.53	0
2018-08-23 13:00:15 UTC	28.8	72.7	31.56	0
2018-08-23 13:05:12 UTC	29.1	72	31.31	0
2018-08-23 13:10:09 UTC	29.3	71.4	31.72	0
2018-08-23 13:15:00 UTC	29.3	71.8	31.42	0
2018-08-23 13:20:10 UTC	29.4	71.8	31.58	0
2018-08-23 13:25:03 UTC	29.7	71.3	30.39	0
2018-08-23 13:30:11 UTC	29.9	69.9	31.81	0
2018-08-23 13:35:14 UTC	30.8	65.5	31.44	0
2018-08-23 13:40:03 UTC	30	68.2	31.44	0
2018-08-23 13:45:13 UTC	29.7	68.5	32.14	0
2018-08-23 13:50:03 UTC	29.7	69.1	32.44	0
2018-08-23 13:55:10 UTC	30	68.7	33.36	0
2018-08-24 11:45:11 UTC	24.8	59.5	31.83	-1
2018-08-24 11:50:08 UTC	25	58.5	28.67	-1
2018-08-24 11:55:09 UTC	25	61.9	28.86	-1
2018-08-24 12:00:00 UTC	25.1	66.6	31.47	-1
2018-08-24 12:05:12 UTC	26	69	31.17	-1
2018-08-24 12:10:04 UTC	25.2	69.1	30.06	-1
2018-08-24 12:15:19 UTC	26.2	70.3	31.94	-1
2018-08-24 12:20:11 UTC	26.7	71.7	31.5	-1
2018-08-24 12:25:15 UTC	27	71.9	31.56	0
2018-08-24 12:30:06 UTC	27.4	71.2	31.36	0
2018-08-24 12:35:00 UTC	27.6	70.7	32.36	0
2018-08-24 12:40:18 UTC	27.8	70.6	30.97	0
2018-08-24 12:45:16 UTC	27.9	70.5	30.92	0
2018-08-24 12:50:12 UTC	28	70.4	31.31	0
2018-08-24 12:55:03 UTC	28.1	69.9	30.97	0
2018-08-24 13:00:14 UTC	28.2	69.9	31.03	0
2018-08-24 13:05:09 UTC	28.2	69.8	31.64	0
2018-08-24 13:10:02 UTC	28.4	69.4	31.31	0
2018-08-24 13:15:14 UTC	28.6	69.2	31.36	0
2018-08-24 13:20:06 UTC	28.7	69.5	30.44	0
2018-08-24 13:25:16 UTC	28.7	68.8	30.97	0
2018-08-24 13:30:12 UTC	28.7	68.8	31.06	0
2018-08-24 13:35:05 UTC	28.8	68.8	31.14	0

2018-08-24 13:40:12 UTC	28.8	68.8	31.44	1
2018-08-24 13:45:03 UTC	28.9	68.5	31.86	1
2018-08-24 13:50:14 UTC	28.9	68.7	31.5	1
2018-08-24 13:55:10 UTC	28.9	68.8	31.58	1
2018-08-24 14:00:00 UTC	28.9	69	31.06	1
2018-08-25 11:05:06 UTC	24.9	68.9	29.08	-2
2018-08-25 11:10:16 UTC	24.7	73.2	29.97	-2
2018-08-25 11:15:08 UTC	24.2	73	30.36	-1
2018-08-25 11:20:16 UTC	25.4	75.4	30.69	-1
2018-08-25 11:25:09 UTC	25.7	72.5	29.28	-1
2018-08-25 11:30:02 UTC	25.5	78	29.86	0
2018-08-25 11:35:09 UTC	26.1	78.1	32.06	0
2018-08-25 11:40:17 UTC	26.6	78.6	31.44	0
2018-08-25 11:45:28 UTC	26.9	79.5	31.08	0
2018-08-25 11:50:02 UTC	27.1	78.9	31.14	0
2018-08-25 11:55:15 UTC	27.4	78.5	30.92	0
2018-08-25 12:00:08 UTC	27.6	78.5	30.97	0
2018-08-25 12:05:16 UTC	27.7	78.6	31.67	0
2018-08-25 12:10:07 UTC	27.8	78.5	31.94	0
2018-08-25 12:15:00 UTC	27.9	78.1	31.31	0
2018-08-25 12:20:08 UTC	28.2	77.1	31.58	0
2018-08-25 12:25:15 UTC	28.4	76.4	31.17	0
2018-08-25 12:30:09 UTC	28.6	76	31.36	0
2018-08-25 12:35:02 UTC	28.4	76.7	30.97	0
2018-08-25 12:40:10 UTC	28.4	76.6	30.69	0
2018-08-25 12:45:04 UTC	28.3	77	30.28	0
2018-08-25 12:50:13 UTC	28.4	77.1	30.78	0
2018-08-25 12:55:05 UTC	28.7	76.4	30.89	0
2018-08-25 13:00:16 UTC	28.9	75.7	31.28	0
2018-08-25 13:05:06 UTC	28.8	76	31.44	0
2018-08-25 13:10:12 UTC	28.7	76.3	31.06	0
2018-08-25 13:15:06 UTC	28.7	76.3	31.33	0
2018-08-25 13:20:14 UTC	28.6	76.7	31.03	0
2018-08-25 13:25:05 UTC	28.6	77	31.44	1
2018-08-25 13:30:12 UTC	28.7	77.1	30.97	1
2018-08-25 13:35:06 UTC	29	76	31.78	1
2018-08-25 13:40:13 UTC	29.1	75.8	31.5	1
2018-08-25 13:45:08 UTC	29	76.1	31.36	1
2018-08-25 13:50:17 UTC	29	76.2	30.92	1
2018-08-25 13:55:10 UTC	28.8	76.8	30.64	1

2018-08-25 14:00:03 UTC	28.8	77.3	31.36	1
2018-08-26 12:15:03 UTC	24.1	69	30.53	-1
2018-08-26 12:20:11 UTC	24.7	69.2	29.61	-1
2018-08-26 12:25:02 UTC	25.1	75.9	30.67	-1
2018-08-26 12:30:12 UTC	25	76.9	31.64	0
2018-08-26 12:35:04 UTC	25.8	78.3	30.97	0
2018-08-26 12:40:14 UTC	26.3	80.2	31.31	0
2018-08-26 12:45:06 UTC	26.4	79	30.17	0
2018-08-26 12:50:14 UTC	25.9	79	31.03	0
2018-08-26 12:55:04 UTC	26.5	80.1	31.14	0
2018-08-26 13:00:12 UTC	26.9	80.3	31.47	0
2018-08-26 13:05:08 UTC	26.1	78.8	31.39	0
2018-08-26 13:10:02 UTC	26.7	79.8	31.58	1
2018-08-26 13:15:11 UTC	27	81.1	31.25	1
2018-08-26 13:20:03 UTC	27.2	82	31.11	1
2018-08-26 13:25:13 UTC	27.4	82.1	31.69	1
2018-08-26 13:30:09 UTC	27.4	82.3	31.56	1
2018-08-26 13:35:01 UTC	27.8	81.5	31.64	1
2018-08-26 13:40:11 UTC	27.9	80.6	31.33	1
2018-08-26 13:45:05 UTC	27.8	81.2	30.94	1
2018-08-26 13:50:14 UTC	27.8	81.6	30.72	1
2018-08-26 13:55:05 UTC	27.8	81.8	30.56	1
2018-08-26 14:00:14 UTC	27.9	81.6	30.92	1
2018-08-27 10:40:02 UTC	26.3	59	31.44	-1
2018-08-27 10:45:29 UTC	26.2	56.3	29.94	-1
2018-08-27 10:50:05 UTC	26.1	55.4	31.78	-1
2018-08-27 10:55:15 UTC	25.9	54.3	30.72	-1
2018-08-27 11:00:12 UTC	26.4	59.9	30.78	-1
2018-08-27 11:05:01 UTC	26.1	55.7	30.42	-1
2018-08-27 11:10:10 UTC	25.9	54.5	30.5	-1
2018-08-27 11:15:03 UTC	26.3	60.1	31.28	0
2018-08-27 11:20:00 UTC	26.6	59.1	31.08	0
2018-08-27 11:25:01 UTC	26.9	62.9	30.53	0
2018-08-27 11:30:11 UTC	27.1	67.1	31.72	0
2018-08-27 11:35:06 UTC	27.4	70.8	31.53	0
2018-08-27 11:40:18 UTC	27.5	67.5	30.31	0
2018-08-27 11:45:10 UTC	27.6	73	31.72	0
2018-08-27 11:50:22 UTC	27.8	74.6	31.92	1
2018-08-27 11:55:29 UTC	28.1	75	31.86	1
2018-08-27 12:00:01 UTC	28.4	75.3	32.33	1

2018-08-27 12:05:12 UTC	28.3	76.8	31.19	1
2018-08-27 12:10:05 UTC	28.3	76.9	30.64	1
2018-08-27 12:15:13 UTC	28.5	76.6	31.03	1
2018-08-27 12:20:07 UTC	28.5	77.8	31.03	1
2018-08-27 12:25:02 UTC	28.5	77.1	31.25	1
2018-08-27 12:30:11 UTC	28.6	77.2	31.19	1
2018-08-27 12:35:06 UTC	28.8	76.8	31.11	1
2018-08-27 12:40:00 UTC	28.7	77.1	31.28	1
2018-08-27 12:45:09 UTC	28.8	77.4	31.06	1
2018-08-27 12:50:35 UTC	28.7	77.8	31.14	1
2018-08-27 12:55:11 UTC	28.7	77.8	30.58	1
2018-08-27 13:00:02 UTC	28.7	77.8	31.19	1

Chapter 5: Thermal comfort data for female subject

time	temperature	humidity	skin	sensation
2018-08-21 11:45:15 UTC	24.3	57.8	25.58	0
2018-08-21 11:50:15 UTC	23.1	59	28.53	1
2018-08-21 11:55:02 UTC	23.8	58.6	30.89	0
2018-08-21 12:10:02 UTC	25.6	61	29.06	0
2018-08-21 12:15:16 UTC	25.9	63.3	31.61	1
2018-08-21 12:20:09 UTC	25.5	58.7	30.42	1
2018-08-21 12:25:00 UTC	26	67.5	31.72	0
2018-08-21 12:30:08 UTC	26.1	62.9	31.28	1
2018-08-21 12:35:15 UTC	26.4	67	31.39	0
2018-08-21 12:40:09 UTC	26.4	69.6	32.64	0
2018-08-21 12:45:05 UTC	26.5	67.3	32.61	1
2018-08-21 12:50:10 UTC	26.9	71.9	32.47	0
2018-08-21 13:15:07 UTC	28.1	77.2	31.08	1
2018-08-21 13:20:16 UTC	28.2	76.6	31.72	1
2018-08-21 13:25:09 UTC	28.3	76.5	32.39	0
2018-08-21 13:30:17 UTC	28.5	76.5	31.83	1
2018-08-21 13:35:07 UTC	28.6	75.9	31.92	1
2018-08-21 13:40:04 UTC	28.7	75.8	32.03	2
2018-08-21 13:45:14 UTC	28.6	75.7	31.83	2
2018-08-21 13:50:05 UTC	28.6	75.7	32.31	2
2018-08-21 13:55:13 UTC	28.6	75.4	31.94	2
2018-08-21 14:00:04 UTC	28.7	75.5	31.69	2
2018-08-23 11:35:17 UTC	27.6	53.4	31.36	0
2018-08-23 11:40:09 UTC	27.5	50.1	31.06	0
2018-08-23 11:45:02 UTC	27.3	49.3	31.58	0
2018-08-23 11:50:29 UTC	27.3	56.4	31.97	1
2018-08-23 11:55:05 UTC	27.5	55.7	31.86	0
2018-08-23 12:00:16 UTC	27.5	55.9	32.11	0
2018-08-23 12:05:08 UTC	27.7	61.6	32.61	0
2018-08-23 12:30:00 UTC	28.2	67.5	31.75	1
2018-08-23 12:35:14 UTC	28.4	69.2	31.53	0
2018-08-23 12:40:07 UTC	28.5	70.1	31.42	0
2018-08-23 12:45:03 UTC	28.4	65.5	31.42	1
2018-08-23 12:50:12 UTC	28.5	70.4	31.39	0
2018-08-23 12:55:04 UTC	28.7	70.9	31.42	0
2018-08-23 13:00:19 UTC	28.9	70.6	31.92	0
2018-08-23 13:10:08 UTC	29.2	70.9	32	1
2018-08-23 13:15:00 UTC	29.2	71	32.03	1

2018-08-23 13:20:10 UTC	29.3	71.3	31.81	1
2018-08-23 13:25:04 UTC	29.4	71.2	32.47	0
2018-08-23 13:30:14 UTC	29.4	70.1	31.72	1
2018-08-23 13:35:08 UTC	29.4	69.6	31.94	1
2018-08-23 13:40:03 UTC	29.4	69.8	31.67	2
2018-08-23 13:45:13 UTC	29.4	69.4	31.86	2
2018-08-23 13:50:08 UTC	29.4	69.6	32.11	2
2018-08-23 13:55:05 UTC	29.5	69.3	31.86	2
2018-08-23 14:00:40 UTC	29.5	68.4	31.19	2
2018-08-24 12:25:04 UTC	27.4	69.4	32.58	0
2018-08-24 12:30:13 UTC	27.5	68.2	32.31	0
2018-08-24 12:35:09 UTC	27.7	68.7	32.33	0
2018-08-24 12:40:19 UTC	27.7	68.3	31.36	0
2018-08-24 12:45:15 UTC	27.7	69.5	31.64	0
2018-08-24 12:50:08 UTC	27.8	68.9	31.64	0
2018-08-24 12:55:02 UTC	27.8	68.7	31.64	0
2018-08-24 13:00:15 UTC	27.9	69	31.47	0
2018-08-24 13:05:08 UTC	28	68.9	31.67	0
2018-08-24 13:10:03 UTC	28	68.8	31.33	0
2018-08-24 13:15:15 UTC	28.1	68.8	31.69	0
2018-08-24 13:20:06 UTC	28.2	68.8	31.97	0
2018-08-24 13:25:01 UTC	28.2	68.8	32.14	0
2018-08-24 13:30:12 UTC	28.2	68.8	31.75	0
2018-08-24 13:35:05 UTC	28.3	69.1	31.89	0
2018-08-24 13:40:16 UTC	28.3	69.1	32.08	-1
2018-08-24 13:45:07 UTC	28.3	69.1	31.64	-1
2018-08-24 13:50:16 UTC	28.3	69.1	31.94	-1
2018-08-24 13:55:08 UTC	28.4	69.2	31.92	-1
2018-08-24 14:00:00 UTC	28.4	69.2	31.58	-1
2018-08-25 11:00:14 UTC	26.2	62.8	31.17	0
2018-08-25 11:15:15 UTC	26.7	63.5	32.33	0
2018-08-25 11:20:06 UTC	26.8	68.1	32.81	0
2018-08-25 11:25:16 UTC	27.2	69.3	32.67	0
2018-08-25 11:30:08 UTC	27.1	69	32.56	0
2018-08-25 11:35:16 UTC	27.2	71.3	32.53	0
2018-08-25 11:40:07 UTC	27.4	73.5	32.89	0
2018-08-25 11:45:16 UTC	27.6	75.3	32.97	0
2018-08-25 11:50:06 UTC	27.8	74.6	33.19	0
2018-08-25 11:55:16 UTC	27.9	74.6	33.33	0
2018-08-25 12:00:08 UTC	27.8	75	33.28	0

2018-08-25 12:05:00 UTC	28	76.5	33.53	0
2018-08-25 12:10:08 UTC	28.2	75.6	33.5	0
2018-08-25 12:15:01 UTC	28.2	75.6	32.36	0
2018-08-25 12:20:09 UTC	28.3	75.8	31.69	0
2018-08-25 12:25:00 UTC	28.4	75.3	31.92	0
2018-08-25 12:30:09 UTC	28.5	75.4	32.58	0
2018-08-25 12:35:03 UTC	28.5	74.9	32.53	0
2018-08-25 12:40:11 UTC	28.6	75.2	32.72	0
2018-08-25 12:45:04 UTC	28.3	75.7	31.42	0
2018-08-25 12:50:13 UTC	28.3	76.1	32.33	0
2018-08-25 12:55:05 UTC	28.3	76.1	32.14	0
2018-08-25 13:00:13 UTC	28.5	75.7	32.92	0
2018-08-25 13:05:06 UTC	28.6	75.6	31.69	0
2018-08-25 13:10:15 UTC	28.6	75.6	32.39	0
2018-08-25 13:15:06 UTC	28.7	75.4	32.61	0
2018-08-25 13:20:14 UTC	28.6	75.8	32.72	0
2018-08-25 13:25:07 UTC	28.6	75.9	32.47	0
2018-08-25 13:30:16 UTC	28.8	75.8	32.64	0
2018-08-25 13:35:07 UTC	28.8	75.9	32.56	0
2018-08-25 13:40:16 UTC	28.8	75.8	32.42	1
2018-08-25 13:45:09 UTC	28.8	76.2	32.61	1
2018-08-25 13:50:01 UTC	28.9	76	32.06	1
2018-08-25 13:55:10 UTC	28.9	76	32.33	1
2018-08-25 14:00:41 UTC	28.9	75.5	32.5	1
2018-08-26 12:00:12 UTC	25.5	81.1	29.64	0
2018-08-26 12:05:04 UTC	25.3	71.9	29.22	0
2018-08-26 12:10:12 UTC	25.3	71.9	29.47	0
2018-08-26 12:15:03 UTC	25.6	67.1	31.81	0
2018-08-26 12:20:14 UTC	25.9	66.9	31.89	0
2018-08-26 12:25:05 UTC	26	70	32.53	0
2018-08-26 12:30:13 UTC	26.1	69.1	32.83	0
2018-08-26 12:35:06 UTC	26.3	73	33.06	0
2018-08-26 12:40:16 UTC	26.4	77	32.69	0
2018-08-26 12:45:08 UTC	26.5	78.3	32.11	0
2018-08-26 12:50:16 UTC	26.6	74.8	33.06	0
2018-08-26 12:55:07 UTC	26.7	77.2	32.64	0
2018-08-26 13:00:15 UTC	26.8	78.7	32.89	0
2018-08-26 13:05:08 UTC	26.8	72.3	31.61	0
2018-08-26 13:10:02 UTC	26.9	77.1	33.11	0
2018-08-26 13:25:15 UTC	27.1	81.2	33.08	0

2018-08-26 13:30:10 UTC	27.3	81.3	33.25	0
2018-08-26 13:35:02 UTC	27.5	81	32.81	0
2018-08-26 13:40:11 UTC	27.7	80.4	32.83	0
2018-08-26 13:45:06 UTC	27.6	80.8	32.42	0
2018-08-26 13:50:15 UTC	27.6	80.8	32.78	0
2018-08-26 13:55:05 UTC	27.7	80.8	32.78	0
2018-08-26 14:00:14 UTC	27.8	81	32.08	0
2018-08-27 11:00:11 UTC	25.3	62.6	31.86	0
2018-08-27 11:05:07 UTC	24.5	60.7	30.33	-1
2018-08-27 11:10:16 UTC	23.9	59.9	31	-1
2018-08-27 11:15:07 UTC	25.3	67.5	33.17	0
2018-08-27 11:20:00 UTC	25.1	64.1	31.92	-1
2018-08-27 11:25:04 UTC	25.6	67.5	31.58	-1
2018-08-27 11:30:16 UTC	26.2	74	32.83	0
2018-08-27 11:35:08 UTC	26.8	76.6	32.94	0
2018-08-27 11:40:00 UTC	26.5	71	30.97	-1
2018-08-27 11:45:11 UTC	27	77	33.14	0
2018-08-27 11:50:06 UTC	27.6	78	32.56	0
2018-08-27 11:55:14 UTC	27.9	79	33.36	0
2018-08-27 12:00:05 UTC	28.2	79	33.39	0
2018-08-27 12:05:15 UTC	28.2	79	32.33	0
2018-08-27 12:10:07 UTC	28.3	79	32.25	0
2018-08-27 12:15:15 UTC	28.4	78.8	31.94	0
2018-08-27 12:20:08 UTC	28.5	78.9	32.56	0
2018-08-27 12:25:02 UTC	28.7	78.6	32.64	0
2018-08-27 12:35:06 UTC	28.8	78.2	32.83	1
2018-08-27 12:40:00 UTC	28.9	78.2	32.67	1
2018-08-27 12:45:09 UTC	29	78.1	32.86	1
2018-08-27 12:50:01 UTC	29	78	33.28	1
2018-08-27 12:55:13 UTC	29	77.9	33.28	1
2018-08-27 13:00:05 UTC	29.2	77.5	33.94	1

Appendix C: Checklist for all devices

Item	Budget	Amount/Notes					
Participants fee	$300	spring break					
Participants fee	$461	summer					
cooling device	$120	5					
IR vision sensors	$240	5					
environmental sensors	$135	5					
else	$50						
esp8266	$40	5					
wemo insight	$196	6					
Total	$1,542						
		balance					
environmental sensors	$135	$135					
DHT22_2/3/2018	-$10	$125					
DHT22_3/4/2018	-$4	$121					
DHT22_5/8/2018	-$10.07	$111					
Wind sensor_5/8/2018	-$110.74	$0					
						balance	
		balance		**cooling device**	$120	$120	6.2
IR vision sensors	$236	$236		desktop fan	-$8	$112	
GridEye_2/21/2018	-$49.53	$186		transformer	-11.548387	$100	
GridEye_3/4/2018	-$49.53	$137			0	$100	
Relays_4/17/2018	-$8	$129		plug	-5.8064516	$95	
GridEye_5/8/2018	-$129.43	$0		plugs	-7.5806452	$87	
				breadboard	-3.8645161	$83	
esp8266	$40	$40		mini-fans	-32.177419	$51	
1/25/18	-$8.79	$31.21			0	$51	
5/8/18	-$29.66	$1.55		batteries	0	$51	
				usb	-19.354839	$32	
else	$50	$50		plugs	-15.806452	$16	
energy meters	-12.90322581	$37		adc	-3.5532258	$12	
wall	0	$37		arduino uno	-4.4354839	$8	
GridEye_6/18/2018	-33.70967742	$3		velocity sensor	-6.4516129	$1	
dht222_6/24/2018	-3.193548387	$0					